ELECTROCHEMICAL DETECTION OPTIMIZED FOR CAPILLARY LIQUID CHROMATOGRAPHIC DETERMINATION OF NEUROACTIVE COMPOUNDS

by

Xiaomi Xu

Bachelor of Science, Xiamen University, 2001

Master of Science, Xiamen University, 2004

Master of Science, University of Pittsburgh, 2008

Submitted to the Graduate Faculty of the Kenneth P. Dietrich School of

Arts and Sciences in partial fulfillment

of the requirements for the degree of

Doctor of Philosophy

University of Pittsburgh

2011

UNIVERSITY OF PITTSBURGH

THE KENNETH P. DIETRICH SCHOOL OF ARTS AND SCIENCES

This dissertation was presented

by

Xiaomi Xu

It was defended on

November 10, 2011

and approved by

Stephen G. Weber, Professor, Department of Chemistry

Adrian C. Michael, Associate Professor, Department of Chemistry

Shigeru Amemiya, Associate Professor, Department of Chemistry

John Kitchin, Associate Professor, Department of Chemical Engineering

Dissertation Advisor: Stephen G. Weber, Professor, Department of Chemistry

ELECTROCHEMICAL DETECTION OPTIMIZED FOR CAPILLARY LIQUID CHROMATOGRAPHIC DETERMINATION OF NEUROACTIVE COMPOUNDS

Xiaomi Xu, PhD

University of Pittsburgh, 2011

Miniaturization of the electrochemical flow cell detector is critical to improving the performance of a capillary liquid chromatography-electrochemical detection (LC-ECD) system. Fabricating the spacer in the flow cell using a novel photosensitive polymer coating offers the convenience of controllable thickness and easy assembling, which leads to improvement in detector performance. The advantage of the thin polymer coating as the spacer is demonstrated by comparing the performance with that of a traditional free standing spacer. A dual working electrode electrochemical detector increases detection selectivity based on the difference in the electrochemical reversibility of analytes. Carbon fiber/epoxy composite materials are commercially available in various shapes and sizes at very low cost. Using tube and rod composites, a ring-disk electrode with a 20 μm gap between the ring and the disk is successfully fabricated through a unique two-step insulation-adhesion process. The narrow gap is favorable for mass transfer in the generator-collector experiment. When assembled in an electrochemical radial-flow cell detector, the dual electrode gives high collection efficiency (0.8 for a chemically reversible species), which enhances the detection selectivity. Carbon electrodes can also be replaced with naphthalenethiol modified gold electrodes. The modification monolayer suppresses the background current from Au while giving detectable current for biological analytes with sensitivity comparable to a glassy carbon electrode.

Analyzing microdialysates sampled from the brain area of interest using HPLC is the most popular method among neuroscientists to measure extracellular neurotransmitters. An optimized capillary UHPLC-ECD system is successfully applied to the measurement of serotonin basal concentration in microdialysis samples and the analytical system can be coupled with microdialysis for on-line measurements.

TABLE OF CONTENTS

LIST OF TABLES

LIST OF FIGURES

PREFACE

I would like to take this opportunity to thank people around me who have made the graduate school a fruitful journey of my life. Without their help and guidance, it would not have been possible for me to come this far.

Professor Stephen Weber, my graduate school advisor, has always been a great mentor. He is a true scholar, and more importantly to me, a wonderful teacher. After working under his guidance for several years, his efforts to train us into independent researchers have strongly influenced me, which shape me into who I am academically today. I can never express my deep gratitude to him enough.

My committee members have also guided me over the years. Dr. Shigeru Amemiya is a serious electrochemist, whose expertise has helped to expand my knowledge in this field. Dr. Adrian Michael, who is also my proposal committee member, has given me great advice especially in the bioanalytical field. I would like to thank Dr. John Kitchin for taking his time to serve in my committee.

The Weber group has always been great. Everyone is helpful and knowledgeable. I should especially point out several group members, Yifat Guy, Kristi Kauffman, Amy Rupert, Jing Zhang and Hong Zhang, who I constantly have discussions with about my project and science in general. These conversations have helped me a great deal throughout the years.

The machine shop and electronic shop at the University of Pittsburgh are extremely helpful. Tom Gasmire at the machine shop is so talented that he can make anything upon request. Thanks, Tom.

Last but certainly not the least; it goes without saying that I owe everything to my family. My parents and siblings will probably never be able to read or understand my dissertation, but their selfless love and support have kept me going over the years to pursue my academic dream. My husband, Gabriel Cheung, has been tolerating my emotional ups and downs the past years. To that, I can only say I love you and thanks for everything.

1.0 INTRODUCTION

Microdialysis-HPLC is a widely accepted method among neuroscientists and chemists for measuring neurotransmitters in extracellular fluids due to its versatility, robustness and reproducibility[1-5]. Several reports demonstrate determination of extracellular serotonin (5-hydroxytryptamine, 5-HT)[6-8] and dopamine[9-12] in microdialysate samples using high-performance liquid chromatography (HPLC) with electrochemical detection (ECD). An analytical HPLC system with column ID of 4.6 mm is usually equipped with a 5-20 μL sample loop, which takes 5-20 minutes to fill with a microdialysis flow rate of 1 μL/min. Due to the relatively long sampling intervals (5-20 min) in typical practices of microdialysis, the temporal patterns are partially lost when relatively rapid fluctuations of neurotransmitters take place. When the HPLC analysis is performed offline, the temporal resolution can be improved by decreasing the separation system volume, i.e., using a capillary HPLC column. Newton and Justice demonstrated that 1 min time resolution was possible for microdialysis sampling of dopamine while a 500 μm ID column was used to analyze 0.5 or 1.0 μL microdialysate samples[13]. For online HPLC analysis, the separation speed must be at least as fast as the sampling time in order to achieve near real-time measurement. HPLC separation time can be reduced by optimizing HPLC system parameters, including particle size, system pressure and temperature[14].

Various detection methods can be coupled to HPLC for the analysis of microdialysates. Due to the sensitivity reasons, UV detection is rarely used unless the studied neurotransmitters exist in high concentration, e.g, glutamate, aspartate and GABA[15, 16]. Lately the mass spectrometry (MS) detection has gained popularity as this mode of detection has the advantage of providing additional structural information about the eluted compounds[17-21]. However, electrospray ionization (ESI) MS is not quantitative without using isotopically different standards. The expensive MS instrumentation is also not favorable for its wide application. Fluorescence (FL) detection is another detection method that has found applications in the investigation of neuroactive compounds in biological samples[5, 22, 23], but the utility of FL detection is determined by the availability of suitable fluorescent labels and derivatization requires multiple sample treatment steps[5].

With its high sensitivity and selectivity, electrochemical detection is the most widespread technique for detecting neurotransmitters following the HPLC separation. Electrochemical detection offers unique advantages for capillary column chromatography as it can be miniaturized without a loss in sensitivity because electrochemical reactions are surface reactions and the sensitivity does not depend on the flow cell volume under laminar flow condition which can easily be achieved in the small volume channel flow cell[24]. A number of neurotransmitters are electroactive, e.g., monoamines that can be directly detected at an oxidizing potential. Other neurotransmitters, on the other hand, are not electroactive, for example, some amino acids and neuropeptides. In this case, a derivatization technique/device is needed for electrochemical detection. The use of *o*-phthalaldehyde (OPA) in the presence of a thiol is perhaps the most popular derivatization chemistry for amino acid neurotransmitters. Sixteen amino acids in physiological samples, including all the neurotransmitter amino acids and neuromodulators, have

been successfully determined electrochemically through off-line derivatization with o-phthalaldehyde/tert-butyl thiol[25]. For peptides longer than dipeptides, the classical biuret reaction with Cu(II) yields electroactive Cu(II)-peptide complexes that can be oxidized to the corresponding Cu(III) complexes. The reaction chemistry, which is reversible, allows for the determination of peptides that lack an electroactive group or a primary amine[26]. In order to achieve online analysis of neurotransmitters, the derivatization has to be completed online via a flow reactor. The biggest concern is the additional peak broadening that occurs within the reactor, especially when coupled with capillary columns. Weber group developed a post-column flow reactor from microchannels formed in fluorinated ethylene propylene and fused-silica tubing, which operates in the Taylor dispersion regime and enables complete mixing of analyte and derivatization streams purely by diffusion. It has insignificant effects (i.e., <3%) on peak band spreading used with 100-μm-ID columns[27].

1.1 LOW-VOLUME ELECTROCHEMICAL FLOW CELL

1.1.1 Background

The performance of an HPLC system is affected by extra-column band spreading, especially for columns with a small internal diameter. Several published reports have identified extra-column effects as a major factor that negatively impacts HPLC performance[28-30]. The extra-column contributions to band spreading, both the volumetric σ_v^2 and time-related τ^2, such as the sampling rate and the detector time constant, have been analyzed in detail[31]. The detector volume, besides the injection volume and the volume of the connection tubing between the injector and detector,

can be a significant contribution to the volumetric extra-column band spreading. For a capillary HPLC system, the requirement on reducing the extra-column band spreading is especially critical due to the small peak variance inside the capillary column. Thus, the electrochemical detector volume has to be minimized in order to preserve the separation efficiency achieved in the chromatographic column.

Due to its extremely low dead volume, on-column electrochemical detection has been adopted by some research groups[32-35] for capillary separations, where a single carbon fiber is inserted into the outlet end of the capillary column as the working electrode by using a simple two-electrode arrangement. Figure 1.1[36] shows an optimized in-capillary detection scheme where the inside diameter of the capillary end is enlarged via HF etching and the carbon fiber electrode is inserted in the lumen of the capillary for detection[37, 38]. Using the on-column electrochemical detection with micellar electrokinetic capillary chromatography (MEKC), Ewing[39, 40] achieved the determination of biogenic amine variability among individual fly heads with enhanced sensitivity. Weber's lab used the in-capillary detection scheme combined with post-column biuret derivatization to detect non-electroactive peptides after capillary LC separation[27]. The carbon-fiber microelectrode was placed in a post-column flow reactor built with fluorinated ethylene propylene and fused-silica capillary tubing[27], which allows the post-column reaction to take place without adding significant peak band-spreading.

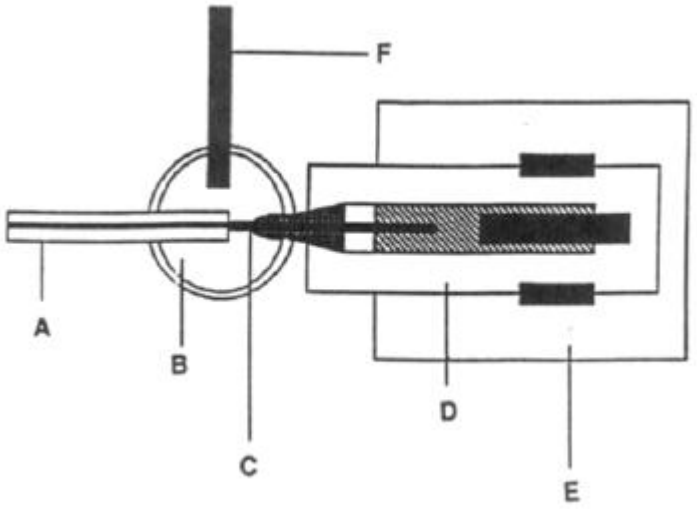

Figure 1.1 End-column amperometric detector: (A) separation capillary; (B) electrochemical cell; (C) carbon-fiber electrode; (D) electrode assembly; (E) micromanipulator; (F) SCE reference electrode. Reprinted with permission from[36]. Copyright 1993 American Chemical Society.

However, single fiber electrodes (several micrometers in diameter) are very fragile and require micro-positioning, not to mention their reproducibility problem and sensitivity to vibration. Thus, they are not ideal LC detectors which require robust design and reproducible electrode response[41]. A thin-layer electrochemical flow cell, on the other hand, provides more stable and reproducible electrochemical response. It also allows more complicated electrode designs, for example, multiple working electrodes, to enhance the detector performance. There are predominately two basic types of EC flow cells with different flow patterns: cross-flow and radial-flow (also called wall-jet). A thin layer of solution flows parallel to a planar electrode surface embedded in the flow channel in the case of cross-flow pattern; the eluent impinges directly upon the working electrode surface and flows away radially in the radial-flow pattern. These two types of flow cell are both commercially available from different manufacturers and

laboratory constructed for particular applications. A recent article reviewed developments in electrochemical flow detections for liquid chromatography in the past 15-20 years[42].

The large majority of reported studies for the determination of neuroactive compounds utilize commercially available electrochemical flow cell detectors for HPLC detection, because they are in general well optimized and continuously improved by manufacturers to compete in the market of analytical instruments [43]. However, most of these commercial electrochemical detectors are not compatible with capillary separation systems due to the inherent high dead volume: electrochemical detectors manufactured by Agilent Technologies and CH Instruments both have detection volume of 0.5 μL; Waters and Shimadzu only offer EC detectors with cell volumes of several microliters. The only commercial electrochemical flow cells that are compatible with capillary systems are UniJet from BASi and DECADE from Antec Leyden. They are both radial flow thin-layer cells and have been applied as the detector following capillary HPLC for the measurement of monoamine neurotransmitters in microdialysate samples[7, 8] and phenols in water samples[44].

1.1.2 Statement of the problem

The limited availability of electrochemical flow cell detectors that are compatible with capillary LC hampers its further application. As the main problem associated with a conventional electrochemical flow cell is its relatively large dead volume, a modification process to decrease cell volume can convert it into a capillary LC detector. Using a photoresist coating in replace of a free-standing polymer film as the spacer/gasket in the flow cell is an innovative method to decrease the flow cell volume. The flow channel volume can be easily reduced due to the conveniently controllable thickness and flexible flow channel shape through a standard

photolithographic process. This modification technique can be applied to electrochemical flow cell detectors of virtually any design for different application purposes. The fabrication, characterization and application of the photoresist flow cell will be demonstrated in detail.

1.2 ELECTRODE MATERIAL AND ITS SURFACE MODIFICATION

1.2.1 Background

Glassy carbon is the most commonly used working electrode material in chromatographic detection as it offers sufficient sensitivity for most applications and exhibits large range of available potentials with low background, high stability and resistance to passivation. Different forms of carbon, including carbon fiber, diamond, reticulated vitreous carbon and graphite, have also been used in various applications. Villalba *et al.* reviewed different carbon materials which have been applied in HPLC-electrochemical detection systems[46]. Carbon composite electrodes consist of two or more components where carbon materials, e.g., carbon particles, carbon nanotubes or carbon fibers, are bound together by a binder. Besides bulk electrodes, carbon film electrodes can also be integrated into the electrochemical flow systems.

Surface modification of carbon electrodes can increase the detection sensitivity and selectivity for measuring neuroactive compounds. Several methods[46, 47] have been utilized including polymer coating, carbon nanotube coating and chemical modification by adsorption or covalent binding. A melanin-type polymer-modified glassy-carbon electrode and graphite carbon electrodes showed sensitivities 3–5 times higher than bare-carbon electrodes and LODs at sub-micromolar levels for neurotransmitters, because of more efficient electron transfer and excellent

permselectivity of the melanin polymers[48]. Nafion is another common polymer coating that enhances the detection of monoamine neurotransmitters as it enhance the adsorption of amines and repels negatively-charged acidic metabolites[49, 50]. Using conductive nanomaterials, e.g., carbon nanotubes[51], to coat the carbon electrode improves sensitivity due to enhanced oxygen rich surface functional groups and subsequent electrocatalytic effect. Some chemicals, e.g., 4-sulfobenzene, have also been utilized to improve the electrode surface properties towards monoamine neurotransmitter detection due to the enhanced adsorption[52].

Metallic electrodes, most commonly platinum and gold electrodes, are also widely employed in amperometric detection in HPLC. Compared to carbon, gold electrodes have narrower electrochemical window because they are oxidized easily especially in alkaline solution. Besides, metallic electrodes tend to become fouled when used for the detection of biological samples. To expand its application for neuroactive compounds, for example, detection of neuropeptides through biuret reaction[53, 54], the electrochemical window has to be expanded. Self-assembled monolayer (SAM)[55] provides a way to control the chemical nature of the electrode solution interface. Although aliphatic thiol monolayers are the most commonly used system for SAM on gold, it essentially forms an insulation layers between the gold substrate and the adjacent electrolyte as the electron transfer through aliphatic thiol SAM occurs with tunneling mechanism. The electron transfer rate constant decays exponentially with the aliphatic chain length[56], which inhibits not only gold oxide formation but charge transfer with redox systems within the electrolyte as well. Aromatic thiol SAM, on the other hand, has higher electron transfer rate owing to the presence of delocalized π-electrons in the aromatic ring[57]. Moreover, when the mercapto group is directly attached to an aryl, the thiolate is less prone to oxidation under ambient conditions. Modification of Au surface with proper aromatic thiols can

essentially broaden the electrochemical window by suppressing Au surface oxide formation, while promoting the electron transfer of the electroactive species in the solution to the electrode.

Thin film metallic electrodes are convenient to fabricate through standard photolithography and sputtering techniques[58]. In a recent publication, Ogburn *et al.* demonstrated the fabrication of disposable electrochemical cell detector which consists of platinum working electrode, platinum auxiliary electrode, and silver/silver chloride coated on Pt reference electrode. However, problems with this detector include high limits of detection compared with those of a commercial electrochemical detector due to its high noise level and short lifetime due to the loss of Ag/AgCl coating during flow through experiments. Metallic electrodes, including gold, platinum, copper and palladium, are commonly used in microfabricated EC detectors due to the relative ease with which they can be evaporated or sputtered[59].

1.2.2 Statement of the problem

Although it provides sufficient sensitivity for most applications, glassy carbon electrode is hard and brittle which limits its available sizes and shapes. Carbon fiber/epoxy composite material, on the other hand, is much more flexible. Taking advantage of its commercial availability in various shapes and sizes, its use as electrode material should be favorable. For example, a ring-disk dual electrode with an ultra-thin gap can be fabricated with carbon fiber composite due to its flexible dimension. Metallic electrodes have limited application in biological sample analysis due to its narrow electrochemical window and tendency to fouling. Surface modification of aromatic thiols on gold electrode suppresses its background current which would otherwise interfere with amperometric detection of peptides and the modified gold electrode has sensitivity comparable to that of a glassy carbon electrode. The self assembled monolayer modification can be easily

applied to other metallic electrodes, e.g., Pt electrode, which will expand the application of metallic electrodes in biological samples.

1.3 DUAL OR MULTIPLE WORKING ELECTRODE ECD

1.3.1 Background

Increasing detection selectivity is always desired especially due to the fact that some neuroactive compounds can be present in complicated matrices with multiple coexisting interfering species. A dual or multiple working electrode detector with different designs, including dual microband or microdisk electrodes, ring-disk microelectrode and interdigitated microelectrode arrays (IDA)[60], can improve the selectivity of the detection. When operated in a generator-collector mode, i.e., electrogenerating a species at one of the electrodes and then collecting the product at the other electrode, a dual-electrode detector can discriminate analyte based on its reversibility. For example, the use of a series dual electrode amperometric detector (upstream anode, downstream cathode) for the selective detection of bioactive peptides has been demonstrated[54].

Collection efficiency is the ratio of the current passed at the downstream electrode to that passed at the upstream one. For a reversible species, the collection efficiency depends on the mass transfer rates, which are partly determined by the flow rate and the cell geometry. When a homogeneous reaction takes place involving the species produced at the generator, the collection efficiency is also dependent on the rate constant of the homogeneous reaction and can be simulated through theoretical modeling[61].

Different designs of dual or multiple working electrodes have been reported with an emphasis to increase the collection efficiency. Use of interdigitated array electrode can effectively improve collection efficiency due to two reasons: the gap between electrodes can be reduced to 1-2 micrometers or less using lithographic technique; the array configuration with low flow rate generates repeated redox cycling between oxidised and reduced states thus improve collection efficiency as well as sensitivity[46]. Carbon film based interdigitated ring array in a thin-layer radial flow electrochemical detector enhances the epinephrine and dopamine signals with a collection efficiency of 83% for dopamine[62]. The collection efficiency for dopamine reaches above 80% on a gold IDA (eight pairs), where both the band electrodes and the gaps are 2 μm in width[63, 64].

1.3.2 Statement of the problem

Dual electrode detector used in conventional LC is not suitable for capillary LC because the relatively large gap between the generator electrode and the collector electrode leads to unfavorable collection efficiency with the inherent low flow rate of capillary LC. Although microfabricated interdigitated array electrodes can improve the collection efficiency, these electrodes are not polishable and are electrochemically less well defined compared to solid electrodes. In addition, microfabrication involves complicated procedures and expensive equipments (vapor deposition, micromachining, etc.), which may not be accessible to most research laboratories. Thus, a dual-electrode based on solid electrode that can be readily applied to commercial electrochemical detectors is preferred. Due to the flexibility of carbon composite material, a ring-disk dual electrode with minimal gap can be fabricated.

1.4 RESEARCH OVERVIEW

HPLC-electrochemical detection following microdialysis sampling is the most widely adopted analysis method for neurotransmitter measurements due to its versatility, high sensitivity and selectivity. In order to preserve the separation efficiency achieved in a capillary LC column, electrochemical detector has to be optimized. Also, due to the low abundance and complexity nature of biological samples, increasing detection sensitivity and selectivity is always desired. Chapter 2.0 describes the design and fabrication of a miniaturized electrochemical flow cell that is compatible with capillary columns. By utilizing a novel photosensitive polymer material, a flow channel is achieved with easily controllable thickness in the μm range. The photosensitive polymer acts as a spacer/gasket in a sandwiched flow cell, which defines the flow channel and helps to hold the pieces together upon the pressure during assembling. Detailed characterization of its mechanical properties shows the photoresist material possess adequate mechanical strength to withstand the stresses and strains that occur during assembly and usage. With the ultra-thin flow channel, the detector is capable of preserving separation efficiency achieved in the capillary column.

In Chapter 3.0, a commercially available and very economical material – carbon fiber/epoxy composite is used as a novel electrode material. A dual working electrode set-up increases detection selectivity based on the difference in electrochemical reversibility of analytes. Collection efficiency is crucial to the performance of a dual electrode detector, which is determined mainly by the gap/distance between the two electrodes. A ring–disk electrode with an ultra-thin gap (20 μm) between the ring and the disk is successfully fabricated using tube and rod carbon fiber composites through a unique two-step insulation-adhesion process. This composite ring–disk electrode is assembled in a thin-layer radial-flow cell and used as an electrochemical

detector with the disk electrode as a generator electrode and the ring electrode as a collector. This electrode, combined with a miniaturized electrochemical flow cell, is proved to achieve collection efficiency of 80% for an electrochemically reversible species.

Chapter 4.0 explores the possibility of using gold as the electrode material for the detection of biological samples. The problem associated with its narrow electrochemical window due to gold oxidation/reduction is solved by the surface modification with a self-assembled naphthalenethiol monolayer, which suppresses the background current from Au while giving detectable current. Thus, we can take advantage of the easy fabrication of gold electrode in a micro-fluidic device and expand its application.

Chapter 5.0 investigates the application of an optimized capillary HPLC-electrochemical detection system in the analysis of serotonin in microdialysate samples. Not only does the use of capillary column reduce the sample amount requirement, the separation of serotonin is also accelerated to within one minute through the use of high pressure and elevated temperature. The optimized capillary HPLC-electrochemical detection system can be coupled on-line with microdialysis for near real-time analysis of neurotransmitters.

2.0 OPTIMIZATION OF AN ELECTROCHEMICAL FLOW CHANNEL FOR CAPILLARY LC USING A NOVEL PHOTOSENSITIVE POLYMER COATING

2.1 INTRODUCTION

HPLC separation coupled with electrochemical detection is a very effective method to analyze bioactive compounds because of the selectivity and sensitivity of an electrochemical detector. A small ID HPLC column is advantageous in handling samples with limited volume and increasing separation efficiency, which is especially important in some biological systems, e.g., cerebrospinal fluid (CSF) and extracellular fluid of the brain tissue. Capillary LC and microbore HPLC are also attractive in that consumption of the mobile phase is dramatically reduced. With the decrease of the column size, flow-rates in capillary LC are reduced to a typical range of 0.5 - 5 μL/min, which leads to a smaller peak volume. The peak volume is in the range of microliters for a microcolumn, depending on system parameters (e.g., separation efficiency, capillary diameter and length). To maintain the inherent separation efficiency, the extra-column peak broadening must not exceed a certain percentage of the column peak broadening. If the observed peak is allowed to have a volume 10% greater than the column peak volume, the extra-column peak volume should be less than one-half (ca. 46%) of the column peak volume[65].

Because of the stringent requirements for negligible post-column effect in a capillary separation system, on-column electrochemical detection has been widely used in capillary LC

and capillary electrophoresis due to its extremely low dead volume. Several research groups[32, 33] have advanced the use of a single carbon fiber electrode as the working electrode inserted into the outlet end of the capillary by using a simple two-electrode arrangement. However, single fiber electrodes (several micrometers in diameter) are very fragile and require micro-positioning, not to mention their reproducibility problem and sensitivity to vibration. Thus, they are not ideal LC detectors which require robust design and reproducible electrode response[41]. The conventional thin-layer flow-through electrochemical detectors are robust during both handling and operating, and provide stable and reproducible electrochemical response as it uses a three-electrode[66] (working electrode, auxiliary electrode and reference electrode) system. They also allow more complicated electrode designs to enhance the detector performance. For example, a dual-working electrode detector is more desirable than a single working electrode detector in some applications, because it offers such benefits as selectivity improvement and signal enhancement in generation-collection measurements[9]. However, such a design would involve extremely complicated fabrication procedures for an on-column carbon fiber detector[67].

To take advantage of the robustness, convenience, and versatility that a commercial electrochemical detector offers, one needs to modify the flow cell to make it applicable for capillary systems. The main problem associated with utilizing a conventional thin-layer flow cell for micro or capillary column LC detection is its relatively large dead volume; a typical electrochemical cell designed for use with conventional HPLC columns has approximately 2-μL volume[68]. Hirata *et al.* successfully modified a commercial electrochemical detector and reduced the flow cell volume to 0.1 μL[68] and applied it for capillary columns. Even though their chromatograms were several hours long and peaks were many minutes wide, which is not

acceptable for current separation purposes, their experiment demonstrated the validity of utilizing a miniaturized flow cell for capillary separations.

The flow cell volume is defined by the spacer sandwiched between two blocks, which house the flow inlet/outlet and the electrodes (working electrode, auxiliary electrode and reference electrode). An open pattern in the spacer should encompass the inlet/outlet openings and the working electrode(s) when aligned within the opposing blocks. The auxiliary electrode and reference electrode can be placed either opposite to the working electrode or in a downstream compartment. The flow cell volume equals the inner area of the spacer times the thickness of the spacer. Therefore, in order to reduce the flow cell volume, the dimensions of the spacer have to be minimized. The spacer in an electrochemical flow cell is usually made from polymer materials, e.g., polytetrafluoroethylene (PTFE or Teflon), polyethylene (PE). Fabricating a small flow cell involves using a thin polymer film. However, in practice, it is very difficult to create a small open pattern in a polymer film with low micrometer thickness and align the spacer in the flow cell.

Because the desired channel volume is in the nanoliters range, micro-fabrication techniques which have been utilized for microfluidic devices[69, 70] are suitable to achieve the appropriate dimensions. Photosensitive polymer, also known as photoresist, is heavily used in various micro-fabrication applications, including printed circuit board (PCB) and microelectromechanical systems (MEMS). By shining light, usually at wavelengths in the ultraviolet spectrum, to a photoresist covered with a photomask, a geometric pattern can be transferred from the mask to the photosensitive coating. Photoresist can be coated on surfaces through different methods, dry film, spin-coating and electrodepostion. Electrodeposited (ED) photoresist is a good way to form a homogenous coating on an electrically conductive surface

and can be used for coating objects of various sizes and shapes because of its electrochemical nature. For example, ED photoresist has been used in our laboratory to coat and insulate carbon fiber microelectrode with controllable electrochemically active area.[71] ED photoresist also has superior adhesion to the substrate compared to spin-coating and dry film.[72] In most micro-fabrication processes, the photoresist is used as a sacrificial layer, where the material serves as a temporary "placeholder" and defines the geometry. The pattern is later engraved into the material underneath the photoresist through a series of chemical treatments, e.g., dry/wet etching. The photoresist is subsequently dissolved or stripped away. However, if it demonstrates good chemical and mechanical resistance, the photoresist material itself can be used as a vital structural component of a device. For example, a microchannel has been created on SU-8, a popular epoxy-based photoresist, which also acts as a microfluidic substrate[73].

In the current study, a photoresist film with the flow channel is used in replace of a free-standing spacer in the electrochemical flow cell detector. The photoresist coating is formed on one half of the flow cell through electrodeposition. A fluidic channel is then created on the photoresist coating through a standard photolithography process. The photoresist material is tough, chemically stable, tack-free and durable, with excellent adhesion to the underlying substrate. Compared to a free-standing polymer spacer, the photoresist spacer offers a conveniently controllable thickness and flexible flow channel design as it is created through a photolithography process. It also eliminates the technical difficulty in physically aligning the free-standing spacer with the flow inlet/outlet and the electrodes in the flow cell. To ensure its application as a structural component in the flow cell, the topographical, mechanical and thermal properties of the photoresist are characterized. The performance of the electrochemical flow cell detector using the photoresist spacer is tested and compared with that of a free-standing polymer

spacer. With the flexibility of flow channel fabrication using photosensitive polymer coating, optimization of the flow cell detector is made easier. Using theoretical simulation, the electrochemical process can be visualized and the effect of detector parameters, for example, gasket thickness and electrode dimensions, on the detector performance can be predicted.

2.2 EXPERIMENTAL

2.2.1 Chemicals and materials

The reagents used were as follows: Acetonitrile (ACN), HPLC grade, (Fisher, Springfield, NJ); disodium EDTA: Fisher Scientific (Fairlawn, NJ); sodium perchlorate: GFS Chemicals (Columbus, OH); sodium acetate: MCB (Cincinnati, Ohio); isopropanol, trifluoroacetic acid (TFA), sodium 1-octanesulfonate (SOS), serotonin hydrochloride, Sigma (St. Louis, MO); Na_2CO_3, $NaHCO_3$ (EM Science, Gibbstown, NJ); des-Tyr-Leu-enkephalin (GGFL), (Bachem, Torrance, CA); copper sulfate pentahydrate (J.T. Baker, Phillipsburg, NJ) was recrystallized once from water and disodium tartrate dehydrate (Baker) was recrystallized from diluted NaOH; all the other chemicals were of analytical reagent grade purity and were used as received. The aqueous solutions were made with 18 MΩ purified water from a Millipore synthesis A10 system (Millipore, Billerica, MA).

The product name of the photoresist is ElectroImage Plus ED Photoresist bath, product code EIV-50006, and was generously donated by PPG industry (Pittsburgh, PA).

2.2.2 Fabrication of the photoresist spacer

The received photoresist is a milky suspension. Before electrodeposition, the suspension was ultra-filtered for purification purposes. The ultra-filtration was performed according to the manufacturer's instruction: 1) shake to suspend solids; 2) add 68 parts of deionized water to 32 parts slurry and call this volume V; 3) add 50 more parts of water to yield 1.5V; 4) ultra-filter with Ultracel-30 k centrifugal filter devices (Millipore, Billerica, MA) until the total volume of filtrate passed is 1.5V; 5) discard the filtrate and resuspend the solids to give the original volume V. The final suspension was stored in a nontransparent container at room temperature. The ultra-filtration step is essential as impurity in the solution alters the pH value and might cause defect in the coating. The electrodeposition was performed in a jacketed beaker (Chemglass, Vineland, NJ) to control the bath temperature. A stainless steel net acted as the counter electrode. The photoresist was electrodeposited for 60 s at -3.25 V onto the target object using controlled potential electrolysis with an Epsilon-EC potentiostat (Bioanalytical Systems, Inc., West Lafayette, IN). The coated object was rinsed with Mill-Q water and then allowed to cure at 120 °C for 1 hour. The photoresist and the coated object were protected from light exposure during these processes.

The equipment for light exposure process is similar to the previous report[71]. A mercury-doped xenon arc lamp (Oriel, Stratford, CT) was used as the light source due to its high output in the UV wavelength range, 320-380 nm, which was required to remove the photoresist. The photo mask was a piece of bronze sheet with desired patterns that were mechanically carved out to allow light to shine through. The photoresist-coated object was covered with the photo mask and exposed to the UV light. Exposure times varied. Following light exposure, the coated object was placed in the developing solution, an aqueous solution of 2% 2-butoxyethanol and 1% lactic

acid, for 30 seconds. The object was rinsed with Milli-Q water and allowed to dry before repeating the exposure and development steps if desired.

2.2.3 Characterization instrumentations

The instrumentations used for characterizing photoresist film properties are listed as follows.

The photoresist film thickness was measured on an Alpha-Step IQ stylus-based surface profiler (KLA Tencor Corporation, Milpitas, CA), which measures surface roughness over short distances with up to 0.1-nm resolution. Scanning electron microscopy (SEM) images were obtained using a Philips XL-30 field emission scanning electron microscope and the samples were sputter coated with Pd before SEM. Atomic force microscopy (AFM) images were obtained on a NanoScope™ system (Veeco Instruments, Plainview, NY). Nanoindentation experiments were carried out on a TriboIndenter (Hysitron, Minneapolis, MN). Dynamic mechanical analysis (DMA) was done on a DMA Q800 system (TA Instruments, Newcastle, DE). Thermogravimetry analysis (TGA) was measured on a TGA Q500 system (TA Instruments, Newcastle, DE).

2.2.4 Capillary liquid chromatography

The capillary HPLC system was described in a previous publication[9] and is briefly summarized as follows.

The mobile phase (0.1% TFA, 3% 1-propanol, 23% acetonitrile) was pumped through a homemade capillary column slurry packed with 3.2-μm C18 reversed-phase particles. A Waters 600 E quaternary pump with a simple tee as a flow splitter delivered mobile phase at 1 μL/min. The injected sample was 2-μL 1-μM peptide GGFL in 0.1% TFA aqueous solution. The

chromatographic eluent was mixed with the biuret reagent (0.24 M carbonate buffer, 12 mM disodium tartrate, and 2.0 mM copper sulfate, pH 9.8) in a homemade Y-shape post column reactor. The post column reaction derivatizes peptides and produces electroactive Cu(II)-peptide, which makes peptides electrochemically detectable.

2.2.5 Electrochemical flow cell

The electrochemical detector was composed of a BASi cross-flow or radial-flow thin-layer auxiliary electrode, a spacer and a homemade glassy carbon electrode block (1 mm diameter single electrode or two 1 mm diameter dual-electrode). The auxiliary electrode is a stainless steel block which contains flow inlet/outlet and a compartment for the reference electrode, which is Ag/AgCl (BASi). The spacer is either a Teflon film or a photoresist coating deposited on the auxiliary electrode, as described on Section 3.2.2. The electrode block was polished with 0.05 μm alumina slurry and sonicated in DI water before being assembled in the flow cell. The pieces are held together by four bolts on the corners. The applied potential was +0.6 V, and +0.05 V at the downstream electrode in the dual-electrode configuration. The potential was controlled by a BASi Epsilon potentiostat. All stated potentials were referred to the Ag/AgCl reference electrode.

2.2.6 Homogenate sample preparation

The procedures to prepare rat brain slice homogenate were described in detail before[74]. Briefly, organotypic slice cultures of the hippocampus were prepared from the brains of six-day-old rats. The slices were transferred to pre-cooled Eppendorf tubes and snap frozen in liquid nitrogen. To

homogenize the tissue, 90% methanol in water (250 µL for four slices) was added and the tube was placed in an ice-bath and sonicated using Microso Ultrasonic cell disruptor XL 2000. To avoid overheating, the sample was sonicated for 3 seconds, and then allowed to cool down for 10 seconds. The procedure was repeated for about 5 times or until the whole solution turned opaque and there was no solid left. After storage at -20 ºC overnight, the tubes were centrifuged at 11000 g using Jouan Centrifuger A-12 for 3 minutes. The supernatant was removed and filtered with 0.22 µm syringe filters (Millipore, Billerica, MA). Finally, the methanol was evaporated to dryness in a speed vacuum. 0.1 % TFA aqueous solution was added to the sample and vortexed for analysis.

2.2.7 Theoretical simulation

Two pre-defined numerical models in Comsol Multiphysics 3.3 were used for simulation: fluid dynamics as well as convection and diffusion. For simplicity purposes, the flow channel was modeled as a two dimensional rectangular and the simulation was steady-state, i.e., the flow through the channel was a solution with constant concentration of analyte, providing the simplest convective diffusion regime. The flow rate was set at 1 µL/min and the corresponding linear velocity depends on the channel geometry. The channel exit was set as convective flux and all the other boundaries were set as insulator. Diffusion coefficient $D_A = D_B = 5 \times 10^{-10}$ m^2/s. The electrochemical reaction was $A - e \rightarrow B$ on the upstream electrode; $B + e \rightarrow A$ on the downstream electrode. In the case where there is chemical reaction following the upstream electrochemical reaction: $B \rightarrow C$, the reaction rate $R = k \times c = 10 s^{-1} \times c$.

2.3 RESULT AND DISCUSSION

2.3.1 Optimization of the electrochemical flow cell detector

The thin-layer flow cell detector is adapted from a commercial electrochemical detector (Figure 2.1), which is composed of an auxiliary electrode piece, a reference electrode, a gasket and a glassy carbon working electrode block. The auxiliary electrode piece includes flow inlet/outlet and an opening in the center to connect to the reference electrode compartment. The working electrode block contains either one glassy carbon electrode or two adjacent electrodes in the dual-working electrode mode. As the original flow cell detector is designed for conventional HPLC columns, several modifications are required to make it compatible with capillary columns: 1) Teflon tubing sleeves together with PEEK fittings are used to connect a capillary to the flow cell inlet/outlet; 2) the 3-mm-diameter glassy carbon electrode is replaced with homemade 1-mm-diameter electrode as the electrode area affects the detector performance[12] and a smaller electrode gives better signal to noise ratio when the flow rates are in the low μL/min range; 3) as it has a relatively wide flow channel to accommodate the dual series crossflow pattern (Figure 2.1), the original gasket contributes significantly to the post-column bandspreading which is detrimental for a capillary HPLC system. In order to reduce the flow cell volume, we carve out a narrower flow channel on a Teflon film to replace the original gasket. The new flow channel is rectangular which is 1 mm wide and 1 cm long and the Teflon film has various thicknesses, i.e., 45 μm, 22 μm, 12 μm and 6 μm.

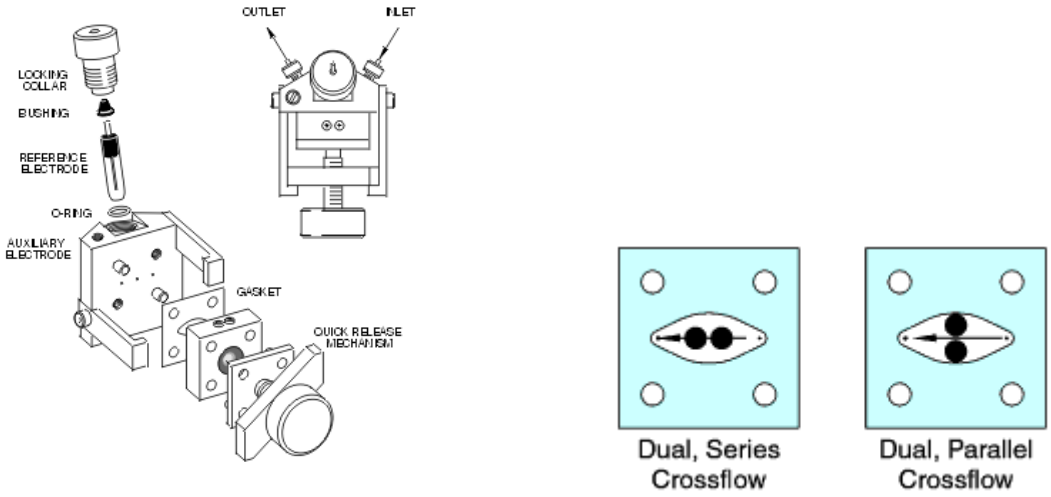

Figure 2.1 Diagram of a BAS thin-layer flow cell. Reprinted from http://www.basinc.com/products/ec/flowcells.php with permission.

Gasket thickness affects the detector performance in a capillary HPLC system. Figure 2.2 shows the chromatograms of des-tyr leu-enkephalin (GGFL) under the same chromatograph conditions with different gasket thickness. The dependence of detector performance on the gasket thickness is summarized in Table 2.1, except for the 6-μm gasket. There is no detectable peak current with the 6-μm thick gasket, because the flow cell detector cannot be properly aligned with this extremely thin gasket. There is possible leakage resulting from bad alignment, which prevents the flow cell from functioning properly. Several parameters are listed on Table 2.1, showing the effect of gasket thickness, including the peak retention time, peak height/area and collection efficiency in a dual-electrode configuration. The retention time is longer with a thicker gasket. Because the chromatograms are collected at the same volume flow rate, the linear flow velocity is lower when the gasket is thicker. So it takes longer time for the analyte to get to the electrode with a thicker gasket. The peak current also shows dependence on the gasket thickness, as it is a function of the flow linear velocity. Although equations relating current and solution velocity have been theoretically derived[75-77], the relationship is more complicated in

practical scenarios. For example, most research work showed that the current output is dependent on the cube root of the linear velocity across the electrode surface; however, this equation is only valid when the coulometric yield of the cell is less than 10%[78]. With the low flow rate involved in capillary LC system, higher values of coulometric yield are often encountered and a more complex behavior is then observed[79]. In addition, there is possibility that the two diffusion layer of working and auxiliary electrodes may overlap and become "coupled"[80] when the gasket is sufficiently thin. So it is possible that the oxidative product on the working electrode may be reduced on the auxiliary electrode and diffused back to the working electrode. Although we cannot provide the exact equation relating the peak current and flow velocity due to these complications, a lower flow velocity will lead to smaller peak height/area, which explains why the current response on a 45-μm gasket is lower than that on a 22-μm gasket. The fact that we observe lower current response with a 12-μm gasket than a 22-μm gasket is also related to difficulty in proper flow cell alignment with a thin gasket. The collection efficiency is calculated as the ratio of the cathode peak current to the anode peak current, which stands for the fraction of upstream products that are converted at the downstream detector. With thicker gasket, the linear velocity is lower, so a larger fraction of the species produced on the upstream electrode will diffuse away before they get to the downstream electrode which leads to a lower collection efficiency. From the results obtained on flow cell detector with different gasket thickness, it is evident that thinner gasket improves detector performance. However, a thin (<22 μm) free standing gasket film is difficult to assemble in a flow cell which limits its application. Using a photosensitive polymer coating as the gasket, on the other hand, will eliminate the technical difficulty in physical alignment and ensure the detector performance.

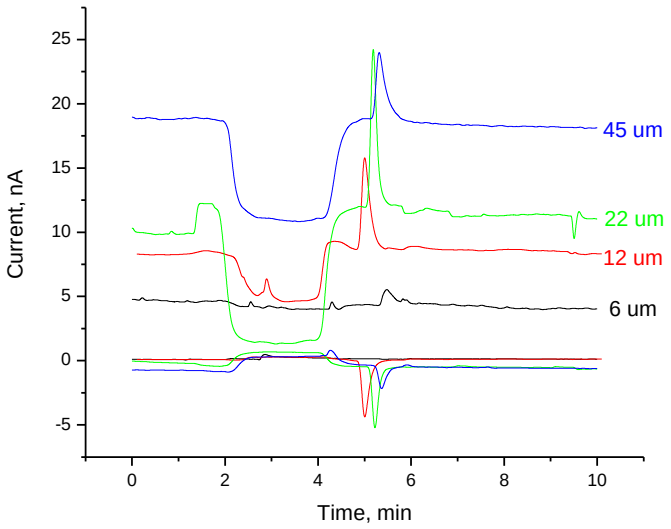

Figure 2.2 The chromatograms of 1 µM GGFL with different gasket thickness

Table 2.1 Influence of the gasket thickness on the cell performance

Gasket thickness (µm)	Retention time (min)	Anode peak current (nA)	Anode peak area (nC)	Cathode peak current(nA)	Cathode peak area (nC)	Sensitivity on anode (nC/pmol)	Collection efficiency
12	5.00	7.1	87	4.4	50	51	0.57
22	5.16	9.4	116	4.6	52	67	0.45
45	5.29	6.1	75	1.8	21	42	0.28

2.3.2 Fabrication of a photoresist spacer in a flow cell and its surface topography

The ED photoresist used in this study is a cathodic photoresist, which is an aqueous emulsion. Under the influence of a suitable electric field, the positively charged micelles migrate electrophoretically toward the cathode - the substrate to be coated. At the same time, the electrolysis of water occurs, generating hydrogen and hydroxide ions at the cathode and oxygen and hydrogen ions at the anode. The micelles reach the electrode and begin to coalesce. Finally they precipitate and form a film on the substrate.[81] As more micelles arrive at the electrode, the resist film grows in thickness and becomes increasingly insulating until further deposition

ceases. This is a self-terminating process as the electrode surface turns insulative. The current vs. time curve (Figure 2.3) demonstrates the deposition process. The deposition current dropped sharply in the first 20 seconds, past which time it started to stabilize and decreased at a very slow rate. The reason why the current did not drop to zero can be explained by the unique structure of the substrate, which is the BASi auxiliary electrode block. The auxiliary electrode block contains deep channels, which are 0.7 millimeter in diameter and several centimeters in length, to house flow inlet and outlet. Coating the inner surfaces of these long and narrow channels is a slow process due to the limited diffusion. However, the surface coating is considered complete when the current starts to decrease at a negligible rate.

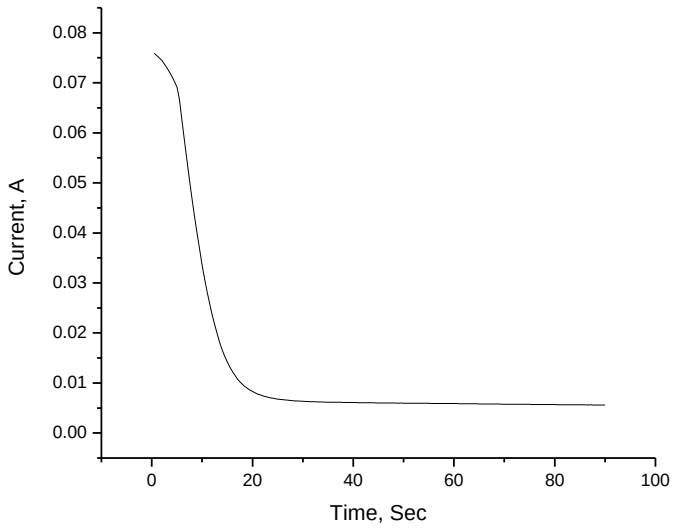

Figure 2.3 Current vs time for the electrodeposition of the photoresist. Applied potential: -3.25 V; Bath temperature: 25 °C.

The photoresist used is positive-acting, implying that irradiation by UV light will cause the exposed part to be solubilized and washed away. A photo-mask with the desired flow channel features is used to cover the photoresist surface during the UV light (range 320-380 nm) exposure; subsequently, the exposed photoresist reacts and becomes soluble in development

solution. Figure 2.4 is an example of the photoresist coating with flow channel, the shape of which is defined by the photomask and is identical with that on the free standing Teflon gasket in Section 2.3.1. The thickness of the deposited photoresist film determines the thickness of the spacer in the flow cell which is related to the cell volume. The photoresist thickness can be controlled by altering the photoresist bath recipe and the experiment conditions, for example, temperature, voltage, etc. The formulation of the photoresist bath, solvent/precipitant ratio, solid content, pH of the medium, has already been optimized by the manufacture to achieve the best coating: tough, durable and tack-free. Therefore, manipulating the deposition conditions is a better method to adjust the film thickness. It is found that temperature is especially efficient in controlling the thickness. The photoresist film thickness is quantified by a profilometer, which can measure surface variations in vertical stylus displacement as a function of position. The diamond stylus is moved laterally across the flow channel to quantify the step height. Figure 2.5 shows the dependence of step height, i.e., film thickness, on deposition temperature. The thickness of the film is 11.0 μm, 4.5 μm and 1.8 μm at deposition temperature 25 °C, 30 °C and 35 °C, respectively.

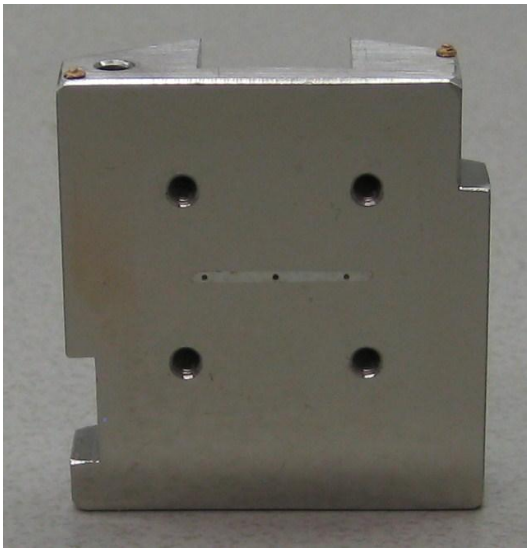

Figure 2.4 A flow channel created on the photoresist film that has been coated on the surface of a flow cell piece.

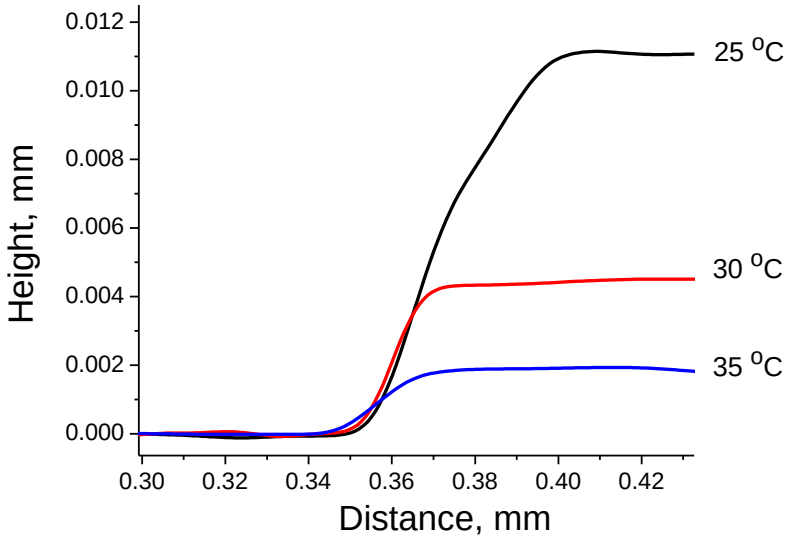

Figure 2.5 The thickness of the deposited photoresist film, measured through surface profiling the channel step height, depends on the deposition temperature.

Besides the profilometric characterization of the film thickness, scanning electron microscopy (SEM) and atomic force microscopy (AFM) are used to provide visual images of the photoresist film surface characteristics. Figure 2.6 shows typical SEM images of the photoresist

film surface, which shows a smooth surface without any visible scratches and defects. However, SEM has limitations in defining three-dimensional surface topography because the electron beam techniques, which relies on the different emission of electrons, cannot give contrast on flat homogeneous surface materials.[82] AFM (Figure 2.7) characterizes the topography of the patterned photoresist surface, which shows both the steel substrate and the photoresist coating. Although the photoresist coating is still relatively smooth judging from the AFM image, it is visible that the surface irregularities of the substrate, e.g, scratches and dents, are also present on the coating. This is due to the fact that the film is fabricated through electrodeposition and the surface features of the substrate will be transferred to the coating. Because the flow cell is a sandwich structure, the smoothness of the surface affects the assembling result. Poor assembly might induce leakage and unstable electrochemical responses in the electrochemical flow cell detector. Thus, both the stainless steel auxiliary electrode block and the working electrode need to be polished well to ensure good performance of the flow cell. The thickness of the photoresist film can also be measured from the AFM characterization, which agrees well with the surface profilometric measurements.

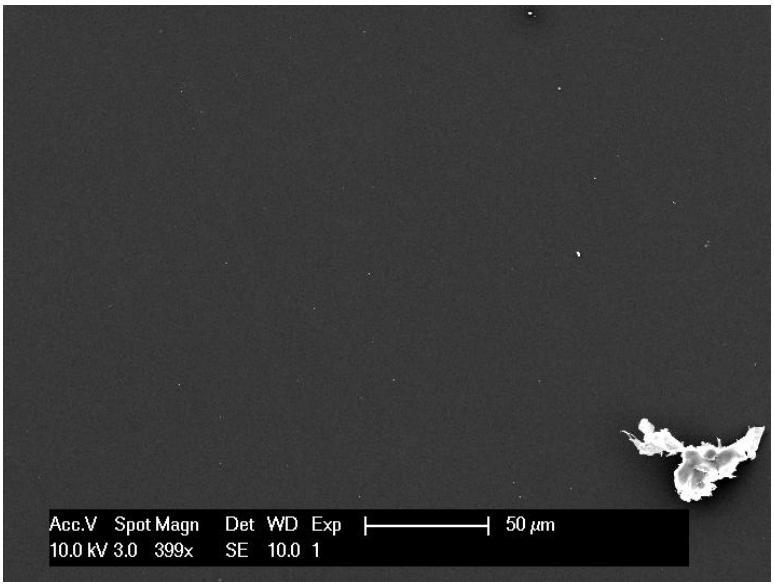

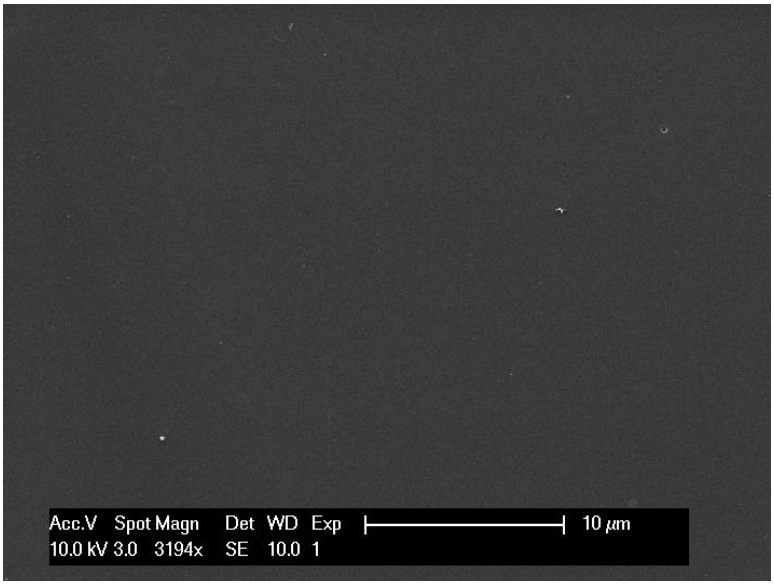

Figure 2.6 SEM images of the photoresist film surface with two different magnification scales.

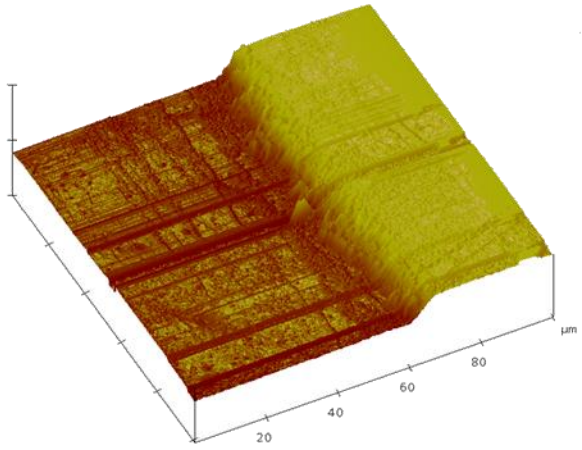

Figure 2.7 Three dimensional AFM image of a photoresist film deposited at 35 °C

2.3.3 Characterization of the mechanical properties of the photoresist film

As a light-sensitive material, the photoresist is often used to transfer the geometric pattern to the underneath material and later stripped away. Because it is not present in the final device, properties of photoresist, other than its photosensitivity, are rarely mentioned in the literature. On the other hand, the properties of photoreist can be very different from those of a model polymer

because of its complex resist formulation, which is a blend of polymer with grafted functionalities to provide etch resistance, solubility switch, adhesion, etc., as well as photoactive compounds and various additives.[83] In the current application, the photoresist material is not only used for its photosensitivity to construct the desired flow channel pattern, but also functions as a structural component in the flow cell. It acts as a spacer/gasket in a sandwiched flow cell, which defines the flow channel and helps to hold the pieces together upon the pressure during assembling. Therefore, the photoresist material must possess adequate mechanical strength to withstand the stresses and strains that occur during assembly and usage.

The mechanical properties of the photoresist film that are most relevant to its application as a spacer/gasket include elastic modulus and hardness. The elastic modulus of materials, also called Young's modulus, describes the material stiffness at small strains, which quantifies the resistance of the material to reversible deformation.[84] The surface hardness of a coating is a measure of its resistance to localized deformation, including reversible and irreversible, and is often used as an indicator of the wear properties. Two methods are used to measure the mechanical properties of the photoresist: depth-sensing indentation (DSI) and dynamic mechanical analysis (DMA). The two techniques are complementary as the indentation measurements can be performed on the photoresist coating, while DMA measures the properties of the photoresist as a free-standing polymer film. In addition, because of the viscoelastic nature of polymers, the dynamic mechanical method is capable of detecting changes in the modulus of a polymeric system and thus measuring the dynamic properties, e.g., glass transition temperature.

2.3.3.1 Depth-sensing indentation (DSI) method – photoresist coating

Depth-sensing indentation is an experimental method to characterize the hardness and elastic modulus of a material from measuring the load applied on a rigid probe and the displacement of

that probe into the surface of the material under investigation simultaneously.[85] DSI is a very suitable technique in the field of thin-film or coating technology, as the properties of the coating can be measured without the need to be peeled from the substrate. Figure 2.8A is a typical load-displacement curve obtained during one cycle of loading and unloading on the photoresist film coated on a steel substrate. The loading function (load vs. time) is shown on Figure 2.8B. After the removal of the indentation impact, there is an impression left on the surface which reflects the shape of the indentation tip (Figure 2.8C). The elastic modulus and hardness values can be derived using Oliver-Pharr method:[85] deformation during loading is assumed to be both elastic and plastic in nature as the permanent hardness impression forms; during unloading, it is assumed that only the elastic displacements are recovered. The hardness H, by definition, is obtained through dividing the peak indentation load P_{max} by the projected area of the impression under pressure A, which can be calculated from h_{max} combined with the knowledge of the indenter probe geometry. Measurement of the reduced elastic modulus E_r follows from its relationship to contact area A and the measured unloading stiffness ($S = dP/dh$) through the relation: $S = \beta \frac{2}{\sqrt{\pi}} E_r \sqrt{A}$, where β is a dimensionless constant. Young's modulus of the specimen is further derived from the reduced elastic modulus taking into account of the mechanical properties of the indenter probe.[84] Because the diamond indenter is much stiffer than the polymer sample and can be modeled as a rigid body, the reduced elastic modulus can therefore be treated as Young's modulus.

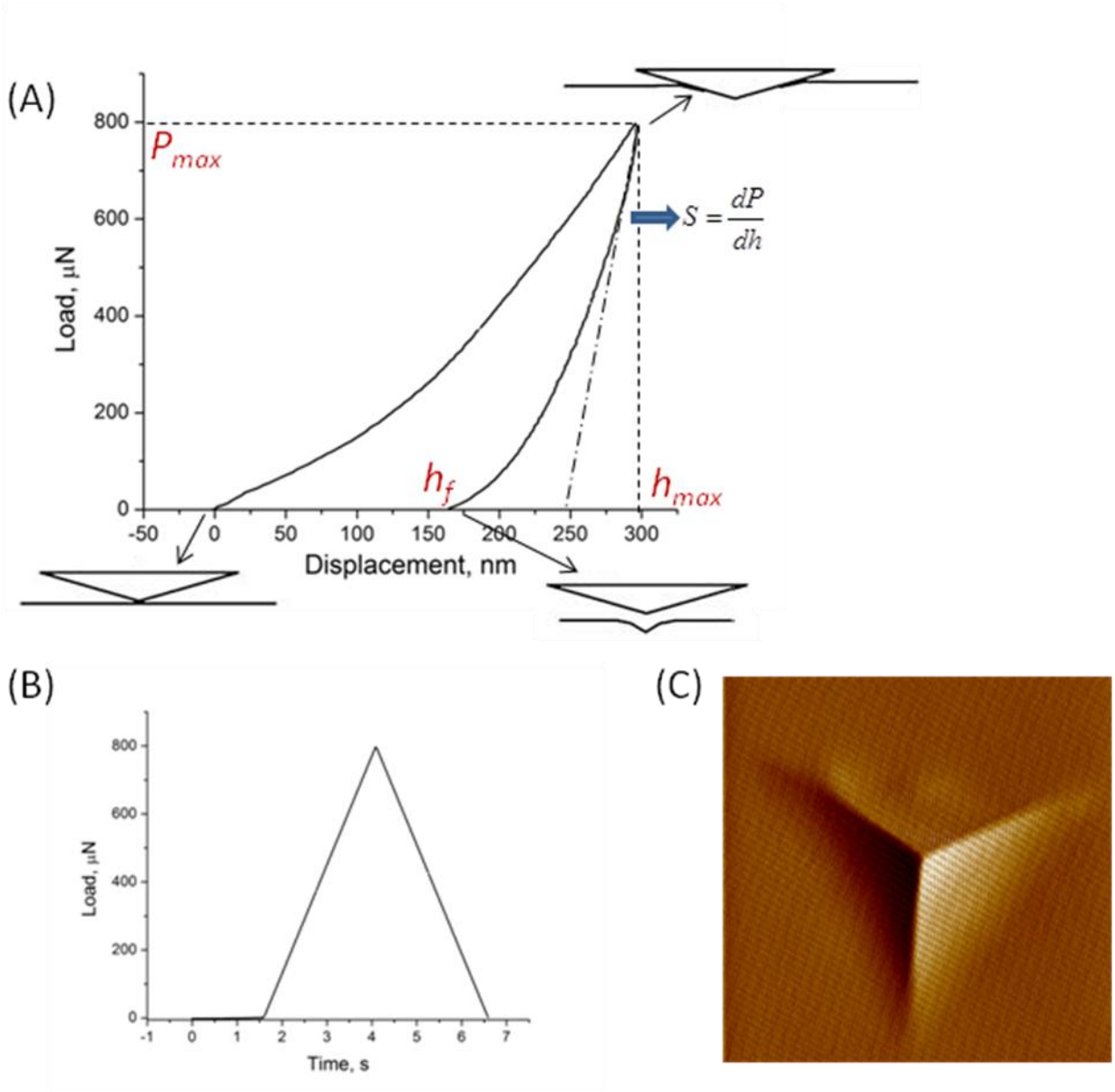

Figure 2.8 (A) A typical loading-displacement curve in a nanoindentation experiment; (B) a triangle shape loading function; (C) a post-indentation image of the surface.

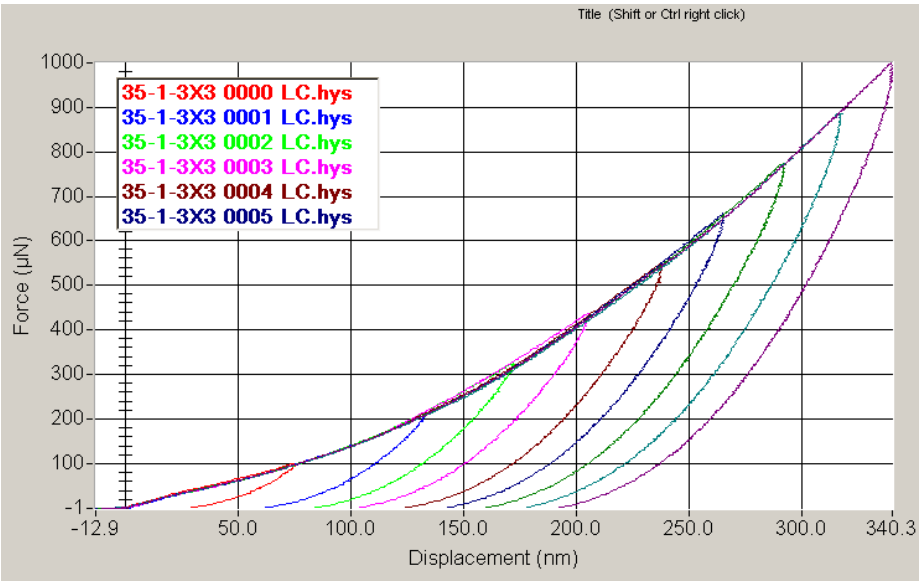

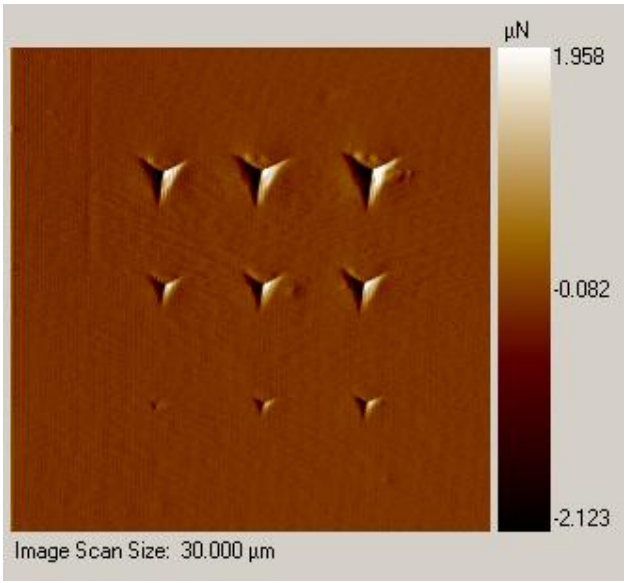

Figure 2.9 The loading and unloading curves of the indentation on the photoresist film deposited on the steel substrate.

Previous investigations have shown that indentation hardness and elasticity values are often a function of the imposed contact conditions, such as the peak load or penetration depth, the loading rate and the operating temperature.[86] This dependence is especially substantial for a polymeric coating system, due to the possible substrate effect and the viscoelastic–plastic response of these materials. Sequences of indentation tests were conducted by a 3x3 matrix, each

spot separated by 5 μm, to test the reproducibility of the experiment and the effect of the experimental parameters. Figure 2.9 shows the superimposed loading and unloading curves of the photoresist film deposited on a steel substrate. The loading/rising data with different peak loads can be fitted by one curve which shows that the sample is homogeneous and have a similar elastic and plastic deformation mechanism for the experimental load range.[87]

Figure 2.10 shows the experimentally determined reduced elastic modulus, E_r, and indentation hardness, H, as a function of the contact depth, for each test spot, respectively. From this figure, it can be seen that both the hardness and elastic modulus values decrease sharply with the contact depth/indentation load and then level off. The dramatically high H and E_r values at shallower depth (<100 nm) have been widely observed in most polymeric systems.[88] This artificial error is usually attributed to indentation size effects (ISEs)[23, 24], including the inevitable indenter tip imperfections and an intrinsic ‘‘blunting effect’’ of the indenter tip, particularly as a pyramidal-shaped sharp tip is used to penetrate the surfaces, and possible tip miscalibration. These effects are especially severe at low indentation load because the contact depth and the impression left on the surface are small (Figure 2.9). Other factors that might cause the artifact include a harder outer skin (i.e., surface hardening) or possible localized oxidation/aging occurring in the top surface layer of the polymer as the experiments are conducted under ambient atmosphere. Although the substrate effect, measurement of hardness and modulus of thin film affected by the substrate due to pile up of the polymer film, has been reported in the literature[88], it is not a problem in the present study: both the H and E_r values do not change significantly with the increase of the indentation depth (>100 nm). The reason is that the substrate effect becomes a concern only if the indentation depth is comparable to the film thickness. The thinnest film in this study is 1.8 μm, and the maximum indentation depth is only about 300 nm. To avoid the

indentation size effects and possible substrate effect, the measurements are conducted with an indentation depth of 250 nm, which is equivalent to 600 μN applied force. Within the range between 100 μN/s and 350 μN/s, the loading rate does not seem to affect the hardness and elasticity measurements. To avoid possible interference from temperature, the indentation experiments are carried out under controlled room temperature. The dependence of mechanical properties on temperature is further investigated with dynamic mechanical analysis.

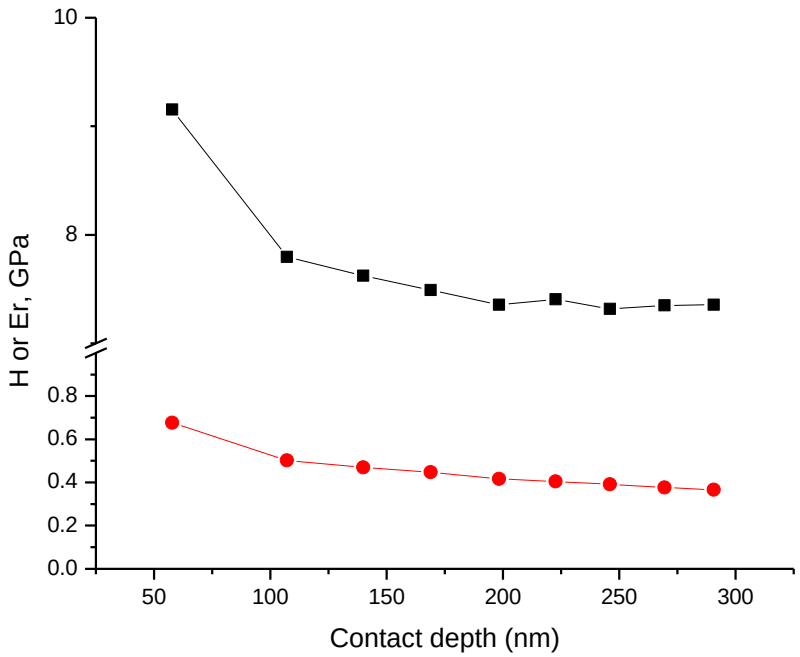

Figure 2.10 The effect of contact depth on the elastic modulus (-■-) and hardness (-●-) measurement through nanoindentation. The film was deposited at 35 °C.

Table 2.2 shows the result of the elastic modulus and hardness values of the photoresist coating at different deposition temperatures. The thickness of the resist film is 11.0 μm, 4.5 μm and 1.8 μm based on the surface profiler measurement. The DSI tests were done at the maximum load of 600 μN. The results show that elastic modulus values increase slightly with the decrease of the film thickness and the hardness values do not vary much with the film thickness. This

slight variation in elastic modulus is probably due to the residual substrate effect as the indentation depth is near or above 10% of the film thickness. It is important to point out that the hardness measurements through DSI test include both the elastic and plastic (inelastic) properties of the material as the penetration depth of the indenter tip h_{max}, and the subsequent area A, includes both recoverable and not recoverable part of deformation. Thus, the DSI method defines the hardness of a surface as its general ability to resist penetration and not as a purely plastic flow property. Also, with the DSI method, the elastic modulus is obtained by calculating the slope of the initial portion of the unloading curve, assuming that all recovery observed during the unloading is elastic recovery.[11] This assumption is true for most ceramics and metals. However, most polymers show strongly viscoelastic behaviors, which imply a time-dependent recovery. Therefore, the unloading portion of the load/displacement data is a convolution of both elastic and viscoelastic recovery, which complicates the explanation of the elastic modulus result.

Table 2.2 Measurement of elastic modulus and hardness of the photoresist at different deposition temperatures.

Deposition temperature (°C)	25	30	35
Film thickness (μm)	11	4.5	1.8
Elastic modulus (GPa)	8.61±0.06	9.36±0.27	9.75±0.20
Hardness (GPa)	0.45±0.0027	0.45±0.0058	0.42±0.0036

2.3.3.2 Dynamic mechanical analysis (DMA) method - the photoresist free standing film

Depth sensing indentation test characterizes mechanical properties of the photoresist as a coating, in which the load is applied vertically to the film and the displacement of the indenter tip is measured as a function of the load. Stress-strain relationship is the basis for measuring mechanical properties of materials, where stress is derived from the load applied on the sample

and strain is the deformation of the sample. Although experimentally simple, the stress-strain relationship in the indentation test is a complex multi-axial situation involved in the contact between two bodies, the sample and the indenter. Tensile test, on the other hand, possesses the simplicity of a uni-axial stress-strain relationship, where the pulling force and the resulting elongation of the sample are recorded. Moreover, because it is conducted on a free-standing sample, the tensile test measures the bulk properties instead of the coating form. A DMA instrument is used to carry out the tensile test. The free-standing photoresist film, carefully peeled off the substrate, is mounted with a dual cantilever fixture. In the current study, the strain/deformation is the controlled input, which is the case for most commercial DMA instruments.

In the DMA test, an oscillating, usually sinusoidal, strain/deformation is applied and the corresponding stress, which may lag behind the strain, is recorded. The complex modulus E* given by the DMA test may be divided into real and imaginary components: $E^* = E' + iE''$, with $E''/E' = \tan\delta$, where δ is phase lag between stress and strain. E' is known as the storage modulus and is a measure of the elastic character or solid-like nature of the material; E'' is known as the loss modulus and is a measure of the viscous character or liquid-like nature of the material.[89, 90] The storage modulus E' of the photoresist film is 1.03 GPa and the loss modulus E'' is 0.12 GPa, which indicates the viscoelastic behavior of the photoresist - exhibits both viscous and elastic characteristics when undergoing deformation. The photoresist is predominantly elastic and stiff at the room temperature as the loss modulus value is much smaller compared to that of the storage modulus. Figure 2.11 shows the effect of the temperature on the storage/loss modulus and tan δ, the ratio of loss modulus to storage modulus. With the increase of the temperature, the storage modulus decreases and the relative viscous contribution

increases. The observation indicates faster molecular motion of the photoresist at higher temperatures and the material becomes more "liquid-like".[91] To avoid the dramatic change in the mechanical properties of the photoresist, the operating temperature needs to be lower than the transition temperature around 50°C, which is defined as the temperature at which a maximum in the loss modulus occurs.

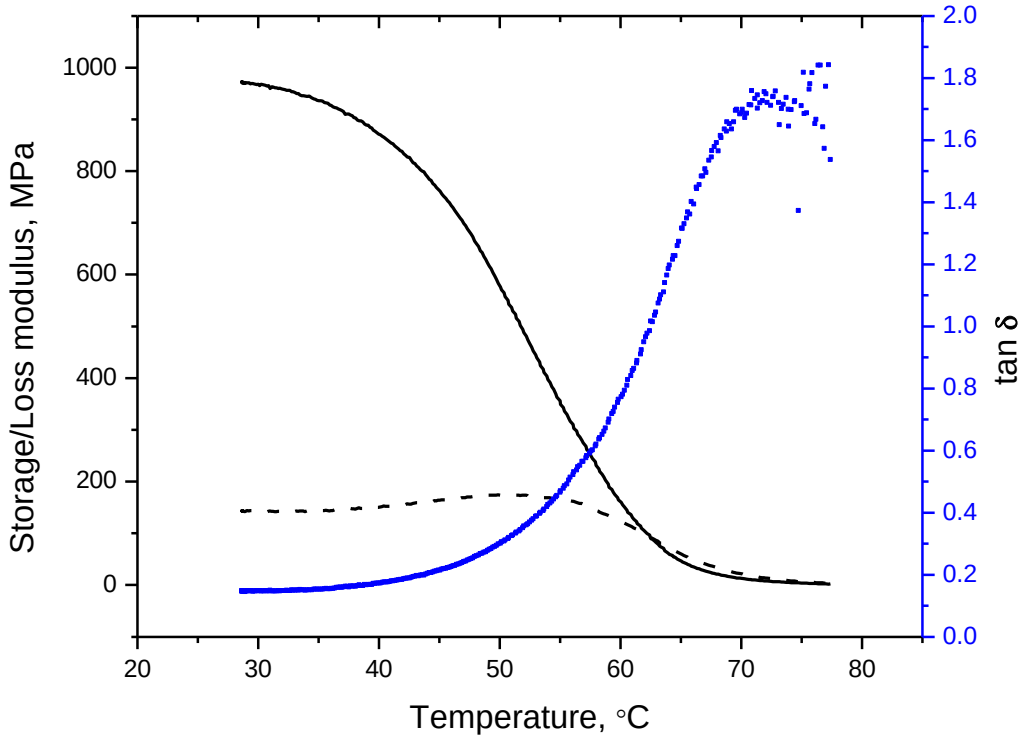

Figure 2.11 Measurement of glass transition temperature of the photoresist by DMA: storage modulus (—), loss modulus (– –) and tan δ (·····).

Another critical temperature of the resist is the onset of the decomposition of the material, which is characterized by thermogravimetric analysis (TGA). From Figure 2.12, the decomposition temperature is 263 °C, which is characterized by the dramatic weight loss. The shoulder peak at 182 °C, more apparent in the derivative of weight percentage curve, may be

explained as the degradation of the side chain or the functional groups on the main polymer chains. The transition temperature and the decomposition temperature are important in defining the temperature processing range of the resist film. A baking process following the deposition is necessary to evaporate any residual solvent and densify the resist.[83] For this step, the onset temperature of thermal decomposition must not be exceeded to preserve the lithographic properties of the resist film. On the other hand, it is usually higher than the transition temperature where the molecular motion of the polymer chain is highly induced to help forming a homogeneous film. Thus, the baking temperature of the photoresist material should be between 50 °C and 182 °C, which is usually set at 120 °C.

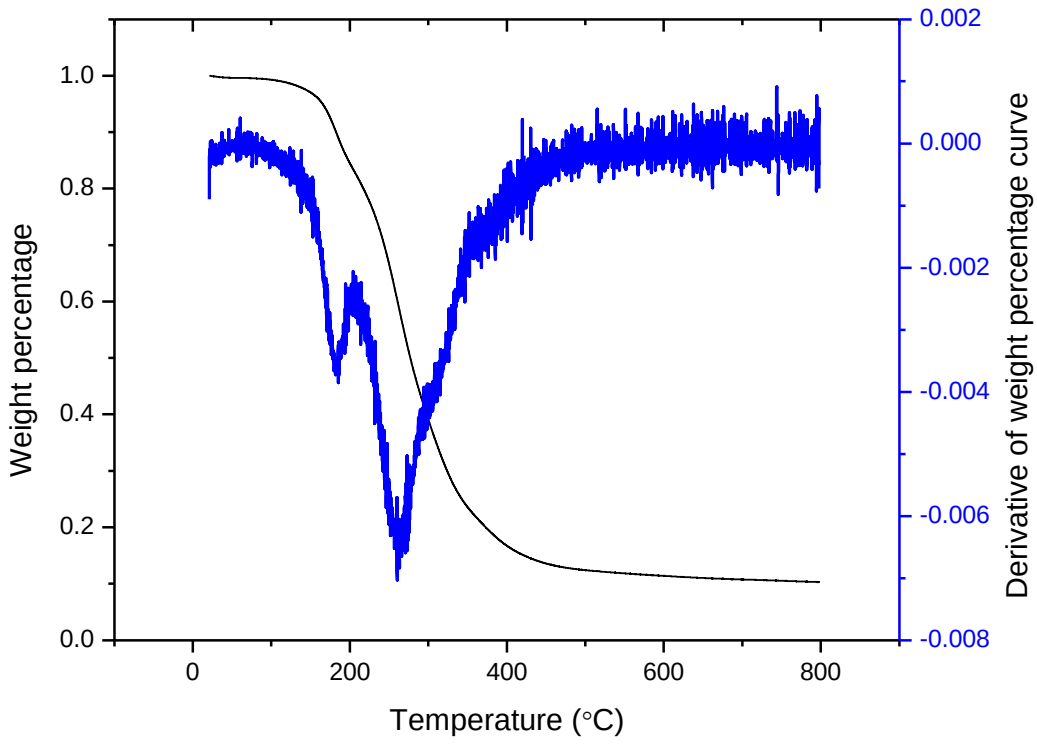

Figure 2.12 The thermogravimetric analysis (TGA) of the photoresist: weight percentage (—) and derivative of weight percentage (—).

The depth sensing indentation and the dynamic mechanical analysis are complementary as they investigate the two different forms of the photoresist film: as a coating and as a free-standing film. Moreover, DMA reveals the thermo-mechanical properties of the resist through measuring its dynamic modulus. There are differences in the modulus value between the two methods, which have been observed by previous researchers especially in the study of polymer materials. The elastic modulus value measured from DSI is higher than the result from DMA tensile test. The possible reasons are the potential substrate effect, surface stratification and the viscoelastic property of polymer.[92,93] In the current application, however, the exact value is not essential. Both the DSI and DMA test prove that the photoresist material possesses typical plastic properties and is mechanically strong enough to be used as a structural component when processed and operated at appropriate temperatures. Specifically, the mechanical and thermal properties of the photoresist are in agreement with those of polyurethane.[94] According to the manufacture's information, this photoresist belongs to the polyurethane family, although the exact formulation is not available due to proprietary reasons.

2.3.4 Application of the photoresist film as a spacer in a miniaturized electrochemical flow cell detector following capillary liquid chromatography

Using the photoresist coating as a spacer in the electrochemical flow cell detector instead of a free-standing polymer film is advantageous because the volume of the flow cell can be easily minimized. Figure 2.13 shows the photographs of an electrochemical flow cell which is composed of the auxiliary electrode block with the photoresist spacer and the working electrode block. In Figure 2.13A, the dimension of the flow channel is 1 mm x 10 mm, which is designed so as to incorporate the flow inlet and outlet on the auxiliary electrode and fit the dimensions of

the working electrode (Φ = 1 mm). It is worth pointing out that the flow pattern on the photoresist spacer is formed through standard photolithographic methods and features in the micrometer range are readily achievable.

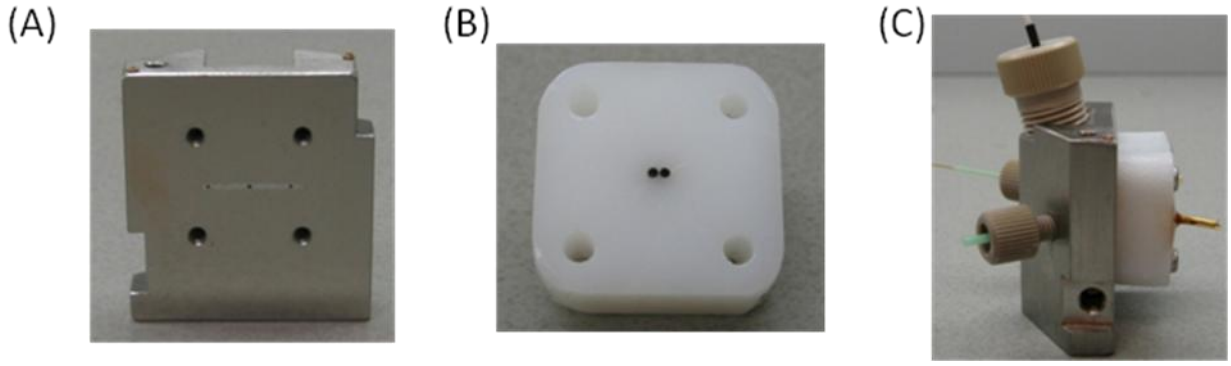

Figure 2.13 (A) A flow channel created on the photoresist film that has been coated on the surface of a flow cell piece; (B) a dual-electrode block; (C) the cross flow cell.

Although minimization of the flow pattern in the current application is limited due to the fixed design of the auxiliary and working electrode blocks, replacing a Teflon spacer with the photoresist film still demonstrates advantages in a capillary separation-detection system. Figure 2.14 shows the comparison of two chromatograms under identical chromatography conditions. Quantitative analysis of the peak shows the improvement of the place number from 6200 with the Teflon spacer to 7300 with the photoresist spacer. The reason is that the thickness of the photoresist spacer is 11 μm while the Teflon spacer is 22 μm thick. The thinner spacer reduces the flow cell volume and thus improves the chromatography.

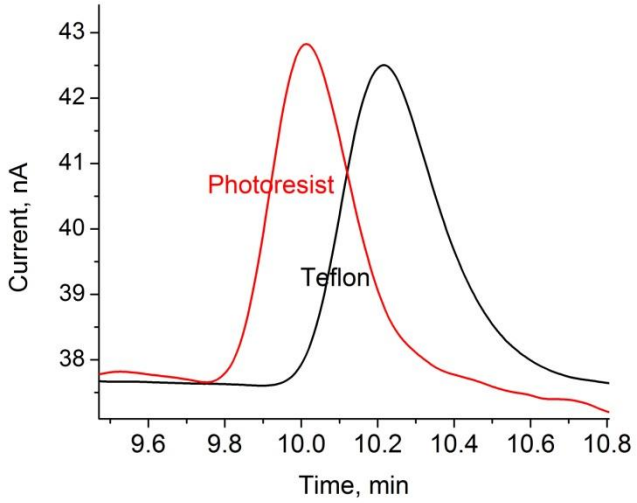

Figure 2.14 Comparison of detector performance with Teflon and photoresist spacer.

Dual-electrode detection has better selectivity than single electrode detection because the potential on the two electrodes can be set at different values for different detection purposes. There are two different dual electrode configurations: parallel and series (Figure 2.1). In a parallel dual electrode configuration, a higher potential can be applied on one electrode so that the hard to oxidize (reduce) components can be detected. But at the same time, the chromatogram will be too complicated and the response from one or more desired components can often be obscured by interferences. The dilemma can be solved by setting the second electrode at a lower potential so that only the more easily oxidized (reduced) components will be detected with great selectivity. The low potential chromatogram usually features better detection limits because of decreased complexity of the chromatogram[95]. In a series dual electrode configuration, the products from the upstream detector can be detected at the downstream detector (oxidative-reductive detection). So those chemically or electrochemically irreversible species are not detected at the downstream electrode, which results in simple chromatograms on the downstream detector and easier peak identification[96]. A rat brain slices homogenate sample

spiked with GGFL was analyzed with capillary HPLC coupled with a series dual-electrode detector. Figure 2.15 shows that the chromatogram on the upstream anode has very many peaks, which makes it difficult to identify the GGFL peptide signal. On the contrary, chromatogram on the downstream cathode provides a much lower background and noise and GGFL identification becomes straightforward. Moreover, although both the anode and cathode give usable signals, the background current and the noise on the downstream cathode are usually much lower than the upstream anode. The background current is principally faradic current arising from the oxidation (or reduction) of electroactive impurities in the mobile phase and post-column reagent. Because the potential on the anode has to be set at a relative high value for the Cu(II)-peptide compound to be oxidized, more species in the system are electroactive, thus creating higher background current. Noise is the random or periodic pattern superimposed on the steady-state background signal[97], representing the summation of spurious contributions from pump pulsation, flow cell hydrodynamics, static electricity, electronic amplification and etc. High background currents increase the susceptibility of the system to noise. The potential on the downstream cathode can be adjusted to give minimum background current, thus low noise. In the current case, the two working electrodes are operated in a serious configuration: the upstream electrode detects the peptide compound through oxidization; and the downstream reduces the oxidized form of the peptide compound. Collection efficiency is the ratio of the downstream response to the upstream response, which is 0.79 on Figure 2.16. The high collection efficiency benefits from the photoresist spacer as the thin and narrow flow channel helps reducing mass loss on the downstream electrode.

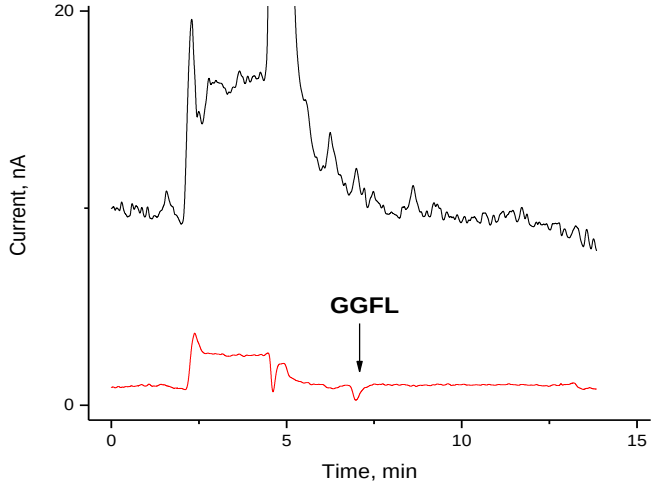

Figure 2.15 The chromatograms of diluted rat brain slices extract sample spiked with GGFL.

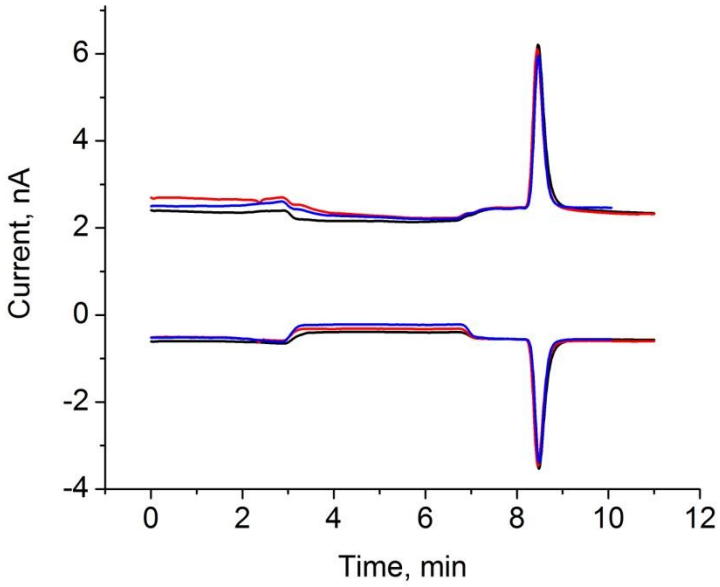

Figure 2.16 Chromatogram of 1 µM GGFL using the EC flow cell with photoresist coating as the spacer.

Achieving high collection efficiency is especially important when the analytes are more complicated. For example, we are interested in enkephalins, a type of neuropeptides, for

understanding the brain chemistry. There are two types of enkephalins: Leu-enkephalin (YGGFL) and Met-enkephalin (YGGFM); GGFL and GGFM are their corresponding hydrolysis products. Our peptide detection scheme is based on the biuret reaction of Cu(II) with peptides and uses a series dual electrode detector. The Cu(II)-peptide/Cu(III)-peptide electrochemistry has a half-wave potential around 0.5 V vs. Ag/AgCl: the Cu(II)-peptide is oxidized at the upstream anode, followed by reduction of Cu(III) back to Cu(II) at a downstream cathode. While the electrochemistry of Cu(II)-GGFL/Cu(III)-GGFL and Cu(II)-GGFM/Cu(III)-GGFM is reversible, it is more complicated with the Cu(II) derivatives of YGGFL and YGGFM. Figure 2.17 shows separation of the four peptides. The current responses of YGGFL and YGGFM on the anode are higher than their hydrolysis products with the same concentration, while lower than them on the cathode. Y (Tyr) is an electroactive amino acid, so peptides with Y are detectable without derivatization, however, the reaction with Cu (II) leads to increases in sensitivity for Y-containing peptides because the anode signal is actually the sum of the electroactive amino acid signal and the Cu (II) signal with appropriate potential applied[98]. This explains why YGGFL and YGGFM give higher current response on anode compared to their hydrolysis products with the same concentration. On the contrary, the cathode signals of Y-containing peptides are lower than their hydrolysis products. There are two reasons for that. First, at the relatively long time scales of the mass transport process from the anode to the cathode in the dual electrode detection, tyrosine oxidations are chemically irreversible. Thus, the only carrier of signal for the cathode is Cu (III). Second, the oxidized product of the Y-containing peptide created on the anode, Y_{ox}-Cu(III)-peptide, can undergo chemical reaction to produce $Y_{ox'}$-Cu(III)-peptide. This process may be followed by further homogeneous intramolecular electron-transfer reaction, $Y_{OX'} - Cu(III) - peptide \rightarrow Y_{OX,OX} - Cu(II) - peptide$. Because the tyrosine oxidation product

$Y_{ox,ox}$-Cu(II)-peptide cannot be reversibly reduced, the net current response on the cathode is depressed. Due to these complications, the current response of Y (Tyr) containing peptides is hard to detect on the downstream cathode and a flow cell detector with high collection efficiency will help increase its detector sensitivity.

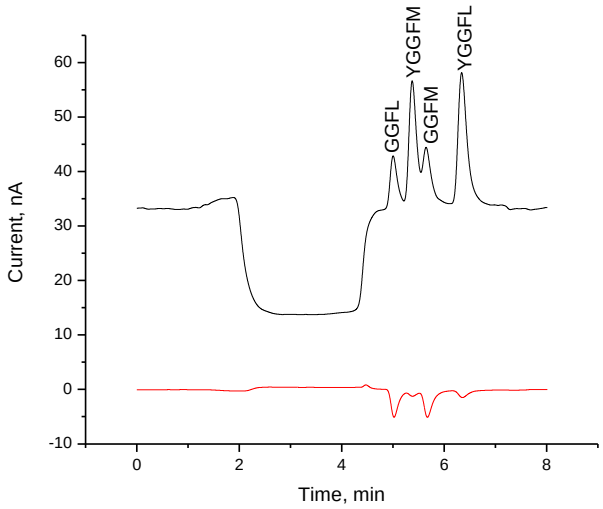

Figure 2.17 The chromatograph of 1 µM enkephalin standard mixture.

2.3.5 Theoretical simulation of the flow channel

Theoretical simulation using numerical models is utilized to visualize the electrochemical process within the flow channel and facilitate its optimization. The potential applied on the working electrode during the amperometric detection is set at a value so that the current response depends entirely on mass transfer. The flow cell detector is simplified as a two-dimensional rectangular channel. A plug of solution containing 1 µM analytes is pumped through the channel under laminar conditions. The concentration on the electrode surface is set to be zero. The result shows the concentration profile after the system reaches the steady state: the analyte concentration in the channel (Figure 2.18 top) depletes rapidly along the electrode; the

concentration gradient (Figure 2.18 bottom) drops sharply along the electrode surface and reaches zero at around 0.4 mm from the electrode starting edge. From the simulation result, it appears that under the specific experimental conditions and flow cell design, an electrode with diameter equal to or smaller than 0.4 mm will help to decrease noise and background current without losing signal.

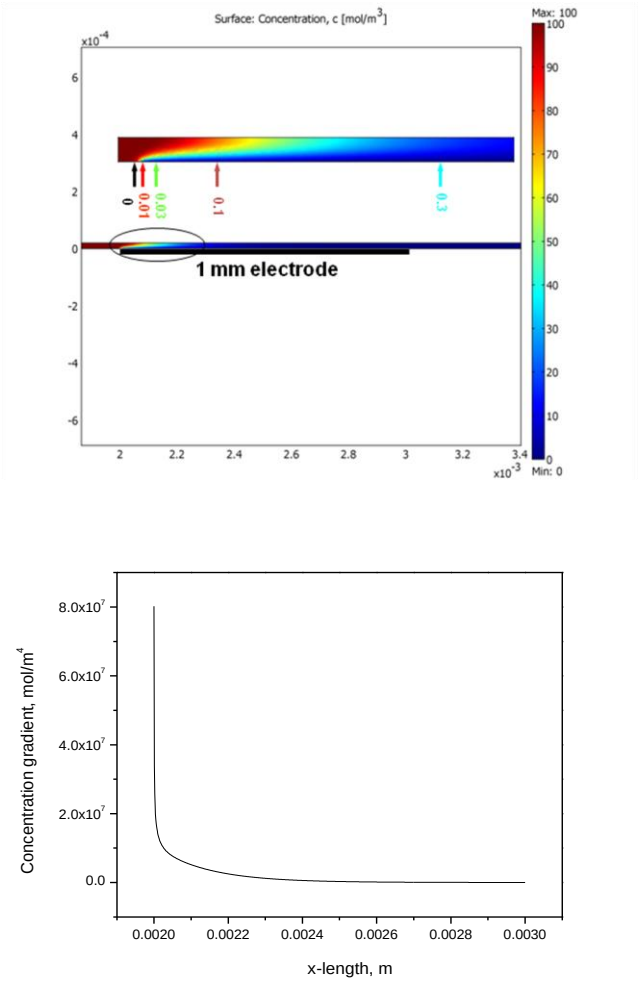

Figure 2.18 Comsol simulation results showing the analyte concentration distribution in the flow channel (top) and the concentration gradient along the electrode surface (bottom). The 1 mm electrode is positioned between 0.0020 m and 0.0030 m.

All the parameters, for example, flow rate, electrode dimensions and flow channel dimensions, can be easily adjusted to reflect the actual experiment parameters. Traditionally, glassy carbon is used as the electrode material and the available dimension of glassy carbon material is limited: to our knowledge the smallest glassy carbon rod is 1 mm in diameter (Goodfellow website). However, both carbon fiber composite and chemically modified gold are also suitable as electrode material for biological applications (see details in Chapter 3.0 and Chapter 4.0). These two materials, compared with glassy carbon, have a much wider selection of sizes, which can be utilized to improve the detection signal/noise ratio.

Theoretical simulation is also performed on a series dual-working electrode detector, where analyte A is oxidized to B on the upstream electrode and B is reduced back to A on the downstream electrode. Potentials on the two electrodes are both set at a mass transfer controlled value. Table 2.3 demonstrates how the collection efficiency is affected by gasket thickness and a thinner gasket (10 μm vs. 20 μm) improves the collection efficiency. Interestingly, although it is shown on Figure 2.18 that a smaller electrode (< 1 mm) will improve signal/noise ratio, the collection efficiency decreases on a dual electrode with smaller dimension (0.4 mm or 0.12 mm). For a reversible redox pair, for example, Cu(II)-GGFL/Cu(III)-GGFL, the current response on both electrodes are determined by mass transfer only and so is the collection efficiency. In a more complex scenario where analyte B undergoes chemical reaction, the reaction rate will affect the current response on the downstream electrode therefore the collection efficiency. For example, it has been discussed in Section 2.3.4 that the oxidative product of Cu(II)-YGGFL undergoes chemical reaction which results in a lower collection efficiency compared with GGFL. Figure 2.19 simulates the concentration distribution of analyte A in the flow channel with two working electrodes, which are both 0.12 mm and separated by a distance of 30 μm. Before

analyte B (oxidation product of A) reaches the downstream electrode, it undergoes chemical reaction with a reaction rate $R = k \times [B] = 10 s^{-1} \times [B]$. Table 2.4 lists the collection efficiency on different dual electrode sets, either with or without chemical reaction involved. Dimensions of both electrodes affect the collection efficiency. Where there is chemical reaction (k = 10 s^{-1}) involved, a small dual electrode set (0.12 mm + 0.12 mm) gives higher collection efficiency than the relatively bigger set (0.40 mm + 0.40 mm), while the opposite is true without chemical reaction. The dual electrode setup with a 0.12-mm upstream electrode and a 0.40-mm downstream electrode gives high collection efficiency with or without chemical reaction. These preliminary simulation results give us theoretical guidance to optimize the electrochemical detector parameters, for example, electrode dimensions and gasket thickness, in different applications.

Table 2.3 Effect of gasket thickness on the collection efficiency

Electrode dimension / Channel height	1 mm + 1 mm	0.4 mm + 0.4 mm	0.12 mm + 0.12 mm
20 μm	98.1%	82.3%	57.0%
10 μm	~100%	95.8%	68.6%

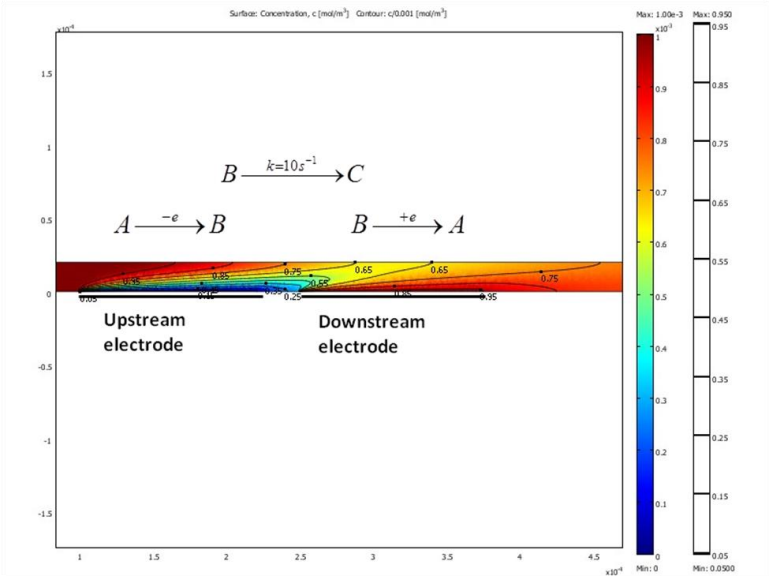

Figure 2.19 Comsol simulation results showing the analyte concentration distribution in the flow channel with dual electrode setup. Upstream electrode is positioned between 0.10 mm and 0.22 mm and downstream electrode is positioned between 0.25 mm and 0.37 mm.

Table 2.4 Effect of dual electrode dimensions on the collection efficiency

Dual electrode dimensions	Collection efficiency (without chemical reaction)	Collection efficiency (with chemical reaction)
0.12 mm + 0.12 mm	54.7%	13.3%
0.12 mm + 0.40 mm	84.0%	14.6%
0.40 mm + 0.40 mm	81.3%	5.7%

2.4 CONCLUSION

Using a novel photosensitive polymer coating to replace the traditional free-standing polymer film as the spacer in an electrochemical flow cell detector has been shown to offer the convenience of controllable thickness and easy assembly, which leads to improvement in detector performance. Fabrication of the photosensitive coating is reported, along with its detailed characterization. Although most photoresist films are traditionally used for sacrificial purposes only, the mechanical characterization results prove its usefulness as a structural component below the glass transition temperature. The advantage of the thin coating as the spacer is shown in electrochemical detection following capillary separation, in compassion with a traditional free-standing gasket.

3.0 CARBON FIBER/EPOXY COMPOSITE RING-DISK ELECTRODE: FABRICATION, CHARACTERIZATION AND APPLICATION TO ELECTROCHEMICAL DETECTION IN CAPILLARY HIGH PERFORMANCE LIQUID CHROMATOGRAPHY

Carbon fiber/epoxy composite materials, which are manufactured using the pultrusion process, are commercially available in various shapes and sizes at very low cost. Here we demonstrate the application of such a material as an electrochemical detector in a flow system. Cyclic voltammetry shows that the material's electrochemical behavior resembles that of glassy carbon. Using tube and rod composites, we successfully fabricated a ring-disk electrode with a 20 μm gap between the ring and the disk. The narrow gap is favorable for mass transfer in the generator-collector experiment. This composite ring-disk electrode is assembled in a thin-layer radial-flow cell and used as an electrochemical detector. The disk electrode, placed directly opposite to the flow inlet, is operated as a generator electrode with the ring electrode being a collector. The high collection efficiency on the ring electrode (0.8 for a chemically reversible species) enhances the detection selectivity.

3.1 INTRODUCTION

Carbon composites are composed of carbon and nonconducting binders that are mixed according to specific ratios and allowed to cure to a rigid solid, the shape and size of which are defined by the mold used. Many types of carbon materials can be used in composite fabrication, including carbon fibers[99-102], carbon foam[103], carbon nanotubes[104], and particulate forms of graphite[105-108], glassy carbon[109], and diamond[110]. The composites can be regarded as ensembles of microelectrodes, the properties of which depend on the carbon material used in the composite, the binders, and the volume fraction of conducting material. Carbon composite electrodes are widely used in electrochemistry for sensing and detection applications due to their flexible shape, controllable electrochemical properties and low cost. The binder material and fabrication process affect whether a composite electrode is suitable for detection in a flow system. Some graphite composite electrodes, such as Kel-F graphite[111, 112], PVC graphite[113, 114], PTFE graphite[115], epoxy graphite[116] and sol-gel derived ceramic graphite[106, 108, 117], are good for flow system detection purposes, while paraffin carbon paste electrodes suffer practical difficulties.

Most carbon composites used in electrochemistry are fabricated in individual laboratories and vary in properties, which makes general application difficult. Carbon fiber composites, which are widely used as structural reinforced plastics, are available on a commercial scale at very low cost. They are composite materials combining carbon fibers (short or continuous, unidirectional or multidirectional) and a 'plastic' material such as epoxy or vinyl ester. Carbon fiber composites made from unidirectional carbon fibers have constant cross sections and are usually manufactured using the pultrusion process[118], in which fibers are drawn from spools, passed through resin bath for impregnation, and gathered together to produce a particular shape before entering a heated die. There have been a few studies related to their electrochemical

properties[99-101], but the application as electrochemical detectors has not been explored. Taking advantage of their commercial availability in various shapes and sizes, their use in novel detector design for biological environments and miniaturized devices should be favorable.

We report the fabrication of a ring-disk electrode using the carbon fiber/epoxy composite tube and rod and its application as a dual-electrode detector for a capillary HPLC system. The ring–disk electrode in a radial flow cell is equivalent to a dual-series electrode in a thin-layer cross flow cell. When a dual-series detector is assembled in a flow separation system [54, 119], the analytes are first oxidized/reduced on the generator electrode and the products stable on the timescale of the transit time from the generator to the collector are then reduced/oxidized on the collector electrode. It has been shown that dual-series/generator-collector detection can reduce noise and increase selectivity. For example, biological samples are complicated matrices containing oxidizable species which results in many overlapping peaks with single electrode detection. Dual-electrode detection is selective for electrochemically reversible analytes (e.g., catecholamines) [120-122]. The selectivity inherent in the dual-electrode approach typically lowers detection limits for electrochemically reversible analytes.

Although selectivity is improved with a dual-series detector, the current response is lower on the collector electrode because some of the analyte that is oxidized or reduced at the generator is transported away from the surface and does not reach the collector. Thus, a small gap between the two electrodes is crucial to achieving high collection efficiency on the collector electrode, especially for a capillary HPLC system due to the potentially low solution velocity. The common dual-series electrode composed of two disc electrodes has a relatively large gap between the two electrodes. A ring-disk electrode with proper alignment has the potential to show high collection efficiency. Past efforts towards making ring-disk electrodes include: alternate vapor deposition

of insulating and conducting material around a disk electrode (carbon fiber, metal wire, etc.) [67, 119, 123]; aligning microelectrodes around the disk electrode as the ring electrode[124, 125]; using photolithography and dry etching[126, 127] or sputtering[128] to fabricate carbon or metal thin film ring-disk electrode. These ring-disk electrodes have been applied in certain areas, but the drawbacks are obvious: vapor deposition results in a very thin conducting layer (micrometers thick) as the ring electrode; thin film electrodes are not polishable and electrochemically less well defined compared to solid electrodes; the fabrication methods involve complicated procedures and expensive equipment (vapor deposition, micromachining, etc.). Based on these reasons, we developed a simple and effective method of making a ring-disk electrode from a carbon fiber/epoxy composite tube and rod. The resulting ring-disk electrode has a relatively thin gap (20 μm). We have applied it successfully as a dual-series detector in a capillary HPLC system.

3.2 EXPERIMENTAL

3.2.1 Chemicals and materials

The reagents used were as follows: $K_4Fe(CN)_6 \cdot 3H_2O$, $K_3Fe(CN)_6$ (Fisher Scientific, Fair Lawn, NJ); $Ru(NH_3)_6Cl_3$ (Polysciences, Inc., Warrington, PA); KCl, Na_2CO_3, $NaHCO_3$ (EM Science, Gibbstown, NJ); Leu-enkephalin (YGGFL), des-Tyr-Leu-enkephalin (GGFL), (Bachem, Torrance, CA); copper sulfate pentahydrate (J. T. Baker, Phillipsburg, NJ) was recrystallized once from water and disodium tartrate dehydrate (Baker) was recrystallized from diluted NaOH; all the other chemicals were of analytical reagent grade purity and were used as received. The

above solutions were made with 18 MΩ purified water from a Millipore Synthesis A10 system (Millipore, Billerica, MA). Teflon AF 2400 was purchased from DuPont (Wilmington, DE). FC-72 (a mixture of perfluorohexanes) was obtained from 3M (Minneapolis, MN) and was used to dissolve Teflon AF.

The carbon fiber/epoxy composite materials were purchased from A2Z Corp/Peck-polymers (Englewood, CO, USA) – distributor for DPP Pultrusion (Tilburg, the Netherlands). The glassy carbon (dia. 1.00 mm) was obtained from HTW Hochtemperatur-Werkstoffe GmbH (Thierhaupten, Germany).

3.2.2 Carbon Fiber / Epoxy Ring-disk Electrode Fabrication

The ring-disk electrode was made from a carbon fiber/epoxy composite rod (diameter 0.48 mm) and tube (outer diameter 1.00 mm, inner diameter 0.52 mm). The thin gap between the ring and the disk electrode (20 μm on average) was achieved through a two-step insulation-adhesion process. The first step was to make a Teflon AF coating on the outer surface of the rod for insulation purpose. The composite rod was dipped in a 10 mg/mL Teflon AF 2400/FC72 solution following which the solvent was allowed to evaporate naturally (room temperature, no forced convection of air). Although we did not treat the surface, it is worthwhile to point out that the adhesion of Teflon AF to the substrate is usually limited, but can be improved by surface treatment and heating the coated surface. This process was repeated 10 times and then the piece was dried in an oven at 110 °C for 2 hours to ensure a defect-free Teflon AF thin film coating on the composite surface[67]. The resulting Teflon AF film (dip coat/dry 10 times) was about 7 to 8 μm thick (the thickness can be adjusted by increasing or decreasing the number of coating cycles applied). The second step involved placing the coated rod into the tube and gluing them together.

Because the outer diameter of the coated rod was slightly thinner than the inner diameter of the tube by about 12 μm, there existed thin space between them when the coated rod composite was inserted into the tube composite. To fill the space and glue the rod and the tube composite together, the whole set was immersed in Spurr low viscosity epoxy resin (Polysciences, Inc., Warrington, PA). The epoxy resin penetrated the space between the coated rod and the tube. The electrode pair was then transferred to the oven (70 °C) for the epoxy to cure overnight. A simple test was carried out to examine insulation of the ring-disk electrode by measuring the resistance between the ring and the disk electrode. The few electrode sets that showed measurable resistance were discarded.

Electrical contact was made by connecting each carbon fiber/epoxy composite piece to a nichrome wire with silver epoxy H20E (Epoxy Technology Inc., Billerica, MA) (cured at 80 °C overnight). The electrode was insulated either in a glass tube with Torr Seal (Varian, Inc., Lexington, MA) for voltammetry, or in a Kel-F block with EPO-TEK 353ND epoxy (Epoxy Technology, Billerica, MA) for flow experiments. Before electrochemical experiments, the electrodes were wet polished with 0.05 μm γ-alumina slurry (Buehler Ltd., Lake Bluff, IL, USA) and rinsed and sonicated with deionized water.

3.2.3 Microscopy characterization

Scanning electron microscopy (SEM) images were obtained using a Philips XL-30 field emission scanning electron microscope. The samples were sputter coated with Pd before SEM. Compositional analyses were done by the affiliated energy-dispersive X-ray spectroscopy (EDX). Optical microscopy images were obtained using an inverted fluorescent microscope (Model IX71) with Olympus U Plan Apo 4 × and 20 × objective lenses.

3.2.4 Capillary liquid chromatography and electrochemical detection

The capillary HPLC system was described before[27, 129], so the process is briefly summarized as follows.

The mobile phase (0.1% TFA, 3% 1-propanol, 23% acetonitrile) was pumped through a homemade capillary column slurry packed with 3.2 µm prototype bridged hybrid C18 (Waters, Milford, MA) reversed-phase particles using 100 µm ID, 360 µm OD fused-silica capillary (Polymicro Technologies, Pheonix, AZ) as the column blank. A Waters 600 E quaternary pump (Milford, MA) with a simple tee as a flow splitter delivered mobile phase at 1 µL/min. The injected samples were peptide solutions in aqueous 0.1 % TFA. Two µL were injected. A Picoplus syringe pump (Harvard Apparatus, Holliston, MA) was used to deliver the biuret reagent (0.24 M carbonate buffer, 12 mM disodium tartrate, and 2.0 mM copper sulfate, pH 9.8) at 0.3 µL/min into a home-made Y-shape post column reactor[27], where the biuret reagent was mixed with the chromatographic eluent after the column. The Y-shape reactor was composed of three silica capillary tubes (ID = 75 µm, OD = 360 µm), with the junction fixed in a piece of dual shrink/melt tubing (Small Parts, Miami Lakes, FL). The reaction length was 8 cm measured from the confluence. The post column reaction derivatizes peptides and produces electroactive Cu(II)-peptide[26], which makes peptides electrochemically detectable.

The electrochemical detector was composed of a BAS radial-style thin layer auxiliary electrode, a 13 µm thick Teflon spacer and the homemade carbon fiber composite ring-disk electrode block described on section 4.2.2. The disk electrode was placed centered and directly opposite to the flow inlet. The electrode block was polished with 0.05 µm alumina slurry and sonicated in DI water before being assembled in the flow cell. The detection potential was + 0.6 V at the disk electrode, + 0.05 V at the ring electrode. The potential was controlled by a BAS

(W. Lafayette, IN) Epsilon potentiostat. A Ag/AgCl reference electrode (3M NaCl, BAS) was used as a reference electrode. All stated potentials are referred to this reference electrode.

3.3 RESULTS AND DISCUSSION

3.3.1 Carbon fiber/epoxy composite electrode characterization

The carbon fiber/epoxy composite material used in this study is made from unidirectional continuous carbon fibers and epoxy as the binder resin. SEM shows the cross-sectional and longitudinal images of this material (Figure 3.1). The average diameter of the carbon fibers is 7~8 μm and they are densely packed. The area percentage of carbon fibers calculated from the SEM cross section image is 50~60 %, which agrees with the manufacture's value of carbon fiber volume loading.

(A)

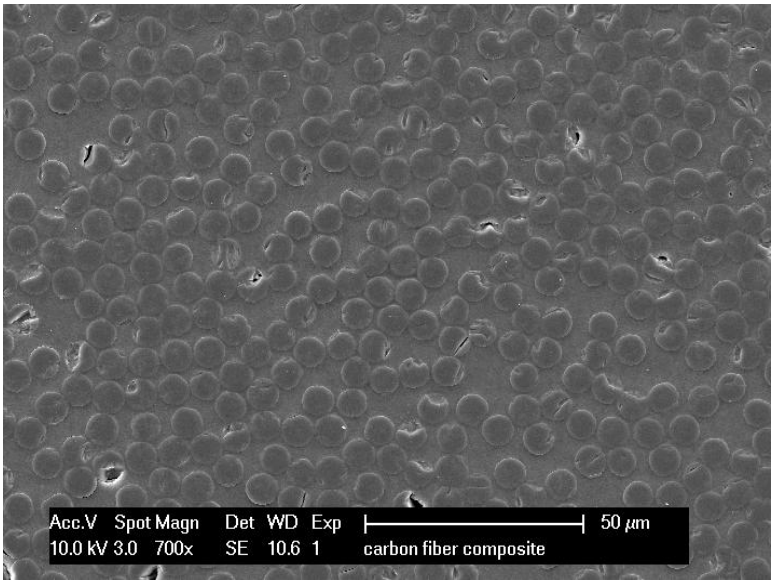

(B)

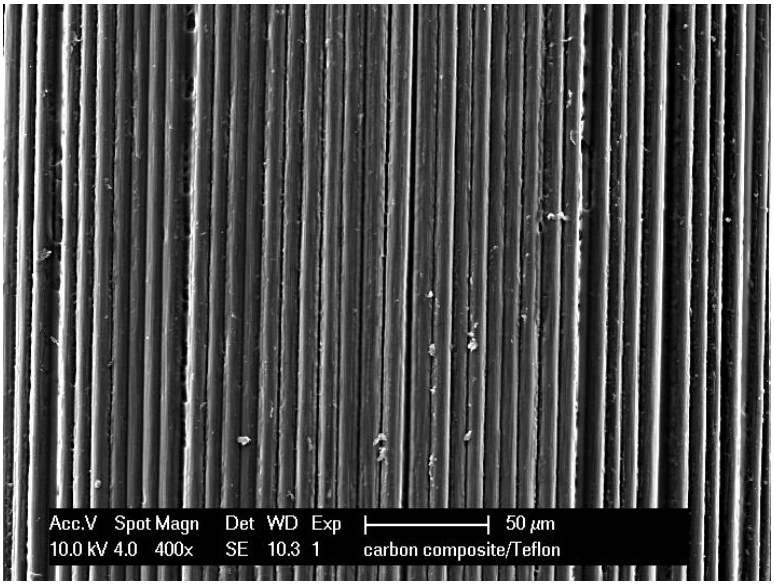

Figure 3.1 SEM images of a carbon fiber/epoxy composite with the 50-µm scale bar: (A) cross-sectional and (B) longitudinal.

The electrochemical behavior of carbon fiber/epoxy composite electrode was evaluated through cyclic voltammetry (CV) in ferrocyanide-containing and ruthenium(III) hexamine-containing solutions at scan rates 20, 50, 100, 200 mV/s (Figure 3.2A and 3.2B). The same experiments were carried out on a glassy carbon electrode with the same geometrical area (both 1.00 mm in diameter) for comparison (Figure 3.2C and 3.2D), as glassy carbon is by far the most commonly used electrode material for electroanalytical purposes. The resulting voltammetric profiles recorded at a carbon fiber composite electrode and a glassy carbon electrode are very similar: the voltammograms display well-defined peak shapes; the peak-to-peak separation is about 65 mV; the peak current is dependent on scan rate (v) in the following way. For the composite electrode: in a solution of $Fe(CN)_6^{4-}$ current is proportional $v^{0.43}$, for $Ru(NH_3)_6^{3+}$ the exponent is 0.44. For the glassy carbon electrode the exponents are 0.46 and 0.45 respectively (see supplementary Figure 3.6 for more details). The peak current dependence of sweep rate indicates that the current is limited by linear diffusion to the electrode instead of radial diffusion.

Also, the similar peak current on carbon fiber composite and glassy carbon electrode indicates that the "effective" electrode area of the carbon fiber composite is the same as the measured physical area. These CV characteristics suggest that the carbon fiber composite material, despite its appearance as a bundle of carbon fibers, behaves like a solid electrode.

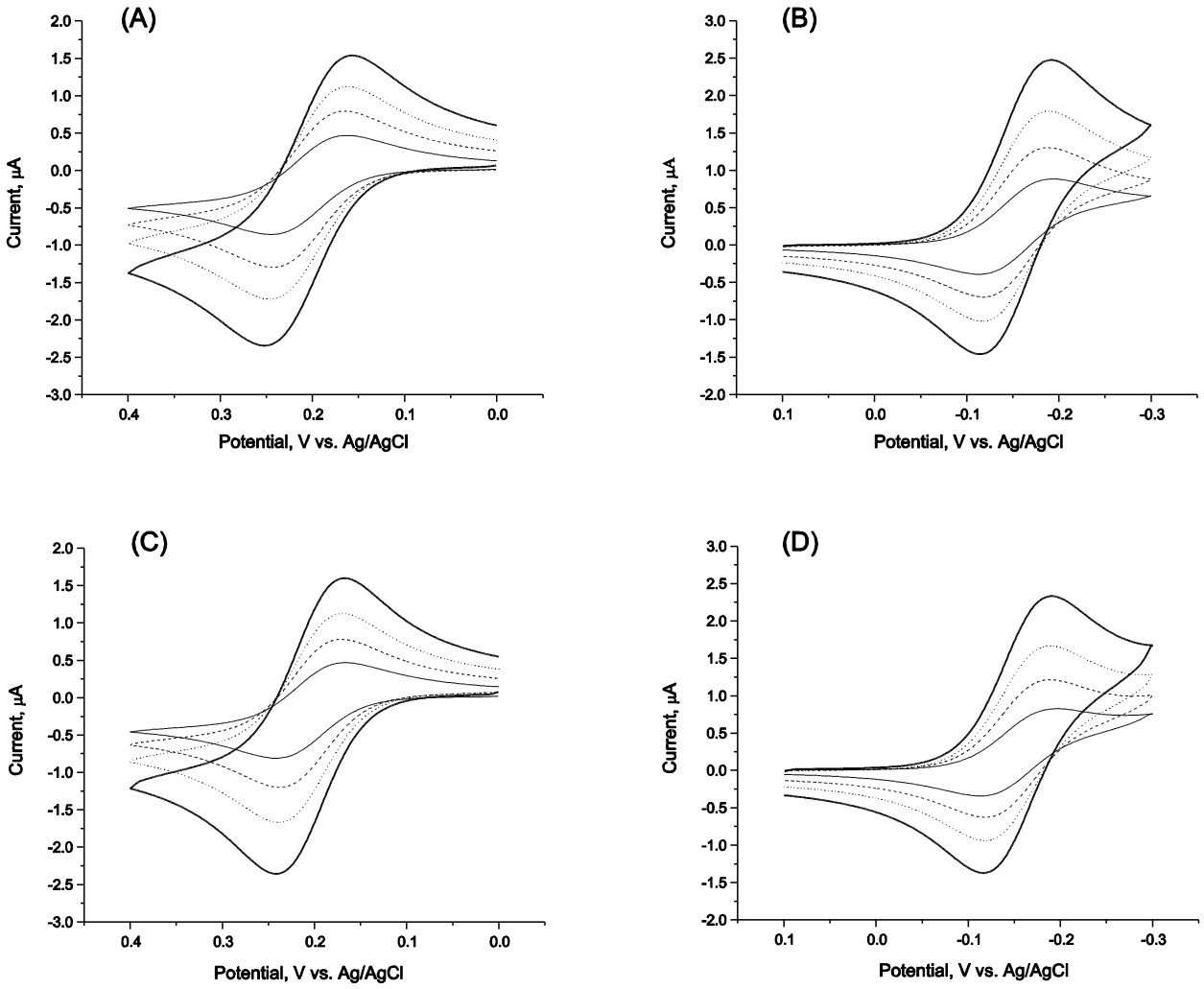

Figure 3.2 Cyclic voltammograms of a carbon fiber/epoxy composite electrode in (A) $Fe(CN)_6^{4-}$ solution and (B) $Ru(NH_3)_6^{3+}$ solution; a glassy carbon electrode in (C) $Fe(CN)_6^{4-}$ solution and (D) $Ru(NH_3)_6^{3+}$ solution. $Fe(CN)_6^{4-}$ solution was 1 mM $K_4Fe(CN)_6$ 0.1 M KCl solution; $Ru(NH_3)_6^{3+}$ solution was 1 mM $Ru(NH_3)_6Cl_3$ 0.1 M KCl solution. Scan rate was 20

mV/s (—); 50 mV/s (---); 100 mV/s (····) and 200 mV/s (—). Both the composite electrode and the glassy carbon electrode have diameters of 1.00 mm.

As the 'active' component of the carbon fiber/epoxy composite electrode, the carbon fibers are usually considered as microelectrodes, the general concept of which is that the electrode is smaller than the scale of the diffusion layer developed in readily achievable experiments[66]. When bundles of carbon fibers are embed within insulating matrix, the diffusion layer of individual microelectrodes can either be isolated or overlapping with each other depending on the gap between the microelectrodes and the experimental time scale. The experimental time scale determines the diffusion layer thickness at individual microelectrodes, which is on the order of $(Dt)^{1/2}$. For a species with a diffusion coefficient of 1×10^{-5} cm^2 s^{-1}, $(Dt)^{1/2}$ is about 30 μm for an experimental time of 1 s. Thus, in an experiment on a carbon fiber composite electrode with a similar or longer time scale, the diffusion layers of the individual carbon fiber microelectrodes start overlapping because the distance between individual carbon fibers in the composite is only 10 μm on average (seen from SEM). In fact, the distance between microelectrodes has to be at least 12 times the radius of microelectrodes[130] for it to behave like a microelectrode array, in which case the total current is the sum of individual microelectrode steady-state current response. The characteristic dimensions of the carbon fiber/epoxy composite determine that it acts like a macroelectrode on the seconds timescale. This explains the similarity between carbon fiber/epoxy composite and the glassy carbon electrode in the current response observed in Figure 3.2.

3.3.2 Carbon fiber composite ring-disk electrode fabrication and characterization

Carbon fiber composite material is commercially available in many shapes and sizes, including rods, tubes, rectangular, strips, etc. Different electrode designs can be fabricated from this composite material taking advantage of its variety in shapes and sizes. A carbon fiber composite ring-disk electrode is composed of a rod fitted inside a tube and separated by an electrically insulating material. The gap spacing between the ring and the disk electrode is determined by the diameters of the rod and the tube. A minimum gap is desirable when the ring-disk electrode is operated in generator-collector mode because of the favorable high collection efficiency. For this reason, we chose a rod and tube pair with these dimensions: Diameter (rod) = 0.48 mm; Inner diameter (tube) = 0.52 mm; Outer diameter (tube) = 1.0 mm. If the rod is fixed perfectly concentrically inside the tube, the gap will be 20 μm. The gap can be filled by allowing a resin, for example, an epoxy adhesive, to penetrate and then cure for hardening. Because the average distance between the rod and the inner tube is only 20 μm, this one-step method can easily fail to form an effective insulation due to the high chance of the rod and the inner tube contacting each other before the epoxy is cured. To prevent this, we added an insulation step before fixing the rod into the tube with the epoxy resin treatment by coating the rod surface with a Teflon AF film. The insulating Teflon AF coating is crucial in the ring-disk electrode fabrication: not only does it create an insulating layer; this step also ensures proper alignment between the rod and the tube.

The carbon fiber composite ring-disk electrode is characterized using optical microscopy (Figure 3.3A). The magnified image (Figure 3.3B) shows the junction between the ring and the disk, which is clearly composed of two layers. EDX results confirm that the layer around the disk periphery is the Teflon AF film, which contains fluorine and carbon as the main elements, and the layer surrounding the Teflon AF film is epoxy. The gap spacing is fairly uniform and is

estimated from the micrograph to be around 20 µm, with Teflon layer around 7 - 8 µm and Epoxy layer 10 - 12 µm thick (as measured on Figure 3.3B). We have fabricated three ring-disk electrodes with the same gap spacing as judged by the optical micrographs.

(A)

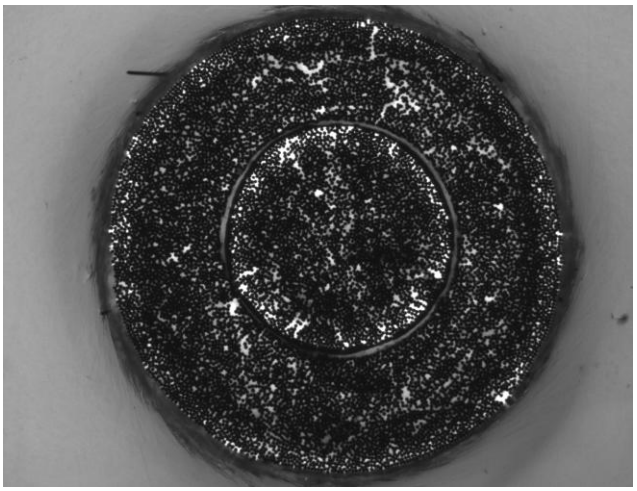

(B)

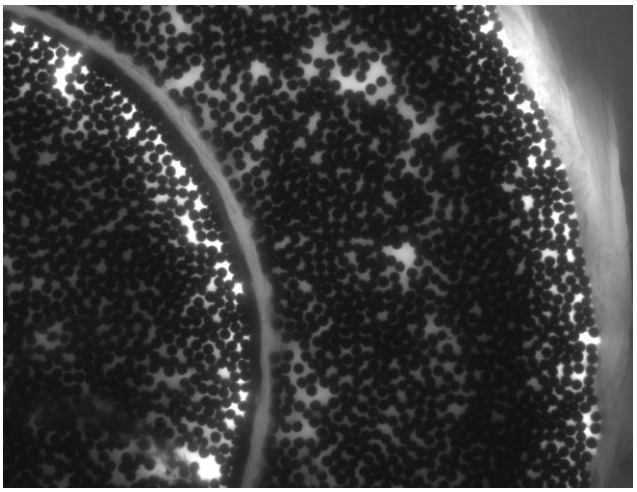

Figure 3.3 Optical microscopy images of carbon fiber/epoxy composite ring-disk electrode: whole ring-disk electrode surface (A) and magnified area showing the 20-µm gap between the ring and the disk (B).

The voltammetric/amperometric experiment[131] in a quiescent solution is a simple and effective method to characterize the quality of a dual-electrode, especially a ring-disk electrode, and demonstrate the thin gap between the two electrodes[124]. In the experiment, the potential at the disk electrode is scanned (voltammetric), while the ring electrode is kept at a certain potential (amperometric) to oxidize or reduce the analyte that is produced from potential scanning on the disk electrode and reached the ring electrode by pure diffusion. Figure 3.4 shows this voltammetric/amperometric experiment in 1 mM $Ru(NH_3)_6Cl_3$ 0.1 M KCl solution. When cathodic current on the disk electrode increases, the anodic current on the ring electrode starts increasing because of the oxidation of $Ru(NH_3)_6^{2+}$ that is produced from $Ru(NH_3)_6^{3+}$ reduction on the disk electrode.

The peak-shaped voltammogram on the disk (generator) electrode resembles that on a single electrode (Figure 3.2B) with a lower peak current value due to the difference in electrode area. The current-potential curve from the ring (collection) electrode, on the other hand, is sigmoidal reaching a steady-state beyond about -0.25 V. The collection efficiency, the ratio of the steady state current on the collector to the peak current on the generator (i_p = 0.215 μA), is 0.404±0.005. Note that this is a ratio of an amperometric steady-state current and a voltammetric peak current.

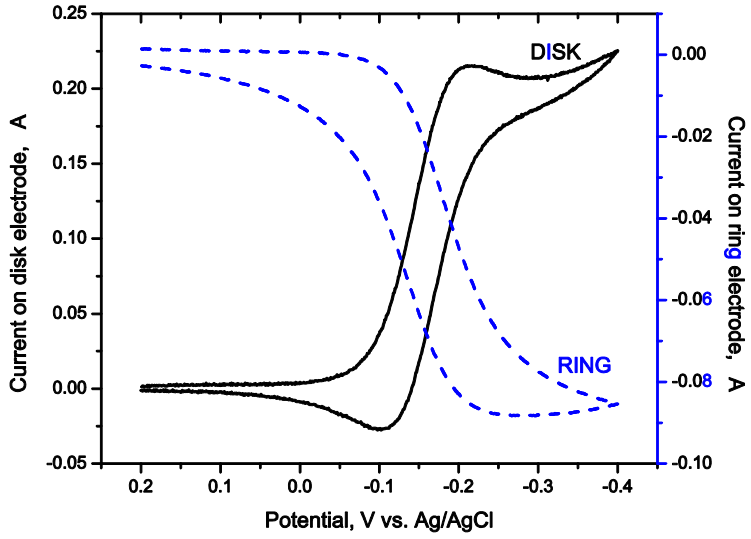

Figure 3.4 Voltammetric/amperometric experiment in 1 mM $Ru(NH_3)_6Cl_3$ 0.1 M KCl solution: cyclic voltammetry on the disk electrode (—), scan rate is 10 mV/s; amperometry on the ring electrode (---), potential = 50 mV.

The same experiment was repeated on another ring-disk electrode fabricated from a composite tube and rod with the same diameters (see supplementary Figure 3.7). The collection efficiency is 0.382±0.005. The very similar collection efficiency, and indeed the similarity of the current magnitudes, indicates the reproducibility of the electrode areas and the gap spacing between the disk and the ring electrode.

3.3.3 Carbon fiber composite ring-disk electrode detection of peptides following capillary HPLC

One application of the carbon fiber composite ring-disk electrode is using it as a dual-electrode detector for a flow system, e.g., flow injection analysis, capillary electrophoresis and liquid chromatography. Because the diameter of the disk electrode (480 μm) is in the same range of a

silica fused capillary lumen (tens to hundreds of micrometers), the ring-disk electrode should be readily applicable for a capillary HPLC separation system. In this experiment, the composite ring-disk electrode was assembled in a thin-layer radial-flow cell with the disk electrode centered and opposite to the flow inlet so that the flow impinges directly on the disk. The disk anode is the generator electrode while the ring cathode is the collector electrode.

Capillary HPLC separation of des-Tyr-Leu-enkephalin (GGFL) and Leu-enkephalin (YGGFL) is shown in Figure 3.5. The peptides (GGFL and YGGFL) are separated on the capillary column. The separated peptides react with biuret reagent in the post column reactor, where the basic copper tartrate solution yields electroactive copper-peptide complexes[26, 53, 54]. The biuret solution is an effective post-column derivatizing reagent for peptides. It interacts with the backbone of the peptides and is thus effective for peptides containing more than two amino acids. The resulting Cu(II)-peptide is oxidized to Cu(III)-peptide on the disk/generator electrode and reduced back to Cu(II)-peptide on the ring/collector electrode. The ratio of current on the collector electrode to that on the generator electrode is defined as collection efficiency. The difference in collection efficiency for GGFL (0.8) and YGGFL (0.05) results from the homogeneous chemical reactions that follow the anodic oxidation of YGGFL. We note that a similar ring-disk electrode showed a collection efficiency value near 0.40 in a voltammetric experiment. The large difference between the collection efficiencies in the quiescent solution experiment (0.40) and the flowstream experiment (0.80) results from the faster mass transport carrying the product of the disk electrode to the ring electrode in the latter case.

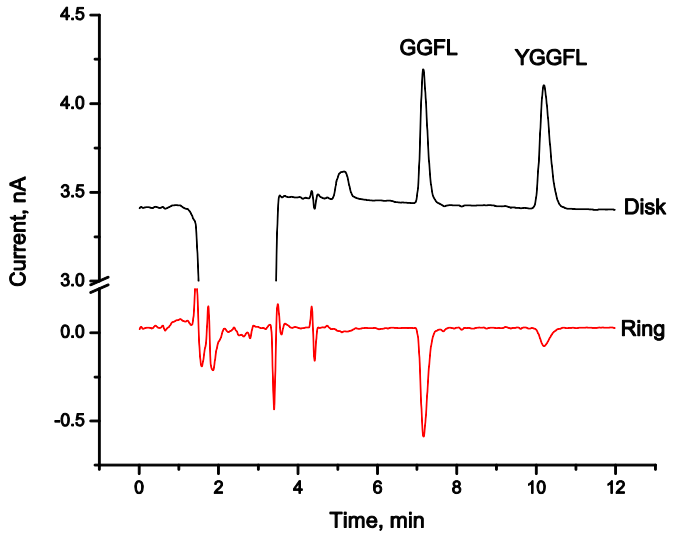

Figure 3.5 Chromatogram of a standard solution containing 1 µM GGFL and YGGFL. The potentials at the disk and the ring electrode are 0.6 V and 0.05 V, respectively.

The Cu-GGFL$^{3+/2+}$ reaction is a reversible one-electron redox process on the timescale of this experiment[132], which means that the current response on the collector electrode is controlled by mass transfer only. Ring-disk electrode and flow cell parameters, as well as flow velocities, affect the collection efficiency. In general, increasing the area of the downstream electrode and reducing the gap between two electrodes[124] are favorable for achieving high collection efficiency. The collection efficiency cannot be simply compared with literature values because of the differences in flow cell design (distance between flow inlet and the electrode), flow rate, etc. In one example of the ring-disk electrode fabricated through vapor deposition, the collection efficiency is reported to be ~0.3[119]. The limited collection efficiency is due to the fact that the ring electrode is only a thin CVD film. Ring-disk electrodes fabricated through micromachining have a higher collection efficiency (close to 0.9) because the gap is small (5 µm)[126].

The electrochemistry of Cu-peptide$^{3+/2+}$ is reversible, but there are possible complications especially for the peptides that contain the amino acids tyrosine and tryptophan. In the case of

YGGFL, the cathodic current on the ring electrode is much lower than for GGFL due to the homogenous chemical reaction that occurs after the oxidation of Cu(II)-YGGFL on the disk electrode. The current response on the disk electrode comes from the oxidation of Cu(II) to Cu(III). In addition, tyrosine can be oxidized at the disk. However, tyrosine oxidation is chemically irreversible on our experimental time scale. Thus, the only carrier of signal for the cathode is Cu(III). At the same time, there is an intramolecular reaction between Cu(III) and a reaction product resulting from the oxidation of the tyrosinyl residue[98] that forms an electroinactive product. The presence of the homogenous chemical reaction is responsible for the low current response on the collector electrode.

The results on the peptide solution demonstrate the ability of the ring electrode to emphasize signals from analytes that are chemically reversible. This is advantageous in biological sample analysis. There are many oxidizable species present in typical biological samples which would result in many overlapping peaks with single electrode detection. The fraction of oxidizable species that is chemically reversible is unknown, but small. The dual-electrode detection in the generator-collector mode enables selective detection of reversible species, e.g., Cu-peptide$^{2+/3+}$, as the chromatogram on the second (collector) electrode will be free from interfering peaks of irreversible species, thus reducing noise and increasing selectivity. The high collection efficiency ensures high sensitivity on ring collector electrode which is crucial for low concentration detection.

3.4 CONCLUSION

A carbon fiber/epoxy composite ring-disk electrode has been fabricated with thin gap between the disk and the ring electrode. The fabrication process is simple and does not require complicated machinery. The composite electrode is commercially available at very low cost and demonstrates well-behaved electrochemistry. The ring-disk electrode features high collection efficiency for electrochemically reversible species.

3.5 ACKNOWLEDGEMENTS

Support from the National Institutes of Health (GM 44842) is gratefully acknowledged. The authors thank Tom Gasmire for his assistance in making the Kel-F block for the ring-disk electrode. We also acknowledge helpful discussions with Professor Danny O'Hare, and the gift of the reversed phase packing material from Dr. Ed Bouvier at Waters.

3.6 SUPPORTING INFORMATION

This section contains supporting information (Figure 3.6 and 3.7).

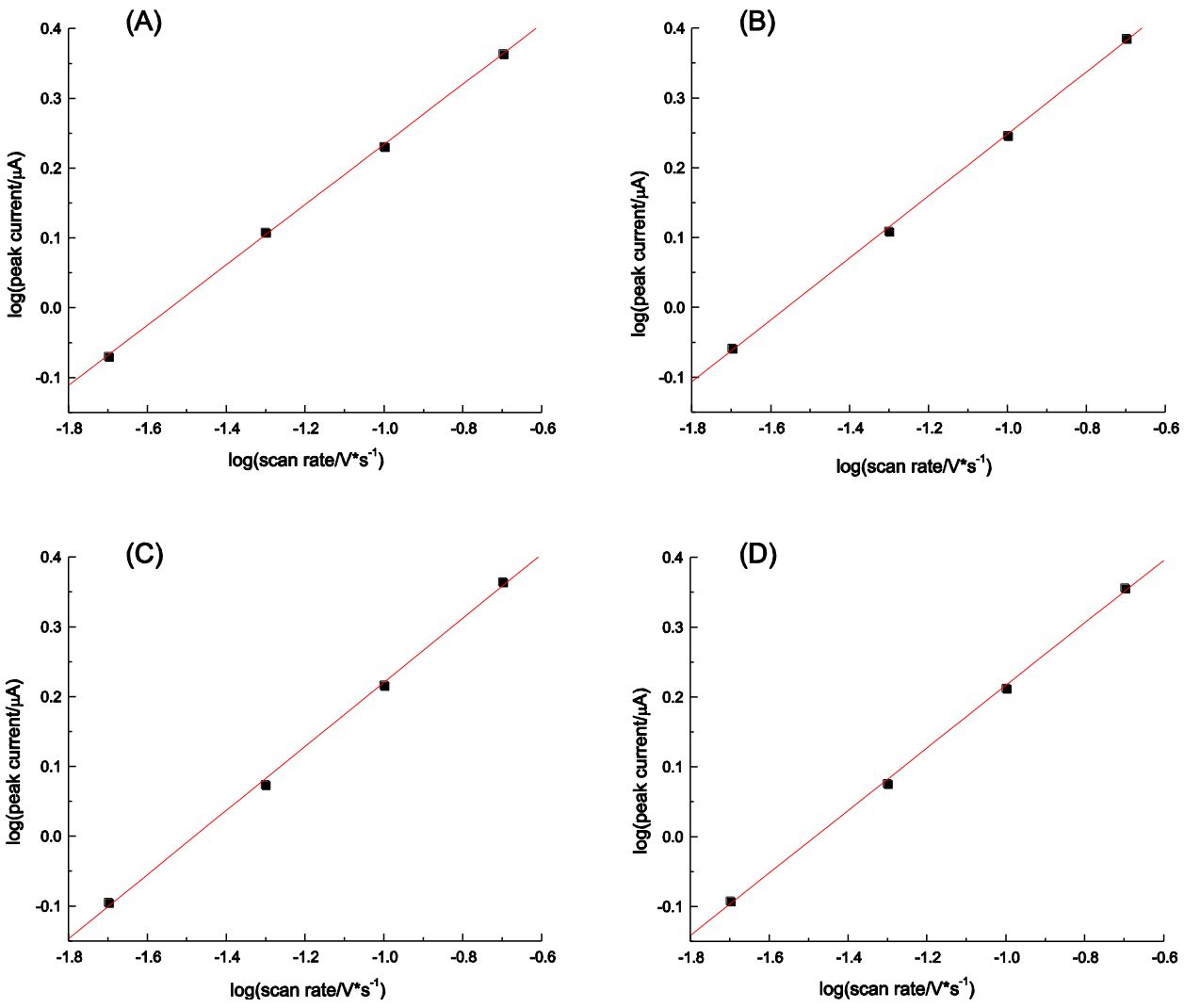

Figure 3.6 log(peak current) vs. log(scan rate) with linear fit: the carbon fiber/epoxy composite electrode in $Fe(CN)_6^{4-}$ solution (A) and $Ru(NH_3)_6^{3+}$ solution (B); a glassy carbon electrode in $Fe(CN)_6^{4-}$ solution (C) and $Ru(NH_3)_6^{3+}$ solution (D). $Fe(CN)_6^{4-}$ solution was 1 mM $K_4Fe(CN)_6$ 0.1 M KCl solution; $Ru(NH_3)_6^{3+}$ solution was 1 mM $Ru(NH_3)_6Cl_3$ 0.1 M KCl solution.

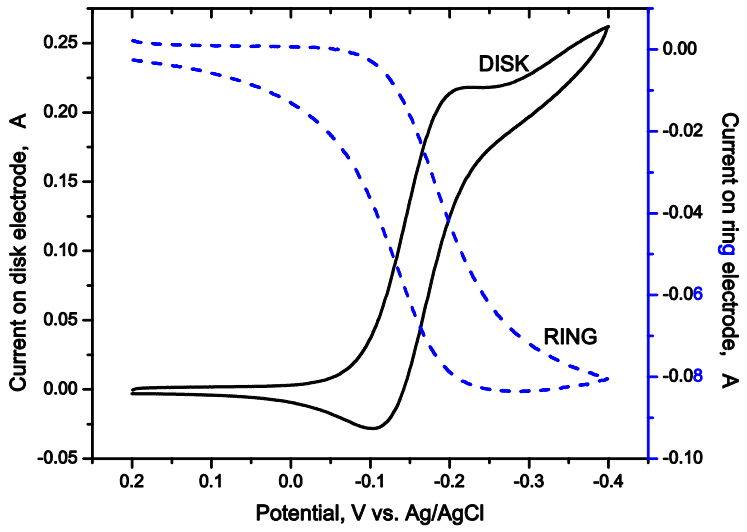

Figure 3.7 Voltammetric/amperometric experiment on a different ring-disk electrode. The experimental conditions are the same as those in Figure 3.4.

4.0 MODIFICATION OF A GOLD ELECTRODE FOR BIURET-BASED PEPTIDE AMPEROMETRIC DETECTION

4.1 INTRODUCTION

Our attempt to miniaturize the separation and detection system will lead us to the "lab-on-a-chip" field, so we need to consider both the chemistry and the technical feasibility in choosing electrode material. Carbon is widely used for electroanalytical purposes, due to its low cost, minimal fouling and wide useful potential range especially in the positive direction[133]. Carbon electrodes used in a microchip are usually in the forms of carbon fiber, carbon paste or carbon ink[134]. However, screen-printed carbon ink electrodes and carbon paste electrodes are not compatible with organic solvents, and carbon fibers are generally not rugged[135]. Metal electrodes, including gold, platinum, copper and palladium, are commonly used for microchip EC due to the relative ease with which they can be evaporated or sputtered[58]. One drawback to the use of metal electrodes is their tendency to become fouled when they are used for the detection of peptides, amino acid and biological samples. Chemically modifying the electrodes can change the surface properties of the metal electrodes. It is well known that gold can form covalent bond with thiols by self-assembly[136]. This method is advantageous: the process is simple which only involves immersing the electrode into a dilute thiol solution; the self-assembled monolayer is stable and can be easily removed when needed.

In the biuret-based peptide detection scheme, Cu(II)-peptide is oxidized to Cu(III)-peptide above 0.5 V vs. Ag/AgCl in pH 10 buffer. Gold gives high oxidative background current in that potential range, which makes quantitative peptide detection very difficult. Thus, there are some requirements in choosing appropriate thiol molecules to modify Au: 1) it should block gold surface from water to suppress background current; 2) electron transfer can still happen through the layer; 3) the modification material should be inert and stable in the media (mobile phase and biuret reagent). Alkanethiol, which is often used in gold modification, is not desirable because electron transfer can only happen through tunneling which is not sensitive enough for detection purpose. Aromatic thiol with extended and closed aromatic system, on the other hand, is possible because electron transfer can occur through delocalized π bond. Based on these concerns, aromatic thiol compounds seem to be a good candidate.

This part of the work will focus on two commercially available aromatic thiols, 4, 4'-dithiodipyridine and 2-naphthalenethiol. 4, 4'-Dithiodipyridine (PySSPy) will form 4-mercaptopyridine (PyS) monolayer on gold surface during the self assembly process[137].

4.2 EXPERIMENTAL

4.2.1 Reagents

Reagents and sources were as follows: 2-naphthalenethiol, 4, 4'-dithiodipyridine, ACS grade sodium carbonate and sodium bicarbonate, Sigma-Aldrich; disodium tartrate dihydrate and copper sulfate pentahydrate, J. T. Baker (Phillipsburgh, NJ); des-tyr leu enkephalin (GGFL), BACHEM (King of Prussia, PA).

The copper sulfate pentahydrate was recrystallized from water. The disodium tartrate dihydrate was recrystallized from dilute NaOH. All other reagents were used without further purification.

All solutions were made with Milli-Q (Millipore, Billerica, MA) house-deionized water.

4.2.2 Electrode pretreatment and thiol adsorption

Immediately before use, the electrode was polished successively with 1, 0.3 and 0.05 μm Buehler (Lake Bluff, IL) alumina in aqueous slurries, and ultrasonicated in Millipore water to remove alumina particles. Then it was rinsed thoroughly with Millipore water and ethanol before thiol modification.

The thiol monolayer was prepared by keeping the gold electrode in 10 mM 2-naphthalenethiol or 4, 4'-dithiodipyridine ethanol solution for 1 hour. After the adsorption of thiol, the electrode was rinsed with ethanol, then Millipore water.

Electrode surface cleaning before modification is crucial to the modification layer quality. Also, modification conditions, e.g. the solvent used to dissolve the modification molecules in and the immersion time, are important for the result. For example, short immersion times result in self-assemble monolayer with defects which allow easy water access to the surface and result in local oxide growth.

4.2.3 Cyclic voltammetry

Gold working electrode of 2 mm diameter (CH Instruments, Inc.) was used as the substrate for thiol modification test and CV characterization. The glassy carbon electrode used as comparison

was homemade. It was constructed by sealing glassy carbon (Sigradur) of 1 mm diameter in a glass tube with Torr Seal (Varian Vacuum Technologies). A platinum electrode was used as the auxiliary electrode, and an Ag/AgCl, 3 M NaCl (BAS, Model RE-5B) reference electrode was used and all the potentials were referred to it. The barrier property of the monolayer was studied using pH 10 buffer solution (0.24 M $NaHCO_3$ / Na_2CO_3). The Cu-peptide solution was prepared by adding peptide to the biuret reagent (0.24 M $NaHCO_3$, 0.24 M Na_2CO_3, 12.0 mM Na_2Tar and 2.0 mM $CuSO_4$) with the final concentration of 10 µM Cu-GGFL.

Cyclic voltammetry was also done on the cathode(downstream) electrode in a dual-electrode flow cell, while the potential on the anode(upstream) electrode was kept at an oxidative potential (600 mV vs. Ag/AgCl). The solution pumped through the flow cell was 50 µM Cu(II)-GGFL in the biuret reagent. The 3-mm-diameter dual gold working electrode block from BAS was used as working electrode. A BAS Epsilon EC potentiostat with Epsilon EC software was used to control and record the cyclic voltammograms. The electrochemical equipment was housed in a faradaic cage to reduce electronic noise. The potential ranges and scan rates used are shown in the respective diagrams.

4.3 RESULTS AND DISCUSSION

4.3.1 Electrochemistry of modified Au electrode

Cyclic voltammetry is used for electrochemical characterization of 2-naphthalenethiol modified gold electrode. Figure 4.1 shows the cyclic voltammograms of a bare gold electrode and a 2-naphthalenthiol modified gold electrode in the carbonate buffer solution and Cu(II)-GGFL

solution. At a bare gold electrode (Figure 4.1A), anodic current arises at a potential positive than 0.5 V vs. Ag/AgCl in the buffer solution, followed by the corresponding cathodic peak at approximately 0.3 V, indicating the gold oxidation and reduction. Scanning potential on the bare gold electrode in Cu(II)-GGFL solution gives an ill-defined cyclic voltammogram. Because the gold surface properties will change when the applied potential is above the gold oxidation onset value, the Cu(II)-GGFL/Cu(III)-GGFL redox is superimposed with the Au oxide formation/removal which complicates the voltammogram.

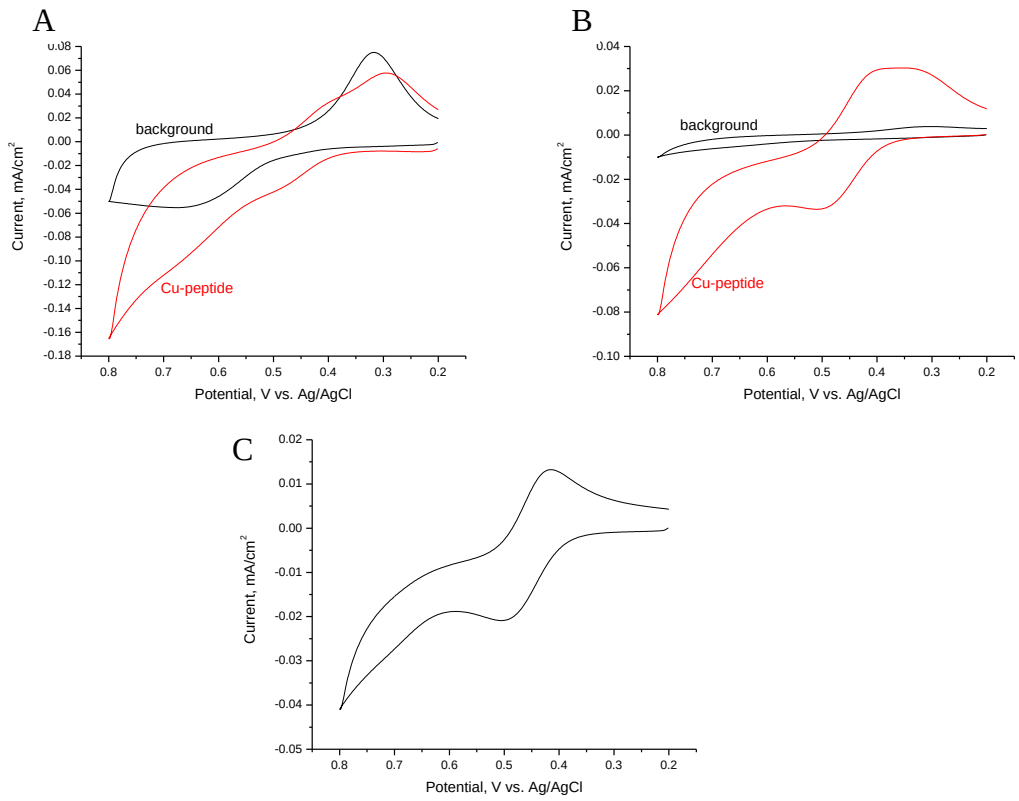

Figure 4.1 Cyclic voltammograms of different electrode surfaces in buffer and Cu-peptide solution (pH 10.4 carbonate buffer and 10 µM Cu-GGFL biuret solution).

Modification of Au electrode with 2-naphthalenthiol suppresses anodic current from gold surface oxide formation and thus the stripping peak from the surface oxide reduction (Figure 4.1B). It indicates that 2-naphthalenethiol forms a barrier-type film which prevents the formation

of anodic oxide on a gold electrode. Ideally, the monolayer is well-ordered and dense enough so that water cannot penetrate to the Au surface where its presence is required for oxide growth. This is similar to the behavior of self-assembled monolayer (SAM) of alkanethiol on gold surface[55, 138-144]. The cyclic voltammogram of the redox couple, Cu(II)-GGFL/Cu(III)-GGFL, shows well-defined redox peaks. There are two oxidative peaks in the voltammograms. This is in agreement with the rotating ring-disk electrode study[53] that there are two generic forms of the complexes, Cu(II)-NNNN and Cu(II)-NNNO, with respective $E_{1/2}$ values of 0.45 V and 0.7 V vs. Ag/AgCl.

The peak potential, peak shape and separation are similar to those on a glassy carbon (Figure 4.1C). However, the current density of the modified Au is higher than that of a glassy carbon under the same conditions. Previous research work on alkanethiol SAM shows that the integrity of the monolayer is seldom perfect[55, 139, 144]. Pinholes are usually present in the monolayer, so both the electrolyte and redox couple have access to the gold substrate at the pinholes. The behavior exhibited by the alkanethiol modified electrode with pinholes resembles a microarray electrode[145-147]. The proposed reason why the current density of 2-naphthalenethiol modified Au is higher than that of a glassy carbon is that the current response in this case is a sum of the pinhole microelectrode effect and the electron transfer through the monolayer. The electron transfer through the monolayer is much more effective than that through alkanethiol SAMs, because the tunneling process is highly facilitated through the delocalized π-electrons[148].

It is also known that 4, 4'-dithiodipyridine (PySSPy) can form 4-mercaptopyridine (PyS) monolayer on Au, which has been used to immobilize proteins for direct electrochemistry study[137, 149-151]. However, CV result (Figure 4.2) shows that Au oxide formation is not completely hindered on the PyS modified gold surface. In this case, it is hard to quantify the

current response generated from the electroactive species in the electrolyte. The CV results indicate that the pyridinethiol monolayer has more defects and is less dense compared to naphthalenethiol. In the case of well studied alkanethiol SAMs, it is known that the chain length has a significant effect on the structural properties of the monolayer: longer-chain alkanethiols form ordered films on gold because of increased van der Waals interactions between chains, and shorter-chain alkanethiols are generally more disordered[143, 152]. This can be one of the reasons why PyS monolayer quality is poorer than naphthalenethiol monolayer. Another possible reason is that PyS modified surface showed more hydrophilicity than the 2-naphthalenethiol modified surface due to the pyridine ring.

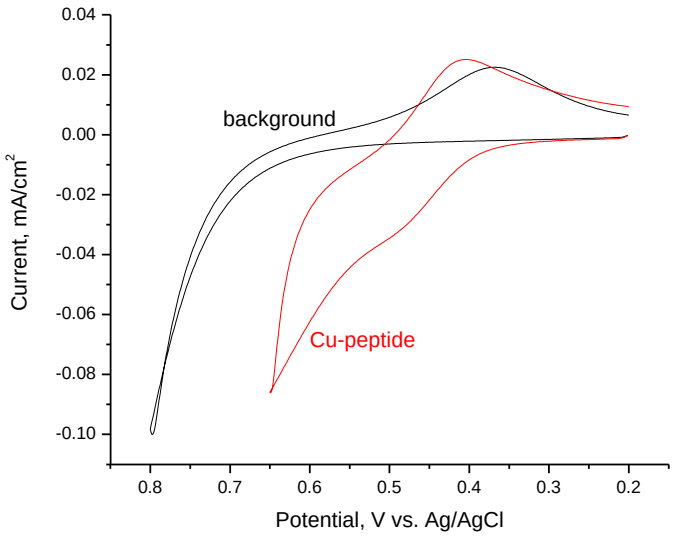

Figure 4.2 Cyclic voltammograms of a pyridine thiol modified Au in (a) pH 10.4 carbonate buffer and (b) 10 µM Cu-GGFL biuret solution.

Due to the above reasons, 2-naphthalenethiol is chosen over PyS to modify gold electrode and the following discussions are based on experiments done with 2-naphthalenethiol monolayer. It is expected that aromatic thiol with larger conjugated π system should form even more ordered

monolayer and have better conductivity because of decreasing band-gap (or HOMO-LUMO separation)[153]. But at the same time, the solubility decreases and synthetic routes become increasingly more difficult. Thus, anthracenethiol seems to be a promising molecule and its synthesis is relatively easy, which makes it a possible molecule to test in the future.

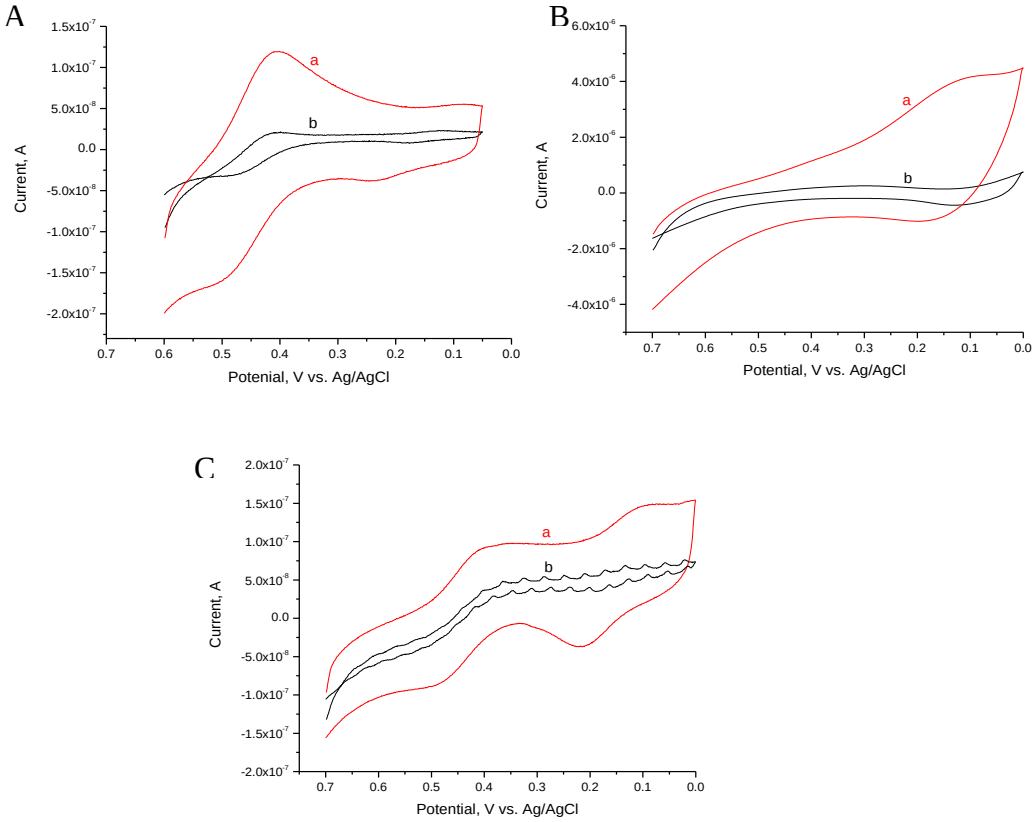

Figure 4.3 Cyclic voltammograms of the cathode in the flow cell at different scan rates (a 200 mV/s, b 20 mV/s) with potential on the anode kept at 700 mV vs. Ag/AgCl.

Voltammetry on 2-naphthalenethiol modified gold electrode is carried out in a flow cell in order to determine the optimal detection potential on the downstream cathode under the flow conditions. Based on the CV results in the quiescent solution, the potential on the upstream anode in the dual-electrode flow cell detector is set at a potential above 0.55 V vs. Ag/AgCl to oxidize Cu (II)-peptide, while the potential on the cathode is scanned from positive to negative (Figure 4.3A). There is a reductive peak at ~0.4 V vs. Ag/AgCl, which is expected to be the

reduction of Cu(III)-peptide. When the potential goes more negative, another reductive current peak appears at ~0.15 V, which can be attributed to Cu(II)-peptide/Cu(I)-peptide reduction. The standard $E_{1/2}$ for Cu^{2+}/Cu^{+} is 0.153 V vs. NHE[114], which equals -0.056 V vs. Ag/AgCl. However, by the presence of ligand, peptide in this case, the reduction potential of Cu^{2+} shifts. It was found that the Cu(II) is reduced to Cu(I) at 0.096 V vs. Ag/AgCl in the presence of Ac-PHGGGWGQ-NH_2, a unit of the octarepeat peptide of the prion protein[129]. The results are comparable to those on a glassy carbon electrode (Figure 4.3C), while no apparent reduction peak can be seen on a bare Au electrode (Figure 4.3B).

4.3.2 Capillary liquid chromatography

Results in the previous section give the criteria for choosing appropriate potentials for peptide detection following capillary liquid chromatography separation. Figure 4.4 shows the simple chromatograph of GGFL detected using bare Au and 2-naphthalenethiol modified Au. A bare gold electrode gives very high background current and the signal is very low. 2-naphtalenthiol modified Au shows good detection trace and the signal current is comparable to that on a glassy carbon electrode.

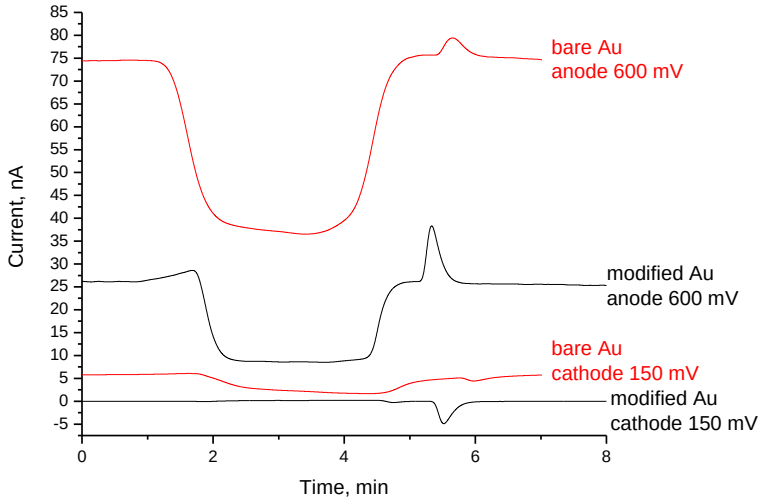

Figure 4.4 Chromatograms of 1 µM GGFL with bare Au and 2-naphthalenethiol modified Au.

4.3.3 Stability of 2-naphthalenethiol modification monolayer

The chromatogram shows that 2-naphthalenethiol modified Au electrode works well in biuret based peptide detection. However, stability of the modified electrode needs to be tested before it can be used in routine detection work. The stability test is done by repeating sample injections and recording the current response over time. The potential was kept on with flow running through the cell within the same day of experiments. The current decreases by about 5% over 3 hours (Figure 4.5) on the first day, which shows fairly good stability of the modification layer. However, the current decays exponentially over days (Figure 4.6). During these days, the flow was kept running through the flow cell but the potential was turned off between days. Current difference within a day of experiments on the 2nd and the 3rd day shows faster deterioration of the modification layer with the applied potential.

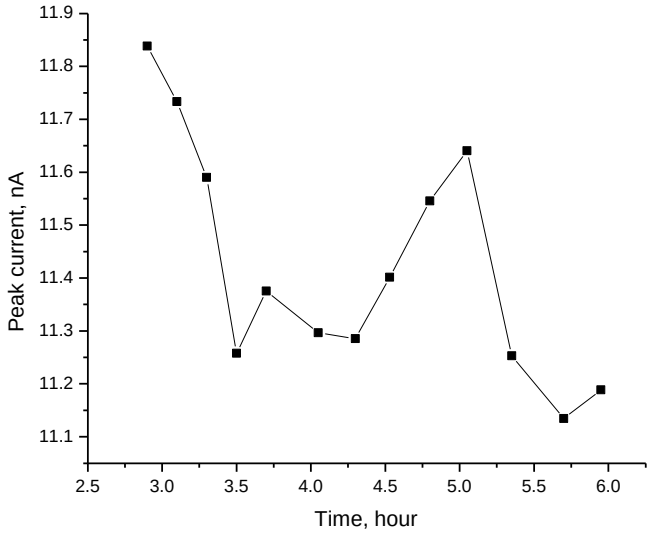

Figure 4.5 Current response of repeated GGFL injection on modified Au electrode over hours.

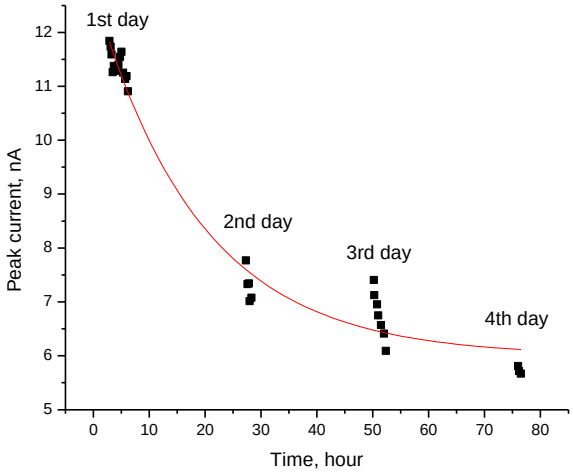

Figure 4.6 Current response of repeated GGFL injection on modified Au electrode over days.

The possible reason for deterioration is the change of modification layer structures over time, with the modification monolayer becoming less ordered or even desorbed from the Au

surface. The modified electrode is exposed to the biuret reagent/mobile phase flow, which is basic with pH value of 10. It is known that alkanethiol head group is electrochemically oxidizable or reducible in strong base[94, 154]. The reductive desorption, $AuSR + 1e^- \rightarrow Au(0) + RS^-$, has a half wave potential of -0.9 V vs. Ag/AgCl in 0.5 M KOH. The oxidative desorption is related to the reaction $AuSR + 2H_2O \rightarrow Au(0) + RSO_2^- + 3e^- + 4H^+$, which has a half wave potential of 0.9 V vs. Ag/AgCl in a pH 10 buffer. So it is possible that the naphthalenethiol desorbs from the gold surface in the basic buffer over time. But as long as the applied detection potential is not extremely positive or negative, the desorption process is fairly slow. Based on the experimental results, the modification monolayer can last for hours without significant sensitivity loss. Thus, the best approach is to perform gold surface cleaning and monolayer assembly each day before assembling the detector flow cell in order to achieve optimal results. Another possible solution is to add a small amount of thiol to the LC eluent, which is expected to inhibit the thiol molecules from desorbing from the electrode surface due to the dynamic exchange of the surface immobilized thiol with the thiol in the solution.

4.4 CONCLUSION

Self-assembled naphthalenethiol monolayers on a gold electrode suppress the background current from Au which would otherwise interfere with amperometric detection of peptides. The modified gold electrode is used in a capillary HPLC-ECD system and is proved to have sensitivity comparable to a glassy carbon electrode. Aromatic thiols with more conjugated benzene rings can improve the modification quality, including higher electron transfer rate and

fewer defects, and replacing naphthalenethiol with anthracenethiol for gold modification is expected to improve the electrode performance and stability.

5.0 DEVELOPMENT OF A CAPILLARY UHPLC-ECD SYSTEM FOR THE FAST ANALYSIS OF SEROTONIN IN MICRODIALYSATE SAMPLES

5.1 INTRODUCTION

Serotonin, also known as 5-Hydroxytryptamine or 5-HT, is a monoamine neurotransmitter synthesized in the serotonergic neurons of the central nervous system and the enterochromaffin cells of the gastrointestinal tract[155]. In the central nervous system, serotonin is stored in secretory granules and released from presynaptic neurons[155] into a synapse upon arrival of an action potential. In a synapse, it binds to specific receptors on the membrane of the postsynaptic cell and leads to a change in ion permeability of the membrane, which can thus generate an action potential and a sequence of these events constitutes neurotransmission. Serotonergic neurotransmission affects a wide range of behaviors, from food intake and reproductive activity, to sensory processing and motor activity, to cognition and emotion[156]. One key regulator is the serotonin transporter (SERT) located in the membrane of presynaptic neurons, which removes extracellular serotonin from the synaptic cleft and the action of serotonin is thus terminated[157]. Serotonin transporter is the site of action of selective serotonin reuptake inhibitor (SSRI) antidepressants (i.e., clomipramine, fluoxetine, citalopram and paroxetine) and some illicit drugs (i.e., cocaine and 3,4-methylenedioxymethamphetamine (MDMA))[158] which bind to the transporter protein with high affinity and inhibit serotonin reuptake or cause reverse transport.

The SERT protein is encoded by a single gene, SLC6A4[156], and its polymorphism has been linked to a poor response to SSRIs and the side effects in some individuals[159-161].

Monitoring the serotonin level in the extracellular brain fluid is an important approach to understanding serotonin neurotransmission and the therapeutic treatment which targets its malfunction, for example, SSRI antidepressants affect SERT and result in an increase of serotonin level in the extracellular fluid. In genetically engineered SERT-deficient mice, i.e., SLC6A4 knockout ($SET^{-/-}$) mice, serotonin level in the extracelluar fluid is elevated compared with wildtype ($SERT^{+/+}$) mice[162]. Measurement of serotonin level includes its basal concentration and its changes above or below baseline level over time. In order to meet these requirements, an analytical system has to be sensitive enough to detect its baseline level and fast enough to capture the dynamics. Carbon fiber microsensors are microelectrodes placed directly inside the brain. When coupled with fast scan cyclic voltammetry (FSCV) technique, carbon fiber microsensor has very high temporal resolution (milliseconds to seconds)[51, 163]. However, it is not able to measure baseline 5-HT concentration due to the fact that the FSCV background current at a carbon fiber microelectrode drifts over time[164]. In addition, its selectivity is limited due to the fact that extracellular components are not separated. A different approach is to sample extracellular fluid followed by analysis. Microdialysis is a commonly adopted sampling technique as it poses minimal disturbance to the studied biological subject and is effective in obtaining protein free microdialysate samples. Analysis of microdialysate samples can reveal crucial information including the basal concentration of serotonin and the dynamic changes in the extracellular fluid. Prior to detection, separation of microdialysates sorts the components and thus improves the method selectivity. Compared with capillary electrophoresis (CE) which is suited to small volume samples[165, 166], high pressure liquid chromatography (HPLC) is a much

better choice for separating and measuring serotonin from brain dialysate samples because of its superior robustness, reproducibility, and wide acceptance among neuroscientists.

The temporal resolution of the microdialysis-HPLC system defines its ability to monitor the dynamic changes of serotonin level in the extracellular fluid[4]. For an off-line system, i.e., collecting the microdialysis sample in aliquots and then injecting them to the HPLC system, the HPLC sample volume, therefore the microdialysis sample collection time, determines the system temporal resolution. By using a capillary system to reduce dilution of chromatographic separation, the sample volume requirement is highly reduced from conventional 20 μL to 500 nL (the sample loop volume of our system), thus reducing sampling time from minutes to seconds, i.e, from 20 minutes to 0.5 min when microdialysis sampling rate is 1 μL/min. For an on-line system where sample collection, injection, and separation-detection are all integrated on one system in a continuous fashion, the separation time has to be equal or shorter than the sampling time in order to avoid overlap between the samples. Thus, a fast HPLC analysis of serotonin is necessary. Several parameters can be utilized to speed up the separation speed while maintaining sufficient separation efficiency. Two parameters used in this study are ultra high pressure (also called UHPLC) and elevated temperature, thanks to the availability of new commercial stationary phases which can withstand high pressure and elevated temperature without compromising the performance[167].

Sensitivity of the analysis system is determined by the detector following separation. Electrochemical detection is simple, sensitive and compatible in nature with serotonin as it is electroactive without the need for derivatization. A carbon fiber microelectrode inserted directly into the capillary lumen as the detector is commonly used in the capillary separation system[6]. While it reduces the post-column band broadening to a minimum, the carbon fiber electrode is

fragile and unstable. An electrochemical flow cell, on the other hand, usually has a relatively large cell volume, which will compromise the separation efficiency achieved in the capillary column and reduce system sensitivity. Our approach is to modify a commercial electrochemical flow cell to minimize the dead volume while paying close attention to electrode surface treatment to increase sensitivity.

5.2 EXPERIMENTAL

5.2.1 Chemicals and Materials

Sources of chemicals were as follows: serotonin hydrochloride, dopamine hydrochloride, 5-hydroxyindole-3-acetic acid (5-HIAA), 3,4-dihydroxyphenylacetic acid (DOPAC), homovanillic acid (HVA), 3-methoxytyramine hydrochloride (3MT), 5-hydroxy-N-methyltryptamine and sodium 1-octanesulfonate (SOS) were from Sigma (St. Louis, MO); tetraglycine (GGGG) was from BACHEM (King of Prussia, PA); disodium EDTA was from Fisher Scientific (Fairlawn, NJ); sodium acetate was from MCB (Cincinnati, Ohio). Acetonitrile (ACN) was HPLC grade and was purchased from Fisher (Springfield, NJ). The copper sulfate pentahydrate was recrystallized from water. The disodium tartrate dihydrate was recrystallized from dilute NaOH. All other reagents were used without further purification. Solutions were made with 18 MΩ purified water from a Millipore synthesis A10 system (Millipore, Billerica, MA).

Fused silica capillaries were purchased from Polymicro Technologies, LLC (Phoenix, AZ). The stationary phases (2.6 μm XTerra C18 and 1.7 μm BEH C18) were generous donation from Waters (Milford, MA).

5.2.2 Flow injection

The aqueous flow solution containing 0.24 M $NaHCO_3$, 0.24 M Na_2CO_3, 12.0 mM Na_2Tar and 2.0 mM $CuSO_4$ was pumped with a Harvard Apparatus (Holliston, MA) pico plus syringe pump and 5 mL Hamilton (Reno, NV) Gas tight syringe. Three different flow rates were used: 10 μL/min, 15 μL/min and 20 μL/min. A VICI 6-valve injector from Valco Instrument (Houston, TX) was used for sample injection with an injection volume of 10 μL. The sample was prepared by adding GGGG to the flow solution (biuret reagent) with the final concentration of 10 μM Cu-GGGG.

Potential was controlled with a BAS (West Lafayette, IN) Epsilon LC potentiostat. An Ag/AgCl, 3 M NaCl (BAS, Model RE-5B) reference electrode was used and all the potentials were referred to it.

Data were imported into Origin 7.5 (OriginLab Corporation) for differentiation, then exported to PeakFit version 4 (AISN Software, Inc.) for determination of the first and second central moments, which represent time and the standard deviation, respectively. The statistical moments were determined by fitting the 5-parameter GEMG function to the data based on the least squares criterion[27].

5.2.3 Capillary UHPLC

The capillary UHPLC system has been described in a previous publication[6] and is briefly summarized. Standard solutions of neurotransmitters (5HT and DA) and acidic metabolites (HVA, DOPAC and etc.) were prepared by successive 10-fold dilutions of stock solutions (1 mM in 0.1 M acetic acid) with 0.1 M acetic acid, except for the final dilution where artificial cerebrospinal fluid (aCSF) was used. The aCSF solution contained (in mM) 147 NaCl, 3.5 KCl, 1.0 $CaCl_2$, 1.2 $MgCl_2$, 1.0 NaH_2PO_4, and 2.5 $NaHCO_3$ at pH 7.4. Mobile phase was 100 mM NaOAc, 0.15 mM Na_2EDTA, 10 mM SOS, pH 4.0, mixed with either 10% or 4% ACN. The pH of the aqueous buffer was adjusted with glacial acetic acid or concentrated NaOH solution to the desired pH. The pump used to deliver mobile phase was Nano LC-1D plus pump from Eksigent Technologies (Dublin, CA) at flow rates from 0.1-10 μL/min without a splitter with operating pressures as high as 10,000 psi. A Valco 10-port valve, which can withstand pressures up to 15 000 psi, was used for manual injections. The fused silica capillary sample loop was 500 nL. Capillary columns were slurry packed with either XTerra or BEH C18 particles using 100 μm ID, 360 μm OD fused-silica capillaries as column blank. The capillary column and the injector were equipped with two separate custom-built heaters to control column and mobile phase temperatures.

5.2.4 Electrochemistry

The cyclic voltammetry was conducted in a three-electrode quiescent electrochemical cell, composing of a 1-mm-diameter glassy carbon electrode, a platinum gauze electrode as the

auxiliary electrode and a Ag/AgCl reference electrode. A BASi Epsilon potentiostat was used to control and record the voltammetry.

The electrochemical detector for capillary UHPLC was composed of a BASi radial-style thin-layer auxiliary electrode (West Lafayette, IN), a 13 μm thick Teflon spacer, and a custom-built 1 mm diameter glassy carbon electrode block. The thin spacer provides a detector volume that minimizes band broadening in the flow cell. The glassy carbon electrode was fabricated by securing the glassy carbon rod in the center of a Kel-F block with Spurr low viscosity epoxy resin (Polysciences, Inc., Warrington, PA), which was allowed to cure at 70 °C for at least 8 h. Electrical contact was made by connecting the glassy carbon electrode to a metal pin using silver epoxy H20E (Epoxy Technology Inc., Billerica, MA), which was cured at 80 °C overnight. The electrochemical detector was housed in a Faraday cage. A short length of 25 μm ID fused silica capillary acted as a connecter between the column and the detector. A BASi Epsilon potentiostat controlled the detection potential at +0.7 V vs Ag/AgCl (3 M NaCl).

A newly fabricated glassy carbon electrode was polished on a metallographic polisher SS-1000 from Buehler (Lake Bluff, IL) using diamond paste then γ-alumina slurry with successively smaller particle sizes. A stream of distilled water was directed at the electrode to eliminate frictional heating[168]. Each day before assembling the electrochemical cell, the electrode block was hand polished with 0.05 μm alumina slurry and sonicated with deionized water.

5.3 RESULT AND DISCUSSION

5.3.1 Electrochemistry of serotonin

Cyclic voltammetry is used as a tool to examine the electrochemical behavior of serotonin which is dissolved in the mobile phase solution used for chromatographic separation. The same experiment is also conducted on dopamine solution for comparison purposes. Figure 5.1 shows the cyclic voltammograms of serotonin and dopamine at a scan rate of 50 mV/s. Electrochemical oxidation of serotonin occurs at 0.53 V vs. Ag/AgCl, while the reduction happens at around -0.10 V. It is known that oxidation of serotonin is a two-electron process, producing quinone imine as the main product[169]. However, the serotonin oxidation electrochemistry is complex, yielding many side-products, as well as post-electrochemistry chemical reactions[170]. Thus, serotonin electrochemistry is not reversible: reduction happens at a much more negative potential with a decreased cathodic current. Electrochemical oxidation of dopamine is also a two-electron process, with dopamine *o*-quinone as the oxidation product[164]. Compared with serotonin, cyclic voltammogram of dopamine gives reversible redox peaks. The oxidation potentials for both serotonin and dopamine are pH dependent, as the electrooxidations of these compounds involve deprotonations. Because the typical mobile phase condition that is used in this study is acidic, potential for the oxidation is moved to a more positive value compared to most literature reported values which are typically conducted under a physiological pH. The surfactant that is present in the mobile phase to enhance chromatographic retention will facilitate the electron transfer between electrode and solution especially for biomolecules due to the synergistic adsorption mechanism[171, 172].

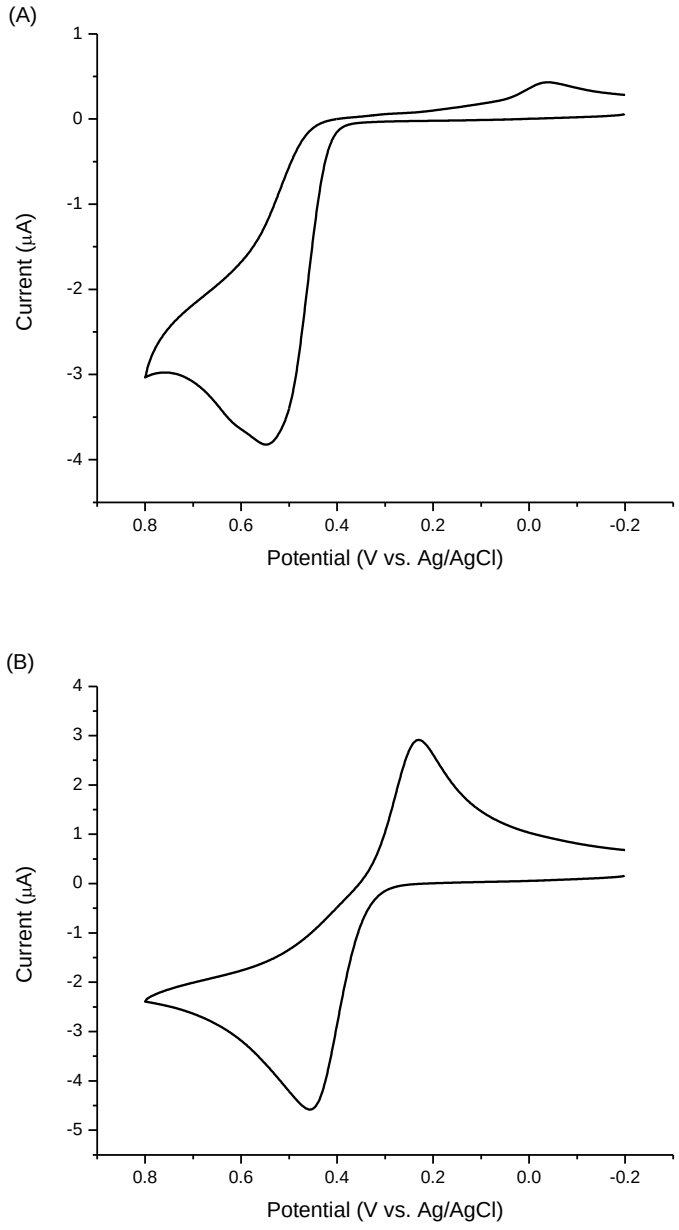

Figure 5.1 Cyclic voltammograms of 2 mM (A) serotonin and (B) dopamine solution on a glassy carbon electrode. Glassy carbon electrode is 1 mm in diameter. Both serotonin and dopamine were dissolved in a typical mobile phase solution: 100 mM NaOAc, 0.15 mM Na_2EDTA, 10 mM SOS, pH 4.0, mixed with 10% acetonitrile. Scan rate is 50 mV/s.

When it is first fabricated, the working electrode is polished using a high-speed metallographic polisher with successively smaller particle size diamond paste and γ-alumina slurry. It is shown in the literature by electron spectroscopy that the highly polished electrodes have a higher oxygen content in the outer 20-30 nm than in the bulk material or in unactivated electrodes[168]. After the initial extensive preparation, only brief repolishing with 0.05 μm alumina slurry between experiments is sufficient to active the electrode surface. Sonication following polishing removes traces of polishing materials from the surface. At this point the glassy carbon had a shiny, mirror like appearance. Mechanical polishing and ultrasonic cleaning yield reproducible activation for glassy carbon electrodes. Satisfactory electrode behavior is shown from the CV result, especially compared with previous literature results on glassy carbon electrode[173].

In order to achieve sufficient system sensitivity, the electrochemical detector has to preserve separation efficiency achieved in the capillary column by minimizing post-column band spreading. A thin-layer cell is the most popular design for HPLC detectors due to the ease of achieving a small volume. Thin-layer cells can be constructed in two ways: cross flow where the fluid flows parallel to an electrode imbedded in a rectangular channel; or radial flow where the fluid stream is directed perpendicular to the electrode surface followed by radial dispersion. The electrode surface is part of the channel wall formed by sandwiching a fluorocarbon gasket between two blocks: working electrode block and auxiliary block which also contains flow inlet/outlet and reference electrode compartment. Figure 5.2A is a photograph of the assembled cell, while Figure 5.2B, C, and D illustrate the radial flow geometry on the auxiliary block, the gasket and the working electrode, respectively. The gasket thickness defines the channel height and the thinnest available gasket (0.0005 inch or 12.7 μm) is chosen in order to reduce cell

volume. Although total detector volume is determined by the channel volume, the "effective" cell volume is calculated from electrode area and channel height. By using a smaller working electrode (1 mm in diameter), the effective cell volume is reduced to 10 nL, which should be compatible with capillary columns without compromising column efficiency.

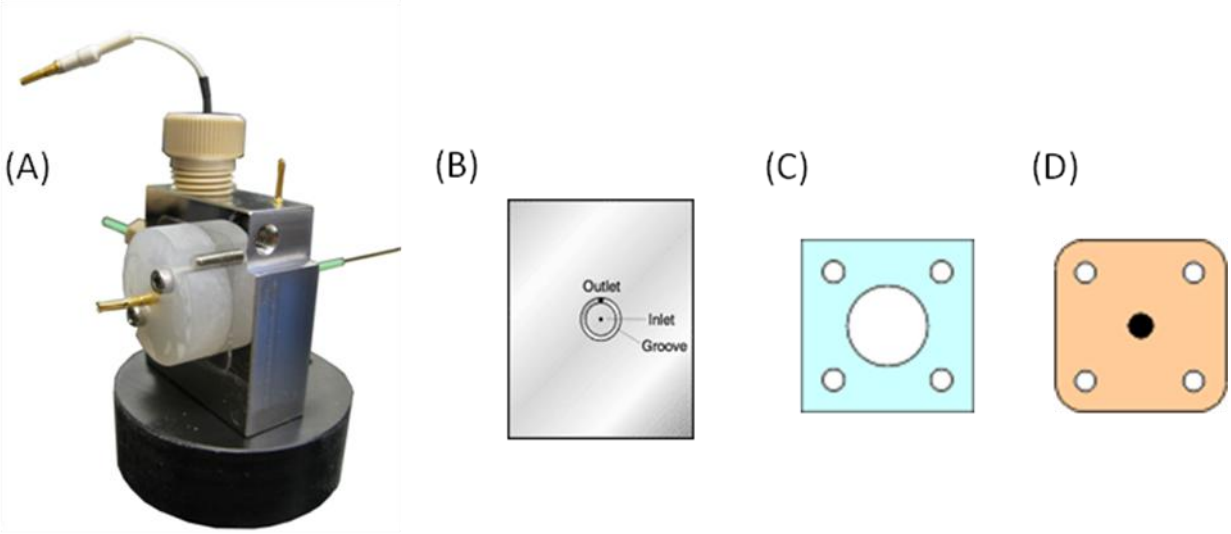

Figure 5.2 The electrochemical flow cell detector. (A) a photograph of the assembled cell; (B) illustration of the auxiliary electrode block showing the radial flow design; (C) the gasket/spacer; (D) the working electrode.

The effect of extra column band broadening in a microchromatographic system can be quantified using a simple method based on flow injection experiments developed by the Weber lab[27]. In this method, a large sample loop is used to produce a steady-state signal that can be differentiated to yield two peaks. Based on the slope of the first and second central statistical moments (time t and standard deviation σ_t^2) of the peaks under different flow rates, the experimental plate height in units of time, "plate time" H_t, can be determined. By comparing the theoretical with experimental values, one can decide whether there is significant band spreading in the system, which is believed to be mainly from the end-column flow cell.

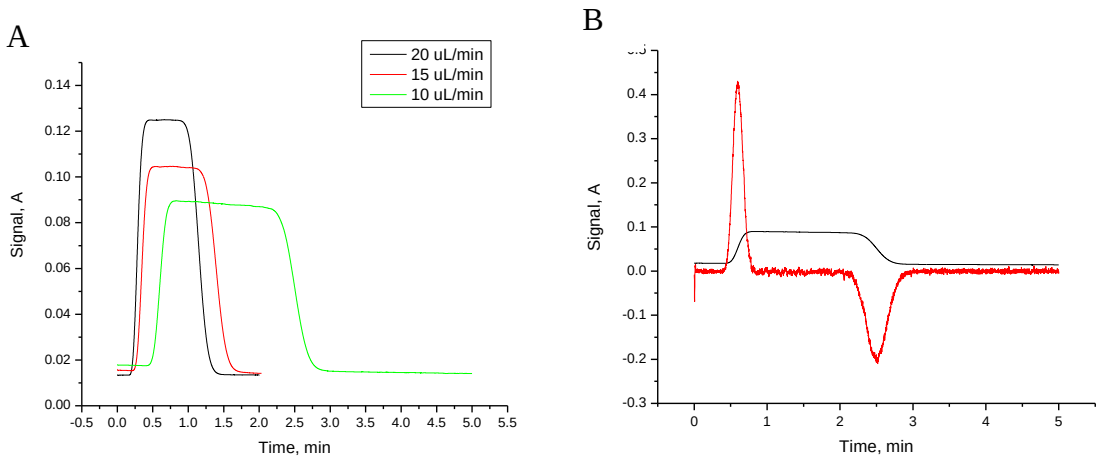

Figure 5.3 Flow injection and data analysis: (A) Flow injection analysis of 10 µM Cu-GGGG. (B) A data trace and the first derivative.

Figure 5.3A shows the signal response at three different flow rates with an injection volume of 20 µL. Flow injection experiments are repeated at least three times for each flow rate. Differentiation of the signal response yields the first derivative of the data trace shown in Figure 5.3B. Sample injection generates a plateau with two steps, which are differentiated to yield two peaks. The following calculation is based on the first step and the corresponding derivative, because the second step includes the information of extra bandspreading caused by diffusion in the loop.

The relationship between the first and the second moments is plotted in Figure 5.4. Linear fit of the data gives the equation, $y = 0.00781x + 0.00039$, $R^2 = 0.994$. The experimental value of the "plate time" H_t is the slope, 0.00781. The theoretical "plate time" can be calculated[27], $H_t = a^2 / 24D$. The capillary radius, a, is 75 µm. The diffusion coefficient, D, of Cu(II)-GGGG is found to be (3.96 ± 0.14) × 10^{-6} cm^2/s in rotating ring-disk electrode study[53]. Based on these two values, a = 75 µm, D = 3.96×10^{-6} cm^2/s, the "plate time" H_t is calculated to be 0.00986 min.

The theoretical value, 0.00986 min, and the experimental value, 0.00781 min, are close, indicating there is some but not significant extra-column band spreading from the detector.

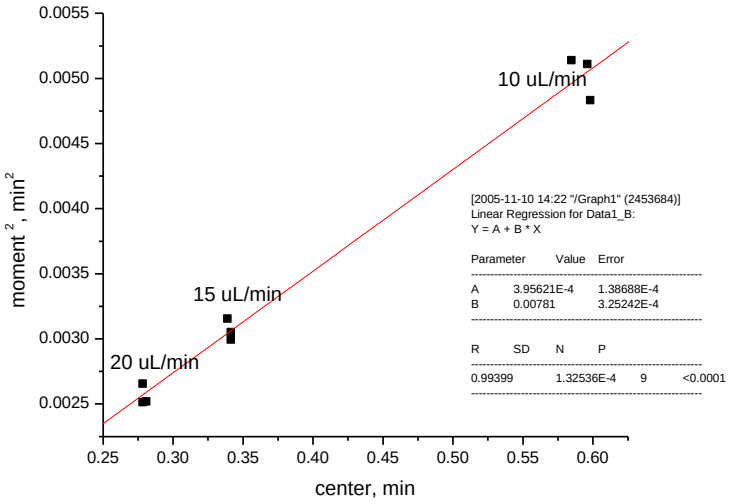

Figure 5.4 Relationship between second central moment and first central moment

5.3.2 Fast separation of serotonin by capillary UHPLC

Reverse-phase ion-pair chromatography is efficient for analyzing biogenic monoamines in rat brain dialysates[57, 174, 175]. For reverse phase separation, mobile phase is acidic (pH = 4) due to the poor stability of silica based columns under a basic environment. The amine functional group in serotonin is protonated under this condition and makes it difficult to retain on the stationary phase. However, when paired with a lipophilic counterion, e.g., sodium octyl sulfate (SOS), charged serotonin forms the neutral complex which helps to retain on a C18 stationary phase. In a typical rat brain dialysate sample, serotonin coexists with acidic metabolites which are usually much more abundant than biogenic monoamines. Metabolic acids interfere with serotonin separation and quantification as the small serotonin peak can be buried by huge peaks of

metabolic acids. Thus, a high concentration of SOS (> 10 mM) is used to retain the monoamines even longer in the column so that they can be distinguished from acidic metabolites. On the other hand, the content of organic modifier, e.g., acetonitrile (ACN), is adjusted to a low percentage (10%) in order to prevent a lengthy separation process. Separation of serotonin from metabolites and other biogenic amines is successfully achieved within 6 minutes using capillary HPLC[57].

Increasing flow rate speeds up the chromatographic process. Compared with a conventional HPLC pump, the UHPLC microfluidic pump capable of delivering fluid at low μL/min to nL/min flow rate range (e.g., Nano LC-1D plus system from Eksigent) can pump against back pressures up to 10,000 psi. Moreover, increasing column temperature reduces mobile phase viscosity and thus lowers the back pressure generated in the column. Figure 5.5 shows the separation of serotonin in a standard mixture that mimics the content of a microdialysate sample, including acidic metabolites (HVA, DOPAC and 5HIAA) and other amines (DA and 3MT). With a higher flow rate (3 μL/min) at an elevated column temperature (50 °C), serotonin elutes within 3 minute and is separated well from other analytes. Other than increasing separation speed, factors like flow rate and temperature also affect separation efficiency. Our goal is not only to shorten analysis time, but also maintain sufficient efficiency to achieve satisfactory separation. Small (sub-2 μm) packing particles have gained substantial popularity as they are capable of improving separation speed and efficiency at the same time. However, the trade-off is higher back pressure. In fact, maximum pressure drop allowed by a chromatographic system is one of the basic limitations on chromatographic analysis efficiency and speed. To effectively optimize all the available system configurations, including pressure, temperature, particle size and column length, Poppe plot or kinetic plot is used as the theoretical guidance in order to minimize tedious experiment work. The result and the detailed discussion

are shown in the recently published paper[6]. Each curve represents the shortest time-per-theoretical-plate, t_0/N, that can be achieved given a certain number of theoretical plates, N, using the given HPLC configuration. It is predicted based on the Poppe plot that serotonin retention time can be reduced to less than 1 minute using a 1.7-μm C18 column at elevated temperature (70 °C) with plate count N = 4000 to achieve the needed separation. This prediction is confirmed by experimental results showing the separation of serotonin within 1 minute using a capillary column packed with 1.7 μm C18 particles[6].

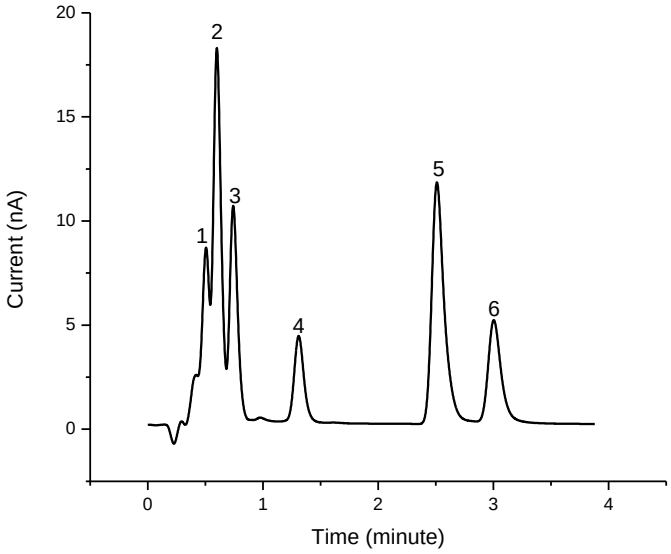

Figure 5.5 Separation of standard mixture containing 1 μM (1) HVA, (2) DOPAC, (3) 5HIAA, (4) DA, (5) 5HT and (6) 3MT. The chromatographic conditions are: injection volume is 500 nL; sample is dissolved in aCSF solution; flow rate is 3 μL/min; column temperature is 50 °C; column is 100 μm-ID and 7.6 cm long packed with 2.6 μm Waters XTerra C18 stationary phase.

Under the established UHPLC system configurations, fast and sufficient separation of serotonin is successfully achieved. Figure 5.6 is a calibration curve showing linear fit for detector

signal (current) versus concentration (0.5, 1, 2 and 10 nM), which guarantees quantification. As microdialysate sample is aqueous, i.e., the sample solution is a weak mobile phase in the case of reverse phase separation, the analytes have a higher capacity factor under the injection conditions and thus pre-concentrate on-column, which improves the concentration limit of detection (LOD)[176]. The 500-nL sample volume, larger than the column volume, helps improving the concentration LOD by taking advantage of pre-concentration. The LOD under this condition is about 0.07 nM calculated on the basis of three times the standard deviation of the noise level around the serotonin peak. This sensitivity was sufficient to measure baseline levels of 5-HT. The detection limit can be further decreased by increasing the detector sensitivity. As the electrochemical detection of serotonin is proton coupled reaction, its interactions with certain functional groups on the surface may lead to an increase in sensitivity. Surface modification method of carbon electrode includes carbon nanotubes, anionic polymer (e.g., most commonly Nafion) and molecular layers.

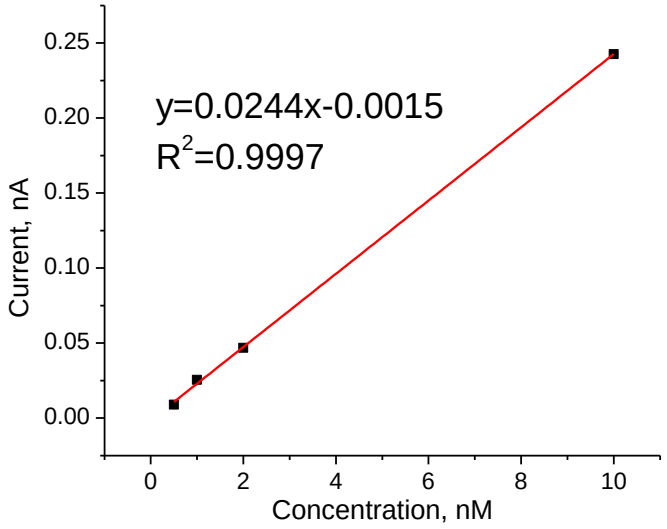

Figure 5.6 Calibration curve of serotonin UHPLC-ECD analysis. The concentration of serotonin is 0.5, 1, 2 and 10 nM in aCSF solution.

5.3.3 Quantization of serotonin in microdialysate samples

Before analyzing microdialysate samples, the UHPLC-ECD system is calibrated with serotonin aCSF standard solution. Figure 5.7A shows the chromatogram of microdialysates sampled from a briefly anesthetized mouse, with aCSF as blank and 1 nM serotonin aCSF as standard for comparison. The 5-HT from chromatographs of dialysate samples was identified by comparing their elution times with those of reference standards. Besides matching the retention time, the serotonin peak position is also confirmed by comparing the microdialysate sample under high K^+ stimulation. When the microdialysis perfusate is changed from aCSF to aCSF supplemented with 120 mM K^+, the neuronal membranes depolarize due to the change of membrane potential and stimulate the elevated release of neurotransmitters. The 5HT level drops after high K^+ is removed from the perfusate. The amount of 5-HT in each dialysate sample was

quantified from their respective peak heights by a linear regression analysis of the peak heights obtained from a series of reference standards. 5HT concentration is 1.1 ±0.01 nM for baseline microdialysate, 5.5±0.2 nM with high K^+ stimulation and 3.3±0.2 nM for post K^+ stimulation sample. The 5HT concentration in microdialysates is determined by microdialysis experiment parameters, including microdialysis flow rate. While 5HT concentration is 1.1±0.01 nM at microdialysis flow rate of 3 μL/min, the level increases to 3.1±0.2 nM when the microdialysis flow rate is dropped to 1 μL/min. The concentration of 5HT in microdialysate sample is related to the actual concentration in the extracellular fluid by a factor of recovery rate. Higher recovery (more concentrated samples) is obtained when the probe is perfused at lower flow rates because this allows more time for the analyte to diffuse from the extracellular fluid across the membrane into the dialysate[2]. In fact, the recovery rate approaches 100% with a flow rate lower than 100 nL/min[177].

Serotonin level in extracellular fluid is regulated by 5HT reuptake transporter (SERT, a Na^+/Cl^- dependent transporter) in the presynaptic cell membrane, as it clears 5HT from extracellular space by transporting it back to presynaptic neurons. SERT has been the subject of some popular antidepressant drugs. There are also biological studies that indicate certain genetic defect can cause deficient SERT protein expression. Figure 5.7A shows the result on a SERT knockout mouse which exhibits a gene dose-dependent decrease in SERT protein levels and subsequently 5-HT reuptake. Compared with the serotonin level in a $SERT^{-/-}$ mouse, a wild type ($SERT^{+/+}$) mouse has significantly lower levels of basal dialysate serotonin under the identical microdialysis conditions (Figure 5.7B).

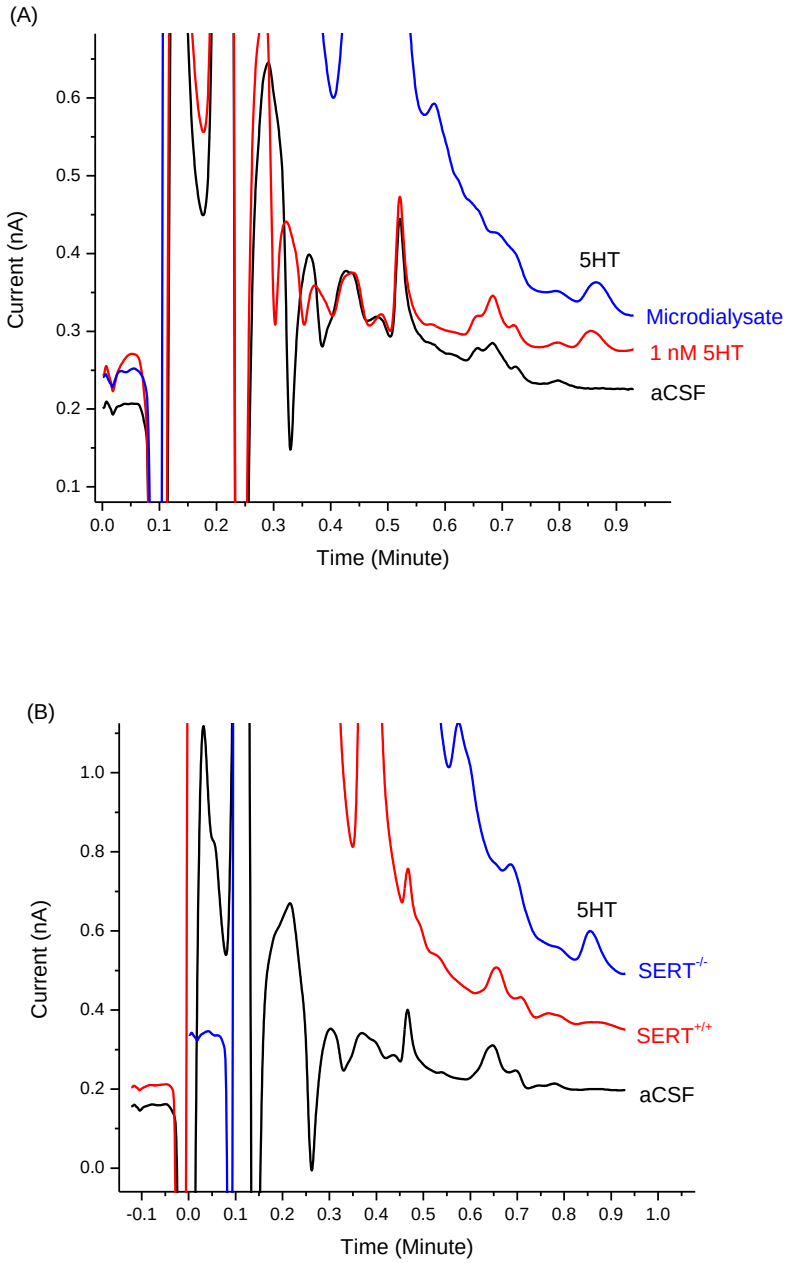

Figure 5.7 (A) the chromatogram of microdialysates sampled from a briefly anesthetized mouse, with aCSF as blank and 2 nM serotonin aCSF as standard for comparison; (B) baseline microdialysate from SERT$^{+/+}$ and SERT $^{-/-}$ mice.

Quantification of basal serotonin in microdialysate samples can be successfully achieved on the UHPLC-ECD system with a high temporal resolution (<1 minute), which enables its

coupling with microdialysis in an on-line setup. The sample loop is 500 nL, which would take 0.5 minute to fill if the microdialysis flow rate is 1 μL/min. The sampling time matches the timescale of UHPLC separation process. Further increase in microdialysis flow rate can increase temporal resolution but also challenges the UHPLC-ECD system sensitivity. On the other hand, if the dialysis flow rate is decreased, the recovery rate will be higher and quantification will be easier and more accurate. Under the on-line real time analysis scenario, the system is calibrated with standard serotonin solutions before connecting to the microdialysis probe. The elution position of serotonin can be confirmed by high K^+ stimulation. We have also noticed that there are likely unidentified impurities in the microdialysates, which may interfere with serotonin quantification if they elute at the same retention time with 5HT. By adjusting column temperature, the impurity peaks can be "moved" to a different time as the retention behavior (retention factor dependence of temperature) is different for serotonin and impurities. We have shown the example in the supplemental information of a recent publication[6].

5.4 CONCLUSION

Equipped with an optimized low-volume electrochemical detector, the capillary UHPLC-ECD system is capable of measuring basal serotonin levels in microdialysis samples with LOD of 0.07 nM. Fast separation of serotonin (< 1 min) is accomplished through a combination of small particles, high pressure and elevated temperature. The high sensitivity and improved temporal resolution of the UHPLC-ECD system make it possible to couple with microdialysis for *in vivo* monitoring of serotonin, including its basal concentration and its changes above or below baseline level over time.

BIBLIOGRAPHY

(1) Perry, M.; Li, Q.; Kennedy, R. T. *Analytica chimica Acta* **2009**, *653*, 1-22.

(2) Nandi, P.; Lunte, S. M. *Analytica chimica Acta* **2009**, *651*, 1-14.

(3) Guihen, E.; O'Connor, W. T. *Electrophoresis* **2009**, *30*, 2062-2075.

(4) Schultz, K. N.; Kennedy, R. T. *Annual Review of Analytical Chemistry* **2008**, *1*, 627-661.

(5) Yoshitake, T.; Kehr, J.; Todoroki, K.; Nohta, H.; Yamaguchi, M. *Biomedical Chromatography* **2006**, *20*, 267-281.

(6) Liu, Y.-S.; Zhang, J.; Xu, X.-M.; Zhao, M. K.; Andrews, A. M.; Weber, S. G. *Analytical Chemistry* **2010**, *82*, 9611-9616.

(7) Parrot, S.; Lambas-Senas, L.; Sentenac, S.; Denoroy, L.; Renaud, B. *Journal of Chromatography, B: Analytical Technologies in the Biomedical and Life Sciences* **2007**, *850*, 303-309.

(8) Gunaratna, P. C.; Cadle, K. K.; Kissinger, C. B. *Journal of Neuroscience Methods* **2006**, *155*, 143-148.

(9) Wen, J.; Zhou, L.; Jin, L.; Cao, X.; Ye, B.-C. *Journal of Chromatography, B: Analytical Technologies in the Biomedical and Life Sciences* **2009**, *877*, 1793-1798.

(10) Santana, M. B.; Rodrigues, K. J. A.; Duran, R.; Alfonso, M.; Vidal, L.; Campos, F.; De Oliveira, I. M.; Faro, L. R. F. *Ecotoxicology and Environmental Safety* **2009**, *72*, 1565-1571.

(11) Jing, F.-C.; Chen, H.; Li, C.-L. *Biomedical and Environmental Sciences* **2007**, *20*, 317-320.

(12) Wang, D.; Zhu, W.; An, Y.; Zheng, J.; Zhang, W.; Jin, L.; Gao, H.; Lin, L. *Chromatographia* **2008**, *67*, 369-374.

(13) Newton, A. P.; Justice, J. B., Jr. *Analytical Chemistry* **1994**, *66*, 1468-1472.

(14) Poppe, H. *Journal of Chromatography, A* **1997**, *778*, 3-21.

(15) Enrico, P.; Mura, M. A.; Esposito, G.; Serra, P.; Migheli, R.; De Natale, G.; Desole, M. S.; Miele, M.; Miele, E. *Brain Research* **1998**, *797*, 94-102.

(16) Sugahara, M.; Asai, S.; Zhao, H.; Nagata, T.; Kunimatsu, T.; Ishii, Y.; Kohno, T.; Ishikawa, K. *Neurochemistry international* **2001**, *39*, 65-73.

(17) Mabrouk, O. S.; Li, Q.; Song, P.; Kennedy, R. T. *Journal of Neurochemistry* **2011**, *118*, 24-33.

(18) Nirogi, R.; Mudigonda, K.; Kandikere, V.; Ponnamaneni, R. *Biomedical Chromatography* **2010**, *24*, 39-48.

(19) Uutela, P.; Reinila, R.; Harju, K.; Piepponen, P.; Ketola, R. A.; Kostiainen, R. *Analytical Chemistry* **2009**, *81*, 8417-8425.

(20) Lanckmans, K.; Sarre, S.; Smolders, I.; Michotte, Y. *Talanta* **2008**, *74*, 458-469.

(21) Buck, K.; Voehringer, P.; Ferger, B. *Journal of Neuroscience Methods* **2009**, *182*, 78-84.

(22) Van Hemelrijck, A.; Sarre, S.; Smolders, I.; Michotte, Y. *Journal of Neuroscience Methods* **2005**, *144*, 63-71.

(23) Yoshitake, T.; Yoshitake, S.; Fujino, K.; Nohta, H.; Yamaguchi, M.; Kehr, J. *Journal of Neuroscience Methods* **2004**, *140*, 163-168.

(24) Hayashi, K.; Kurita, R.; Horiuchi, T.; Niwa, O. *Electroanalysis* **2002**, *14*, 333-338.

(25) Boyd, B. W.; Witowski, S. R.; Kennedy, R. T. *Analytical Chemistry* **2000**, *72*, 865-871.

(26) Warner, A. M.; Weber, S. G. *Analytical Chemistry* **1989**, *61*, 2664-2668.

(27) Sahlin, E.; Beisler, A. T.; Woltman, S. J.; Weber, S. G. *Analytical Chemistry* **2002**, *74*, 4566-4569.

(28) Heinisch, S.; Desmet, G.; Clicq, D.; Rocca, J.-L. *Journal of Chromatography, A* **2008**, *1203*, 124-136.

(29) Cabooter, D.; Billen, J.; Terryn, H.; Lynen, F.; Sandra, P.; Desmet, G. *Journal of Chromatography, A* **2008**, *1204*, 1-10.

(30) Gritti, F.; Felinger, A.; Guiochon, G. *Journal of Chromatography, A* **2006**, *1136*, 57-72.

(31) Fountain, K. J.; Neue, U. D.; Grumbach, E. S.; Diehl, D. M. *Journal of Chromatography, A* **2009**, *1216*, 5979-5988.

(32) Knecht, L. A.; Guthrie, E. J.; Jorgenson, J. W. *Analytical Chemistry* **1984**, *56*, 479-482.

(33) Wallingford, R. A.; Ewing, A. G. *Analytical Chemistry* **1987**, *59*, 1762-1766.

(34) Deng, Q.; Kauri, L. M.; Qian, W.-J.; Dahlgren, G. M.; Kennedy, R. T. *Analyst (Cambridge, United Kingdom)* **2003**, *128*, 1013-1018.

(35) Shen, H.; Witowski, S. R.; Boyd, B. W.; Kennedy, R. T. *Analytical Chemistry* **1999**, *71*, 987-994.

(36) Sloss, S.; Ewing, A. G. *Analytical Chemistry* **1993**, *65*, 577-581.

(37) Powell, P. R.; Paxon, T. L.; Han, K.-A.; Ewing, A. G. *Analytical Chemistry* **2005**, *77*, 6902-6908.

(38) Paxon, T. L.; Powell, P. R.; Lee, H.-G.; Han, K.-A.; Ewing, A. G. *Analytical Chemistry* **2005**, *77*, 5349-5355.

(39) Kennedy, R. T.; Watson, C. J.; Haskins, W. E.; Powell, D. H.; Strecker, R. E. *Current Opinion in Chemical Biology* **2002**, *6*, 659-665.

(40) Kuklinski, N. J.; Berglund, E. C.; Engelbreksson, J.; Ewing, A. G. *Electrophoresis* **2010**, *31*, 1886-1893.

(41) Elbicki, J. M.; Morgan, D. M.; Weber, S. G. *Analytical Chemistry* **1984**, *56*, 978-985.

(42) Trojanowicz, M. *Analytica chimica Acta* **2011**, *688*, 8-35.

(43) Erickson, B. E. *Analytical Chemistry* **2000**, *72*, 353A-357A.

(44) Segovia-Martinez, L.; Moliner-Martinez, Y.; Campins-Falco, P. *Journal of Chromatography, A* **2010**, *1217*, 7926-7930.

(45) Xu, X.; Li, L.; Weber, S. G. *TrAC, Trends in Analytical Chemistry* **2007**, *26*, 68-79.

(46) Villalba, M. M.; Davis, J. *Journal of Solid State Electrochemistry* **2008**, *12*, 1245-1254.

(47) Huffman, M. L.; Venton, B. J. *Analyst (Cambridge, United Kingdom)* **2009**, *134*, 18-24.

(48) Rubianes, M. D.; Rivas, G. A. *Analytical Letters* **2003**, *36*, 329-345.

(49) May, L. J.; Kuhr, W. G.; Wightman, R. M. *Journal of Neurochemistry* **1988**, *51*, 1060-1069.

(50) Hashemi, P.; Dankoski, E. C.; Petrovic, J.; Keithley, R. B.; Wightman, R. M. *Analytical Chemistry* **2009**, *81*, 9462-9471.

(51) Swamy, B. E. K.; Venton, B. J. *Analyst (Cambridge, United Kingdom)* **2007**, *132*, 876-884.

(52) Hermans, A.; Seipel, A. T.; Miller, C. E.; Wightman, R. M. *Langmuir* **2006**, *22*, 1964-1969.

(53) Chen, J.-G.; Woltman, S. J.; Weber, S. G. *Journal of Chromatography, A* **1995**, *691*, 301-315.

(54) Chen, J.-G.; Weber, S. G. *Analytical Chemistry* **1995**, *67*, 3596-3604.

(55) Ulman, A. *Introduction to ultrathin organic films, from Langmuir-Blodgett to self-assembly*; Academic Press, Inc.: New York, 1991.

(56) Wang, W.; Lee, T.; Reed, M. A. *Reports on Progress in Physics* **2005**, *68*, 523-544.

(57) Ulman, A.; Kang, J. F.; Shnidman, Y.; Liao, S.; Jordan, R.; Choi, G.-Y.; Zaccaro, J.; Myerson, A. S.; Rafailovich, M.; Sokolov, J.; Fleischer, C. *Reviews in Molecular Biotechnology* **2000**, *74*, 175-188.

(58) Fischer, D. J.; Vandaveer, W. R. I. V.; Grigsby, R. J.; Lunte, S. M. *Electroanalysis* **2005**, *17*, 1153-1159.

(59) Ogburn, E. T.; Dziewatkoski, M.; Moles, D.; Johnson, J. M.; Heineman, W. R. *Analytical Chemistry* **2011**, *83*, 6963-6970.

(60) Paixao, T. R. L. C.; Matos, R. C.; Bertotti, M. *Electrochimica Acta* **2003**, *48*, 691-698.

(61) Thompson, M.; Klymenko, O. V.; Compton, R. G. *Journal of Electroanalytical Chemistry* **2005**, *576*, 333-338.

(62) Niwa, O.; Morita, M. *Analytical Chemistry* **1996**, *68*, 355-359.

(63) Niwa, O.; Kurita, R.; Liu, Z.; Horiuchi, T.; Torimitsu, K. *Analytical Chemistry* **2000**, *72*, 949-955.

(64) Kurita, R.; Tabei, H.; Liu, Z.; Horiuchi, T.; Niwa, O. *Sensors and Actuators, B: Chemical* **2000**, *B71*, 82-89.

(65) Cazes, J. *Encyclopedia of Chromatography*, 2nd ed.; CRC, 2004.

(66) Bard, A. J.; Faulkner, L. R. *Electrochemical Methods: Fundamentals and Applications*, Second ed.; John Wiley & Sons, Inc.: New York, NY, 2000.

(67) Liu, Y.-S.; Zhang, J.; Xu, X.-M.; Zhao, M. K.; Andrews, A. M.; Weber, S. G. *Analytical Chemistry (Washington, DC, United States)* **2010**, *82*, 9611-9616.

(68) Hirata, Y.; Lin, P. T.; Novotny, M.; Wightman, R. M. *Journal of Chromatography, Biomedical Applications* **1980**, *181*, 287-294.

(69) Metz, S.; Jiguet, S.; Bertsch, A.; Renaud, P. *Lab on a Chip* **2004**, *4*, 114-120.

(70) Pham, N. P.; Boellaard, E.; Burghartz, J. N.; Sarro, P. M. *Journal of Microelectromechanical Systems* **2004**, *13*, 491-499.

(71) Lambie, B. A.; Orwar, O.; Weber, S. G. *Analytical Chemistry* **2006**, *78*, 5165-5171.

(72) Jalonen, P.; Tuominen, A. *Circuit World* **2002**, *28*, 11-13.

(73) Tuomikoski, S.; Franssila, S. *Sensors and Actuators, A: Physical* **2005**, *A120*, 408-415.

(74) Gu, Q.; Shi, X.; Yin, P.; Gao, P.; Lu, X.; Xu, G. *Analytica chimica Acta* **2008**, *609*, 192-200.

(75) Roosendaal, E. M. M. P., H. *Analytica chimica Acta* **1984**, *158*, 323.

(76) Weber Stephen, G. P., W. C. *Analytica chimica Acta* **1978**, *100*, 531.

(77) Meyer, R. E. B., M. C.; Lantz, P. M.; Posey, F. A. *Journal of Electroanalytical Chemistry* **1971**, *30*, 345.

(78) Weber Stephen, G. *Journal of Electroanalytical Chemistry* **1983**, *145*, 1.

(79) Lundqvist, H.; Lubberink, M.; Tolmachev, V.; Lovqvist, A.; Sundin, A.; Beshara, S.; Bruskin, A.; Carlsson, J.; Westlin, J. E.; Department of Oncology, Radiology and Clinical Immunology, Uppsala University, Sweden: Norway, 1999, pp 335-341.

(80) Paddon, C. A. P., Gareth J.; Thiemann, Thies; Marken, Frank *Electrochemistry Communications* **2002**, *4*, 825-831.

(81) Hertlein, W. G.; Tornkvist, K.; Smith, K. *Circuit World* **2001**, *27*, 6-14.

(82) Kakaboura, A.; Fragouli, M.; Rahiotis, C.; Silikas, N. *Journal of Materials Science: Materials in Medicine* **2007**, *18*, 155-163.

(83) Petitdider, C.; Tiron, R.; Derrough, S.; Sourd, C.; Koscianski, L.; Mortini, B. *Proceedings of SPIE* **2007**, *6591*, 659101.

(84) Kranenburg, J. M.; Tweedie, C. A.; van Vliet, K. J.; Schubert, U. S. *Advanced Materials (Weinheim, Germany)* **2009**, *21*, 3551-3561.

(85) Huebner, J.; Nguyen, A.; Turcu, F.; Melchior, D.; Kling, H.-W.; Gaeb, S.; Schmitz, O. J. *Analytical and Bioanalytical Chemistry* **2006**, *384*, 259-264.

(86) Briscoe, B. J.; Fiori, L.; Pelillo, E. *Journal of Physics D: Applied Physics* **1998**, *31*, 2395-2405.

(87) Uzun, O.; Basman, N.; Alkan, C.; Koelemen, U.; Yilmaz, F. *Polymer Bulletin (Heidelberg, Germany)* **2010**, No pp yet given.

(88) Hakiri, N.; Matsuda, A.; Sakai, M. *Journal of Materials Research* **2009**, *24*, 1950-1959.

(89) Menczel, J. D.; Prime, R. B.; Editors *Thermal analysis of polymers: Fundamentals and applications*, 2009.

(90) Chartoff, R. P.; Menczel, J. D.; Dillman, S. H. *Thermal Analysis of Polymers* **2009**, 387-495.

(91) Swaminathan, G.; Shivakumar, K. *Journal of Reinforced Plastics and Composites* **2009**, *28*, 979-994.

(92) Krupicka, A.; Johansson, M.; Hult, A. *Macromolecular Materials and Engineering* **2003**, *288*, 108-116.

(93) Chakravartula, A.; Komvopoulosa, K. *Applied Physics Letters* **2006**, *88*, 131901.

(94) Walczak, M. M.; Popenoe, D. D.; Deinhammer, R. S.; Lamp, B. D.; Chung, C.; Porter, M. D. *Langmuir* **1991**, *7*, 2687-2693.

(95) Lunte, C. E.; Kissinger, P. T. *Analytical Chemistry* **1983**, *55*, 1458-1462.

(96) Roston, D. A., Kissinger, P. T. *Analytical Chemistry* **1982**, *54*, 429-434.

(97) Gratzl, M.; Pungor, E. *Zhurnal Analiticheskoi Khimii* **1988**, *43*, 541-554.

(98) Tsai, H.; Weber, S. G. *Analytical Chemistry* **1992**, *64*, 2897-2903.

(99) Lipka, S. M.; Cahen, G. L., Jr.; Stoner, G. E.; Scribner, L. L., Jr.; Gileadi, E. *Journal of the Electrochemical Society* **1988**, *135*, 368-372.

(100) Nacamulli, L.; Gileadi, E. *Journal of Applied Electrochemistry* **1983**, *13*, 73-78.

(101) Coeuret, F.; Vilar, E. O.; Cavalcanti, E. B. *Journal of Applied Electrochemistry* **2002**, *32*, 1175-1182.

(102) Caudill, W. L.; Howell, J. O.; Wightman, R. M. *Analytical Chemistry* **1982**, *54*, 2532-2535.

(103) Davis, B. K.; Weber, S. G.; Sylwester, A. P. *Analytical Chemistry* **1990**, *62*, 1000-1003.

(104) Zhang, W.; Xie, Y.; Ai, S.; Wan, F.; Wang, J.; Jin, L.; Jin, J. *Journal of Chromatography, B: Analytical Technologies in the Biomedical and Life Sciences* **2003**, *791*, 217-225.

(105) Gerhardt, G. A.; Oke, A. F.; Nagy, G.; Moghaddam, B.; Adams, R. N. *Brain Research* **1984**, *290*, 390-395.

(106) Zhang, W.; Xie, Y.; Gu, J.; Ai, S.; Wang, J.; Yamamoto, K.; Jin, L. *Analyst (Cambridge, United Kingdom)* **2004**, *129*, 229-234.

(107) Pamidi, P. V. A.; Parrado, C.; Kane, S. A.; Wang, J.; Smyth, M. R.; Pingarron, J. *Talanta* **1997**, *44*, 1929-1934.

(108) Tsionsky, M.; Gun, G.; Glezer, V.; Lev, O. *Analytical Chemistry* **1994**, *66*, 1747-1753.

(109) Xu, F.; Gao, M.; Shi, G.; Wang, L.; Zhang, W.; Xue, J.; Jin, L.; Jin, J. *Analytica chimica Acta* **2001**, *439*, 239-246.

(110) Chirita, R.-I.; Finaru, A.-L.; Elfakir, C. *Journal of Chromatography, B: Analytical Technologies in the Biomedical and Life Sciences* **2011**, *879*, 633-640.

(111) Ou, T. Y.; Anderson, J. L. *Analytical Chemistry* **1991**, *63*, 1651-1658.

(112) Kazee, B.; Weisshaar, D. E.; Kuwana, T. *Analytical Chemistry* **1985**, *57*, 2736-2739.

(113) Palenzuela, B.; Rodriguez-Amaro, R.; Rios, A.; Valcarcel, M. *Electroanalysis* **2002**, *14*, 1427-1432.

(114) Ruiz-Jimenez, J.; Luque de Castro, M. D. *TrAC, Trends in Analytical Chemistry* **2006**, *25*, 563-571.

(115) Diego, E.; Agui, L.; Gonzalez-Cortes, A.; Yanez-Sedeno, P.; Pingarron, J. M.; Kauffmann, J. M. *Electroanalysis* **1998**, *10*, 33-38.

(116) Cespedes, F.; Martinez-Fabregas, E.; Bartoli, J.; Alegret, S. *Analytica chimica Acta* **1993**, *273*, 409-417.

(117) Weng, Q.; Xu, G.; Yuan, K.; Tang, P. *Journal of Chromatography, B: Analytical Technologies in the Biomedical and Life Sciences* **2006**, *835*, 55-61.

(118) Chung, D. D. L. *Carbon fiber composites*; Butterworth-Heinemann: Newton, MA, 1994.

(119) Zhong, M.; Zhou, J.; Lunte, S. M.; Zhao, G.; Giolando, D. M.; Kirchhoff, J. R. *Analytical Chemistry* **1996**, *68*, 203-207.

(120) Cheng, J.; Jandik, P.; Avdalovic, N. *Journal of Chromatography, A* **2003**, *997*, 73-78.

(121) Wu, C.-C.; Wu, R.-G.; Huang, J.-G.; Lin, Y.-C.; Chang, H.-C. *Analytical Chemistry* **2003**, *75*, 947-952.

(122) Lu, J.; Zhang, S.; Wang, A.; Zhang, W.; Jin, L. *Talanta* **2000**, *52*, 807-815.

(123) Ghanem, M. A.; Thompson, M.; Compton, R. G.; Coles, B. A.; Harvey, S.; Parker, K. H.; O'Hare, D.; Marken, F. *Journal of Physical Chemistry B* **2006**, *110*, 17589-17594.

(124) Ji, H.; Wang, E. *Talanta* **1991**, *38*, 73-80.

(125) McCreedy, T.; Fielden, P. R. *Analyst (Cambridge, United Kingdom)* **1995**, *120*, 2343-2346.

(126) Hayashi, K.; Kurita, R.; Horiuchi, T.; Niwa, O. *Electroanalysis* **2002**, *14*, 333-338.

(127) Kotani, A.; Kojima, S.; Hayashi, Y.; Matsuda, R.; Kusu, F. *Journal of Pharmaceutical and Biomedical Analysis* **2008**, *48*, 780-787.

(128) Toda, K.; Oguni, S.; Takamatsu, Y.; Sanemasa, I. *Journal of Electroanalytical Chemistry* **1999**, *479*, 57-63.

(129) Xu, F.; Gao, M.; Wang, L.; Jin, L. *Analytical Biochemistry* **2002**, *307*, 33-39.

(130) Wightman, R. M.; Amatore, C.; Engstrom, R. C.; Hale, P. D.; Kristensen, E. W.; Kuhr, W. G.; May, L. J. *Neuroscience (Oxford, United Kingdom)* **1988**, *25*, 513-523.

(131) Nandi, P.; Lunte, S. M. *Analytica Chimica Acta* **2009**, *651*, 1-14.

(132) Margerum, D. W. *Pure and Applied Chemistry* **1983**, *55*, 23-34.

(133) McCreery, R. L., Cline, K. K., *Laboratory Techniques in Electroanalytical Chemistry*; Marcel Dekker: New York, 1996.

(134) Gao, S.; Bhoopathy, S.; Zhang, Z.-P.; Wright, D. S.; Jenkins, R.; Karnes, H. T. *Journal of Pharmaceutical and Biomedical Analysis* **2006**, *40*, 679-688.

(135) Lacher, N. A.; Garrison, K. E.; Martin, R. S.; Lunte, S. M. *Electrophoresis* **2001**, *22*, 2526-2536.

(136) Dubois, L. H. M., R. G. *Anal. Rev. Phys. Chem.* **1992**, *43*, 437.

(137) Wen, J.; Zhou, L.; Jin, L.; Cao, X.; Ye, B.-C. *Journal of Chromatography, B: Analytical Technologies in the Biomedical and Life Sciences* **2009**, *877*, 1793-1798.

(138) Zamborini, F. P.; Crooks, R. M. *Langmuir* **1998**, *14*, 3279-3286.

(139) Vericat, C.; Vela, M. E.; Salvarezza, R. C. *Physical Chemistry Chemical Physics* **2005**, *7*, 3258-3268.

(140) Kato, K. *Encyclopedia of Biomaterials and Biomedical Engineering* **2004**, *2*, 1331-1339.

(141) Schreiber, F. *Progress in Surface Science* **2000**, *65*, 151-256.

(142) Buess-Herman, C. *Progress in Surface Science* **1994**, *46*, 335-375.

(143) Porter, M. D.; Bright, T. B.; Allara, D. L.; Chidsey, C. E. D. *Journal of the American Chemical Society* **1987**, *109*, 3559-3568.

(144) Ulman, A. *Characterization of organic thin films*; Butterworth-Heinemann: Boston, 1995.

(145) Campuzano, S.; Pedrero, M.; Montemayor, C.; Fatas, E.; Pingarron, J. M. *Journal of Electroanalytical Chemistry* **2006**, *586*, 112-121.

(146) Finklea, H. O.; Snider, D. A.; Fedyk, J.; Sabatani, E.; Gafni, Y.; Rubinstein, I. *Langmuir* **1993**, *9*, 3660-3667.

(147) Finklea, H. O.; Snider, D. A.; Fedyk, J. *Langmuir* **1990**, *6*, 371-376.

(148) Scharf, J.; Strehblow, H.-H.; Zeysing, B.; Terfort, A. *Journal of Solid State Electrochemistry* **2001**, *5*, 396-401.

(149) Sawaguchi, T. M., F.; Taniguchi, I. *Langmuir* **1998**, *14*, 3565.

(150) Szucs, A. H., G. D.; Bockris, J. O'M *Electrochimica Acta* **1992**, *37*, 403.

(151) Fedurco, M. *Coordination Chemistry Reviews* **2000**, *209*, 263-331.

(152) Lio, A.; Charych, D. H.; Salmeron, M. *Journal of Physical Chemistry B* **1997**, *101*, 3800-3805.

(153) Kaefer, D.; Witte, G.; Cyganik, P.; Terfort, A.; Woell, C. *Journal of the American Chemical Society* **2006**, *128*, 1723-1732.

(154) Widrig, C. A.; Chung, C.; Porter, M. D. *Journal of Electroanalytical Chemistry and Interfacial Electrochemistry* **1991**, *310*, 335-359.

(155) Jonnakuty, C.; Gragnoli, C. *Journal of Cellular Physiology* **2008**, *217*, 301-306.

(156) Canli, T.; Lesch, K.-P. *Nature Neuroscience* **2007**, *10*, 1103-1109.

(157) Alessandro, S.; Kato, M. *Expert Review of Neurotherapeutics* **2008**, *8*, 111-120.

(158) Mathews, T. A.; Fedele, D. E.; Coppelli, F. M.; Avila, A. M.; Murphy, D. L.; Andrews, A. M. *Journal of Neuroscience Methods* **2004**, *140*, 169-181.

(159) Serretti, A.; Calati, R.; Mandelli, L.; De Ronchi, D. *Current Drug Targets* **2006**, *7*, 1659-1669.

(160) Knobelman, D. A.; Kung, H. F.; Lucki, I. *Journal of Pharmacology and Experimental Therapeutics* **2000**, *292*, 1111-1117.

(161) Schloss, P.; Williams, D. C. *Journal of Psychopharmacology* **1998**, *12*, 115-121.

(162) Murphy, D. L.; Fox, M. A.; Timpano, K. R.; Moya, P. R.; Ren-Patterson, R.; Andrews, A. M.; Holmes, A.; Lesch, K.-P.; Wendland, J. R. *Neuropharmacology* **2008**, *55*, 932-960.

(163) Ogburn, E. T.; Dziewatkoski, M.; Moles, D.; Johnson, J. M.; Heineman, W. R. *Analytical Chemistry (Washington, DC, United States)* **2011**, *83*, 6963-6970.

(164) Robinson, D. L.; Venton, B. J.; Heien, M. L. A. V.; Wightman, R. M. *Clinical Chemistry* **2003**, *49*, 1763-1773.

(165) Kennedy, R. T.; Watson, C. J.; Haskins, W. E.; Powell, D. H.; Strecker, R. E. *Current Opinion in Chemical Biology* **2002**, *6*, 659-665.

(166) Bowser, M. T.; Kennedy, R. T. *Electrophoresis* **2001**, *22*, 3668-3676.

(167) Unger, K. K.; Skudas, R.; Schulte, M. M. *Journal of Chromatography, A* **2008**, *1184*, 393-415.

(168) Kamau, G. N.; Willis, W. S.; Rusling, J. F. *Analytical Chemistry* **1985**, *57*, 545-551.

(169) Jackson, B. P.; Dietz, S. M.; Wightman, R. M. *Analytical Chemistry* **1995**, *67*, 1115-1120.

(170) Wrona, M. Z.; Lemordant, D.; Lin, L.; Blank, C. L.; Dryhurst, G. *Journal of Medicinal Chemistry* **1986**, *29*, 499-505.

(171) Mora, M. F.; Felhofer, J.; Ayon, A.; Garcia, C. D. *Analytical Letters* **2008**, *41*, 312-334.

(172) Chowdappa, N.; Kumara Swamy, B. E.; Niranjana, E.; Sherigara, B. S. *International Journal of Electrochemical Science* **2009**, *4*, 425-434.

(173) Henstridge, M. C.; Dickinson, E. J. F.; Aslanoglu, M.; Batchelor-McAuley, C.; Compton, R. G. *Sensors and Actuators, B: Chemical* **2010**, *B145*, 417-427.

(174) Roach, D. M.; Hooper, S. E.; Anderson, M. R. *Electroanalysis* **2005**, *17*, 2254-2259.

(175) Felice, L. J.; Felice, J. D.; Kissinger, P. T. *Journal of Neurochemistry* **1978**, *31*, 1461-1465.

(176) Boyd, B. W.; Witowski, S. R.; Kennedy, R. T. *Analytical Chemistry* **2000**, *72*, 865-871.

(177) Menacherry, S.; Hubert, W.; Justice, J. B., Jr. *Analytical Chemistry* **1992**, *64*, 577-583.